The University of Aston in Birmingham

FIELD ADSORPTION AND CHARGED SURFACES

Thesis Submitted for the degree of

Doctor of Philosophy

by

Muafak Kamal Wafi

B.Sc., M.Sc.

Department of Physics

October, 1981

Thesis for degree of Ph.D.

by

Muafak Kamal Wafi

The University of Aston in Birmingham

Field Adsorption and Charged Surfaces

Abstract

This thesis deals with the theory of charged surfaces, field adsorption and field-ion imaging.

The existing literature dealing with these subjects is in many ways inconsistent and confusing, and contains conceptual errors. After a brief review of existing ideas, we put forward self-consistent definitions for various parameters, and formulate new models for charged metal surfaces and for field adsorption. The model can be treated analytically, and incorporates the requirements that the crystallographic surface structure, and the localised charge distribution at the emitter surface, be taken into consideration.

This model is applied to a paradigm system, namely helium on tungsten (111). Field and potential variations above a charged surface are explored and it is shown that at a temperature of 80K the field variation in the critical surface is sufficient to explain field-ion image contrast only if a field-adsorbed layer is present. It is also shown that the equipotentials above the planar emitter surface can be imagined to have an egg-box shape, and that the higher the value of the proper polarizability of the surface atoms the further from the emitter surface will be an equipotential of given potential value. An interesting consequence of this is that higher surface-atom polarizability can lead to reduced image contrast.

In the studies of field-adsorption binding energy, the insufficiency of previous treatments is demonstrated. In particular it is shown that neglecting depolarization effects due to mutual interaction between surface atoms leads to marked over-estimation of the binding energy; mutual depolarization in fact means that in some close-packed planes it is impossible to have a fully adsorbed layer. It is also shown that for He on W(111) we cannot have a complete second field-adsorbed layer on top of the first.

When all corrections are taken into account, we have estimated that for the best image field for Helium (45 V/nm), the short-range binding energy for He on W(111) probably lies between 25 and 50 meV. It is concluded that this low value is not sufficient to explain field adsorption and that further modification to our model toward a more realistic model is needed in the future.

Field Ion Imaging, Field Adsorption, Charged Surfaces

TO

MY PARENTS

ACKNOWLEDGEMENTS

I wish to express my gratitude to my Supervisor Dr. R.G. Forbes, for the invaluable help and guidance offered throughout the project.

I wish to thank Professor T. Mulvey, for all the advice and moral support offered whenever needed.

I am very indebted and grateful to my family for their moral and financial support throughout all the years spent in this country carrying on my study, especially to my Mother Fatima and my Father Kamal, my Sister Nawal and her husband Kusay, and my Brother Ageel.

Finally, I wish to thank my wife Margaret, for the patience, understanding and support throughout all the period.

CONTENTS

LIST OF TABLES

LIST OF FIGURES

CHAPTER 1

INTRODUCTION

1.1 General Background

In the last few decades, there has been great improvement in explaining the bulk properties of metals. Bulk theories are now capable of giving qualitatively accurate descriptions of a wide class of metals[1, 2].

Most of this theoretical work relies on the assumption that the body of the metal crystal is homogeneous and continuous, which means that the physical properties of a unit element of the metal are the same, regardless of its location in the whole body[3]. Regarding the real crystal as discontinuous (i.e. atomic) introduced a new factor into bulk theory, namely the "periodicity" of the atomic lattice. Translational symmetry plays a big role in simplifying the formulation of bulk theory. Unfortunately, from this point of view, crystals have surfaces, so there is breakdown in their homogeneous state at the surface. This introduces various difficulties, which have caused the theories of metal surfaces to lag behind relatively[4]. These difficulties mainly result from the loss of translational symmetry, and there is a problem in that the electronic structure must change drastically in consequence of the rapid decrease in electron density near the surface.

A question arises as to the thickness of the "surface". Regarding the crystal interior as homogeneous and continuous might lead to the assumption that surface thickness is zero, on the grounds that the physical properties of any element immediately under the surface cannot be different from that at any other part of the crystal interior. But this approach ignores the behaviour of electrons at surfaces.

The commonest theory of electron behaviour at surfaces is based on the so-called "jellium" model[5]. The ion cores are smeared out to form a continuous rigid positively-charged background, against which the electrons move. Physical properties at and above the surface are then regarded as a combination of bulk and surface effects. At the surface the electrons "spread" into the vacuum, forming a surface double-layer, of finite thickness. Similarly, when we consider structural ("atomic") models, there will be one or more atomic layers that are different in their physical properties from the interior layers. (For example, there is a 5% decrease in inter-atomic spacing, normal to the crystal cube surface, between the outermost layer and the interior layers in alkali halides; but the spacing of the second and third layers is nearly normal[6]). The "surface" is a subject of study in its own right.

Technological advancement in many of the scientific surface techniques (e.g. electron microscopy, field-ion microscopy and related techniques, Auger, X-ray photo-electron spectroscopy) have made it much easier to observe the metal surface in its microscopic details. This has stimulated, and continues to stimulate much advanced research on surfaces, from many viewpoints, in particular those of physics, chemistry, metallurgy and materials science.

One of the most powerful scientific tools in surface studies is the field-ion microscope (FIM)[7], because it allows us to observe the surface in its structural atomic detail. The operation of the microscope requires the application of a very high applied electric field (about 50 V/nm). This leads to a new surface situation, marked by the appearance of new physical phenomena (principally field adsorption, field evaporation and field ionization) and requiring proper theoretical understanding.

The necessary theoretical research is still in its beginnings, and there are many conflicting arguments and hypotheses in the literature.

Meanwhile the accumulating experimental evidence necessitates the re-examination of many parts of the theoretical background both of FIM, and of the theory of charged surfacesand the processes that occur at them. The work presented in this thesis forms part of this theoretical re-examination.

1.2 Field Electron and Ion Emission

Raising the temperature of a metal causes the emission of electrons, a phenomena known for a long time as "thermionic emission"[8], and widely used as an electron source in many electronic instruments. Fig.(1.1) shows that the thermal energy needed to overcome the potential barrier existing at the surface is equal to ϕ, the local work-function of the surface.

However, if a high negative field, of order 3 V/nm, is applied to the surface, as shown in Fig.(1.2), it becomes possible for a fraction of the electrons to "tunnel" through the barrier, instead of going over the hump. This phenomena is known as "field electron emission" and constitutes the basic mechanism of the Field Electron Microscope (FEM)[9].

On the other hand, if a sufficiently high positive field ($\sim$ 50 V/nm), exists at a metal surface then it is possible for an electron (or electrons) in an atom outside the surface to tunnel into the metal, through the barrier shown in Fig.(1.3). The external atom becomes ionized, and is then repelled from the metal surface. This phenomena is known as "field ion emission", and forms the basic process in the Field-ion Microscope (FIM) and related techniques[7, 10].

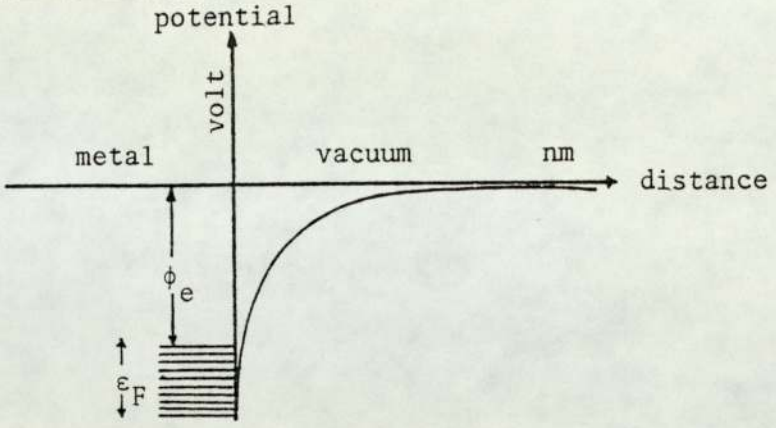

Fig.1.1

Electron potential of metal surface with no external field

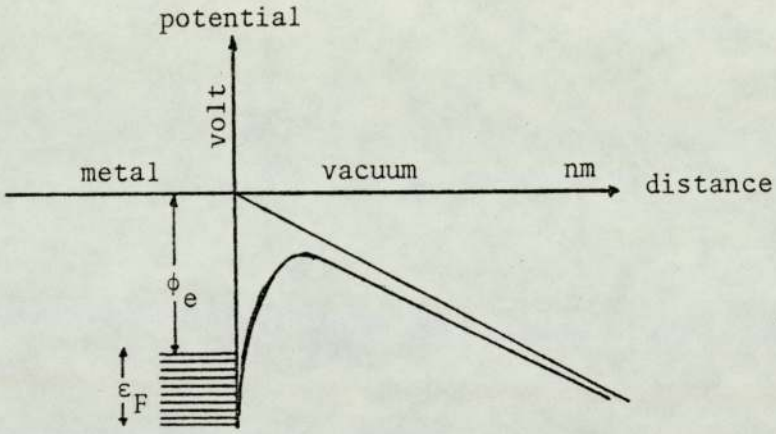

Fig.1.2

Electron potential at metal surface with negative external field

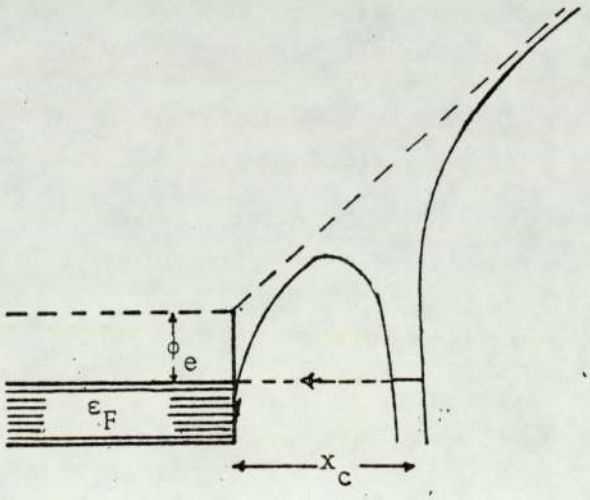

Fig.1.3

Electron potential on metal surface with high positive external field

1.3 The Field Ion Microscope

1.3.1 General Principles

Field-ion microscopy was the first technique capable of giving images of a surface in its atomic details. Historically, the technique developed out of the earlier technique of field electron microscopy[11], when in 1951 Muller[12] applied a high positive field to a pointed field emitter and let hydrogen into the system. An account of the basic technique and its applications was given by Muller and Tsong[7].

Fig.(1.4) shows a schematic diagram of a basic microscope. In this a metallic specimen, shaped as a sharply pointed tip, is mounted in front of a fluorescent screen in a highly evacuated chamber (pressure less than 10^{-6} Torr, and an imaging gas (often helium) is introduced to the chamber at a pressure of few m Torr. A very high positive voltage of the range of 10kV is supplied to the specimen, while the screen is earthed. The effect of the very high field around the tip of the specimen is that the electronic charge distribution of an imaging-gas atom is deformed and the atoms become polarized and so attracted towards the tip. The field is not uniform across the surface of the emitter, but is higher above the positions of protruding atoms such as those at the edges of the planes, and lower over the centre of the planes. As a consequence higher gas concentration (C) and ionization rate-constant (P_e) are expected over these protruding regions, and this leads to a higher rate of ionization in these regions.

The ions thus formed by tunnelling of electrons to the surface are immediately repelled by the positive field at the tip surface, and are accelerated in a direction normal to the tip surface, towards the phosphor screen (or an image intensification device). The impinging of a continuous stream of ions from the protruding sites forms a projection

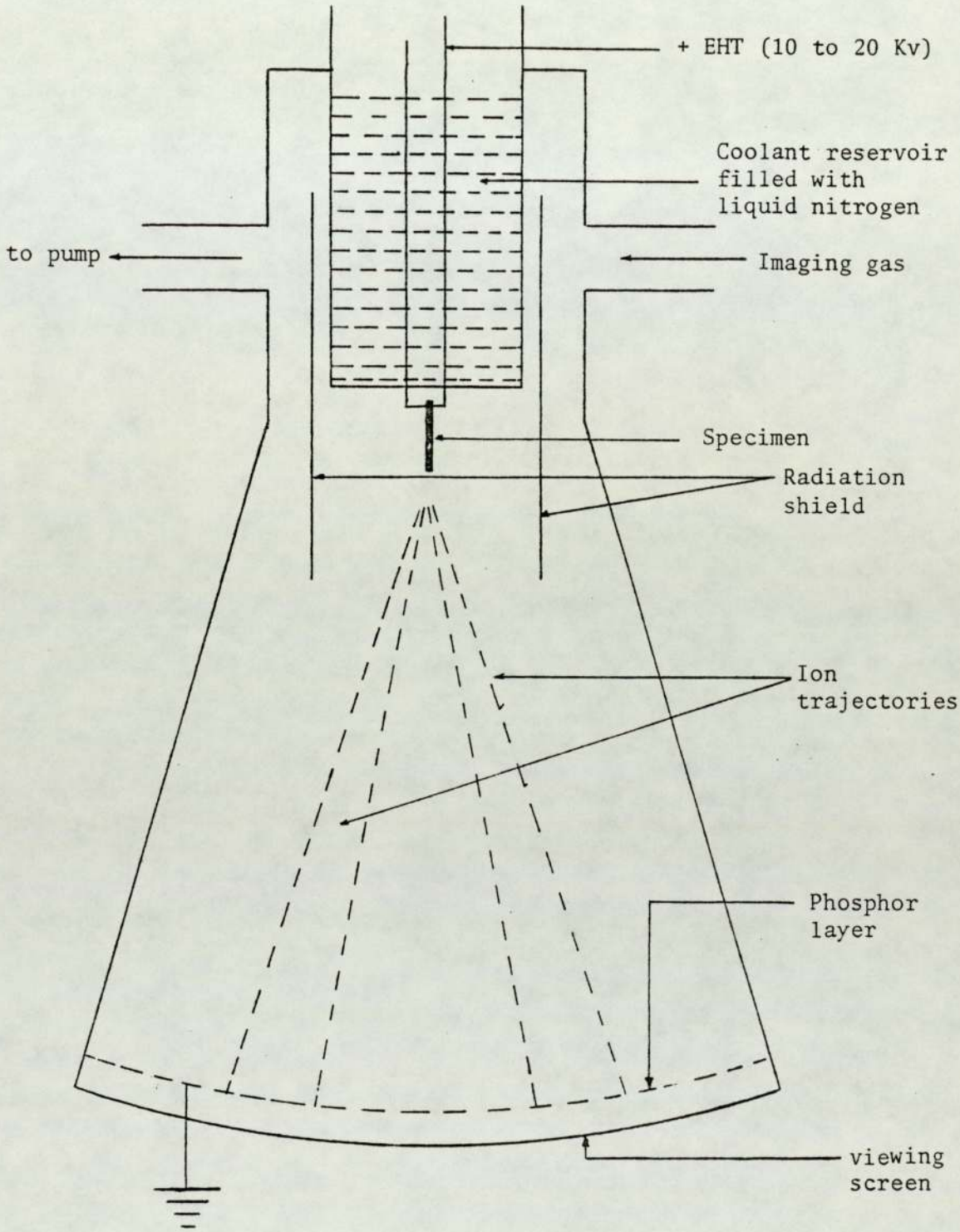

Fig.1.4

A schematic diagram of Field-Ion Microscope

image of these sites. The magnification factor can be found by dividing the tip-to-screen distance by the tip radius-of-curvature, and a very good resolved image can be produced of many millions fold magnification.

The resolution of the image depends on the temperature of the imaging-gas at ionization. Hence the specimen is normally cooled to liquid-nitrogen temperature (78 K) or below.

1.3.2 The Critical Surface

It is well established that neither the attracted imaging gas atoms, nor the desorbed surface atoms, can be ionized inside a geometrical surface, called "the critical surface" that is slightly above metal emitter surface. With a simple "jellium" surface model, this critical surface is located at a critical distance X_c above the emitter surface (Fig.(1.5)), X_c being given by the following approximation[13]:

$$X_c \simeq \frac{\Lambda_o + \sum_n I - n\phi}{neF}$$

where $\sum_n I$ is the ionization energy for n-fold ionization.

Λ_o is the binding energy of neutral atom, in the presence of the field

ϕ is the surface work function

e is the elementary proton charge

ne is the charge on the ion

F is the external field

X_c is a small quantity (i.e. in the range of 0.5 nm). It is often said to be measured from the so-called "the electrical surface" of the emitter. However, difficulties arise over how this surface is to be defined and where it is located (relative to some feature of the real

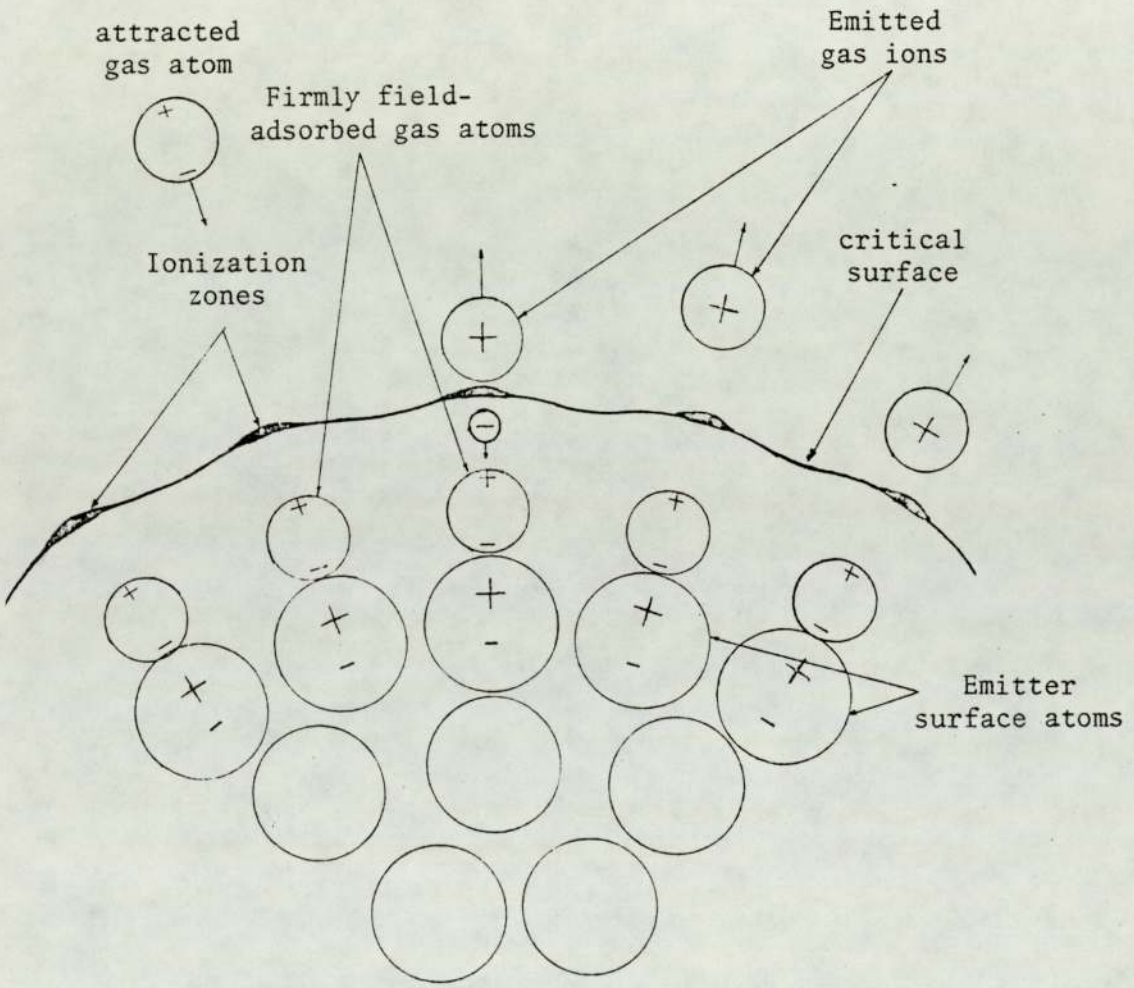

Fig.1.5

A schematic diagram of a FIM tip surface showing the critical surface, ionization zones, field and the field adsorbed gas atoms.

surface). These matters are not well understood, and have sometimes led to conflicting suggestions. Different surface models lead to different results; these matters are discussed in greater detail in later chapters, but we note here that it is desirable in field-ion theory to have a single surface model that can deal both with the position of the electrical surface and with the prediction of field-adsorption binding energies, as described below.

1.3.3 Field Adsorption

Field adsorption[14, 15, 16] is a process that can occur inside the critical surface. If the field is high enough, then imaging-gas atoms can become adsorbed (i.e. bound) onto the emitter surface. Each field adsorbed atom is adsorbed directly above a metal surface atom, as shown in Fig.(1.5).

The short-range field-adsorption binding energy is defined as the work required to detach an adsorbed atom, and to place it at some position in the external field, away from the local variation in field and potential at the surface. These local variations in field and potential are due to the localized (atomic) structure of the real surface, but are enhanced greatly by the existence of adsorbed imaging-gas atoms, which are those believed to have an important role in the process of field ion imaging.

A better understanding of the above is actually the main object of this thesis. The hope is to make some contribution towards answering questions related to the nature of field adsorption, evaluation of the binding energy, and the effect of field adsorption on field and potential variation at the surface and hence on the imaging process.

1.4 Field Evaporation and Associated Techniques

When the field is further increased at a highly positively charged metal surface (typically to more than 50 V/nm) metal surface atoms will at some point detach themselves. The atoms become ionized in the process, with the removed electrons tunnelling back into the metal surface. This process is called "field evaporation".

The concept of field evaporation has been known since the early days of FIM[17], and is used to prepare clean emitter surfaces.

Field evaporation later formed the basic mechanism in the so-called "the atom probe"[18], which provided the means for mass-spectrometric analysis of the detached surface atoms. The time of flight (TOF) atom-probe technique allows the analysis of very small regions of surface or even single atoms. A later development is the so-called "imaging atom-probe"[19], which enables the detection, for a particular species, of its location on the emitter surface.

1.5 Aim and structure of thesis

Having described some of the elementary concepts, we think it helpful to set down the aims and structure of this thesis.

Our primary aims are to develop a theory of highly positively charged metal surfaces, and make it consistent with the theory of field adsorption. For this purpose we shall try to free existing theory from some conceptual errors, and redefine the most important variables (in particular: polarizability, local field, penetration distance) in a self-consistent manner. Then we set up a new self-consistent model for a charged metal surface, using the ideal case of an infinite planar surface.

Finally we apply our model to the practical calculation of field adsorption binding energies, and fields and potentials above a charged

surface, using the system helium on tungsten (111) as a paradigm.

Because of the slightly confused and disjointed nature of existing literature relating to these problems, this thesis has a special structure. Chapter 2 is a review of relevant aspects of existing theories (up until 1978) of field-ion image formation, field adsorption and charged surfaces, essentially considered as separate subjects. In chapter 3 we set down the foundations of a new self-consistent theory, and clarify some basic concepts. Chapter 4 describes the algebraic and mathematical formulation of our model of charged surfaces and field adsorption. In chapter 5 we make practical use of this by devising some computing procedures, which are then implemented in a general computer program. In chapters 6 and 7 we discuss the results: chapter 6 deals with the field and potential variations above a charged surface, with the characteristics of the critical surface, and with the mechanism of field-ion image formation; chapter 7 deals with the calculation of binding energies and makes some comparative studies. Finally, in chapter 8 we summarise our conclusions and discuss some ideas for future work.

CHAPTER 2

REVIEW OF EXISTING THEORIES

2.1 Objectives

As just stated, the intention of this chapter is to summarise relevant aspects of previous work on field-ion image formation, field adsorption and charged-surface theory.

Historically, these three topics developed largely independently of each other, and thus we deal separately with each, at the cost of some slight repetition.

In each case we summarise the development and the main ideas up to about 1978 when the work on this project started.

2.2 Field-ion Image Formation

2.2.1 The Rate-constant and Gas-concentration Hypotheses

The well-defined FIM image is the product of a complex process, in which imaging-gas atoms are attracted towards the emitter tip and (in effect) crowd around the most protruding atoms of the tip surface, before becoming ionized and then repelled from these sites to the phosphor screen (or an image intensification device). The continuation of this process forms a traffic of ions; the number formed per second at a given site is called "site ion current" (or site current), and is denoted by J. The observed brightness of a particular spot depends on the corresponding J value, whereas the total ion current J_{tot} is the sum of all beams, i.e.

$$J_{tot} = \sum_{\substack{\text{all} \\ \text{sites}}} J \qquad \ldots\ldots 2.1$$

Within the framework of a quasiclassical approach,[20], J is the product of a characteristic gas concentration C", a characteristic electron transition rate-constant P_e" and the effective volume of ionization, V. Thus

$$J = C'' P_e'' V \qquad \ldots\ldots 2.2$$

Image contrast can be expressed in terms of relative brightness, which is in turn described by the relative site current (i.e. the ratio of the site currents). If we consider two surface sites A and B then the relative brightness is given by

$$J_A/J_B = (C_A''/C_B'').(P_e''_A/P_e''_B).(v_A/v_B) \qquad \ldots\ldots 2.3$$

If we assume the effective volumes of ionization zone are approximately equal (i.e. $v_A/v_B \simeq 1$) then contrast must be due to the contribution

of the other two factors.

There are two conflicting hypotheses. The more conventional view, originated by Muller[25], and supported by Knor[22, 23] and Tsong[24], is that the more dominant factor is the transition rate-constant. On the contrary, Forbes[23, 25, 26] hypothesised that site-current variations are mostly due to the gas-concentration factor, i.e. the concentration of imaging gas is relatively high above protruding atoms because of relatively high localized field there. This leads to higher probability of finding imaging gas atoms in the right position to be ionized.

An exactly analogous situation arises in the theory of image resolution. Consider points A and M in the critical surface, at positions exactly above an atom and exactly above the position half-way between atoms, as shown in Fig.(2.1). The ratio R of the ionization densities dJ/dV is given by

$$R = (dJ/dV)_A/(dJ/dV)_M = (C_A/C_M) \times (P_{eA}/P_{eM}) \quad \ldots\ldots 2.4$$

So a question arises as to which factor is responsible for the origin of contrast. Forbes (private communication) argues that for atoms in a close-packed plane to be resolved R must be greater than about 1.3. In consequence, if one of the ratios on the r.h.s. is dominant, then this factor must vary by 1.3 as between A and M.

The geometry of the tip surface has a great effect on image formation and on contrast at specific regions. This is because it decides which atom or group of atoms is relatively more protruding and thus at relatively higher field. The relationship between surface geometry and field-ion image contrast is demonstrated by Moore's[27] computer simulation of a structured surface. However, at a more basic theoretical level the question is "how does the surface structure and/or the high field affect the quantities C and P_e?"

For sometime, following Muller's[21] original idea, most of the work done in this field assumed that the dominant factor affecting image contrast was the local variation in the electron-transition rate-constant (i.e. the rate-constant in eq.(2.4)). Knor[22], for example, suggested that there is an enhancement in electron tunnelling in the direction of extending unoccupied bonding orbitals of kink site atoms. Enhanced image brightness in corresponding areas of field-ion images is observed. But there is no reliable calculation to prove that the rate-constant is the dominant factor generally. In particular, Iwassaki and Nakamura[28] found that, if the surface were bare, then they were unable to prove that the rate-constant P_e was higher at point A (above an atom) than at point M (between atoms). They also found, in common with Nolan and Herman[30], that the adsorption of an intermediate helium atom caused a reduction in the electron transition rate-constant; this result is not helpful to a rate-constant explanation of image-contrast.

On the other hand, Forbes[25, 26] put forward a hypothesis that is simplified into a "provisional working rule", suggesting that: "Image appearance is largely determined by the statistics of gas distribution. The overall current generated above an area of surface is primarily determined by supply-and-capture considerations, that is by the number of atoms per unit time that finish or tend to finish accommodation within the area. The distribution of current generated across individual small areas of surface is likely to be significantly affected by gas distribution processes that occur after or near the end of accommodation, these tending to set up local Maxwell-Boltzmann concentration equilibria." Forbes' hypothesis is that the dominant factor in image contrast is due to the gas-concentration factor. The possible significance of the gas-concentration factor was shown in the following argument.

If thermodynamic equilibrium exists, the gas-concentration factor

can be described by the Boltzmann equation[31]:

$$C \propto \exp -U/kT \qquad \ldots\ldots 2.5$$

$$\text{where } U = \tfrac{1}{2} b_A F^2 \qquad \ldots\ldots 2.6$$

U being the gas-atom potential energy, b_A is the polarizibility of the imaging gas atom, and F is the local field.

Applying eq.(2.6) to points A and M gives:

$$C_A/C_M = \exp\left[(\tfrac{1}{2} b_A F^2/kT).(2\delta F/F)\right] \qquad \ldots\ldots 2.7$$

T in these equations is the temperature of the imaging gas. Working out the ratio C_A/C_M for 1% field strength difference at an average field of 45 V/nm then gives (if δF is the field difference) the following results

Temp	C_A/C_M
80K	1.5
20K	5.4
5K	830

Values of C_A/C_M of this size are adequate to explain image contrast. However, it is clear that cryogenic tip temperatures are necessary to cool the imaging gas[32, 33]. Accommodation reduces the large lateral velocity they initially have (as a result of the dipole attractive potential).

The use of cryogenic tip temperatures also increases the probability that incoming atoms will be "captured" by the tip, and reduces the number of "hops" made before trapping occurs into a particular region of the emitter.

There is some evidence[34, 35, 36] that the ionized imaging-gas atoms are not in thermodynamic equilibrium with the emitter tip, and it is convenient to replace T in eq.(2.5) by the effective temperature

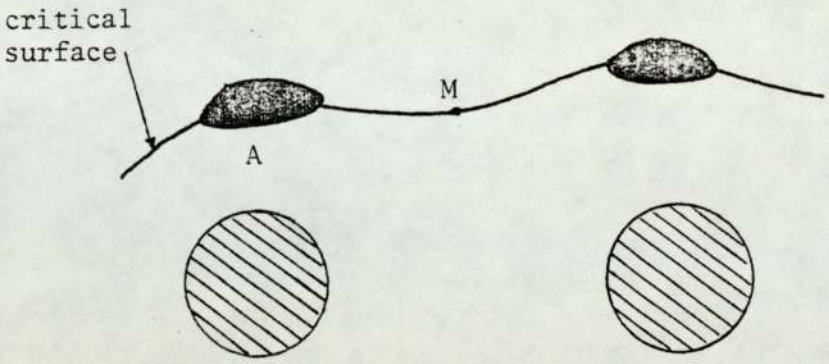

Fig.2.1

A schematic diagram of the critical surface above two adjacent substrate atoms showing point A and M

Fig.2.2

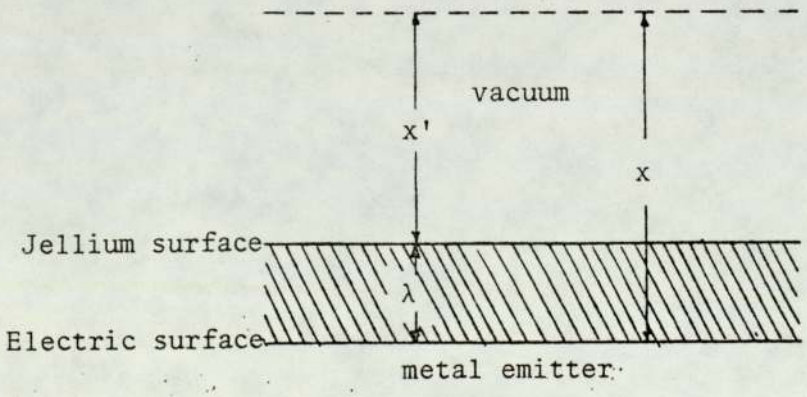

To illustrate the relationship between the jellium surface and the electrical surface

T_{eff}. Ref.(31) suggests that T_{eff} is between 4 to 7 times the emitter temperature.

2.2.2 The effects of Field Adsorption

Although the temperatures are probably low enough to explain image resolution, the question arises: "What is the field variation in the critical surface?" A rough calculation by Forbes[37] suggested that for a bare surface the field variation would be substantially less than 1%. Hence for a bare surface the gas-concentration hypothesis would not explain image contrast.

A solution may lie in the effect of field adsorption on the image formation process. The theoretical explanation of how exactly that happens has not yet been resolved. The first explanation by Muller & Co - workers[8] was that the adsorbed noble gas atoms provide an intermediate collision medium for transferring the dipole energy of the imaging gas atoms to the metal substrate, so accommodation requires fewer hops because of the greater efficiency of energy exchange of equal (or approximately equal) interacting masses. Then we should expect that He adsorption promotes imaging better than Ne adsorption. But this contradicts the fact that the adsorption of Ne is a better image promoter than the He[38].

Another suggestion by Muller[10, 38], but not proved, is that during the ionization process the tunnelling electrons prefer to choose the shortest distance, so they prefer to tunnel through adsorbed atoms. Since Ne is a bigger atom than He there is a smaller gap between Ne and the critical surface, so tunnelling is more efficient than with He.

Theoretical quantum mechanical calculation of tunnelling through an adsorbed noble gas atom have been made by Nolan and Herman[30] using the time dependent perturbation theory, including exchange effects. They

obtained enhancement factors of 3 to 5 for He adsorbate and 30 to 90 for Ne adsorbate. But when they included polarization they obtained an enhancement factor of 0.4 to 1 for He, 2 to 10 for Ne. This reduction in ionization rate-constant due to the adsorption was shown again in the work of Iwassaki and Nakamura[28].

On the other hand, Forbes' "gas concentration" hypothesis could still explain the effect of field adsorption on imaging process, if adsorption led to greater field variation in the critical surface.

Rendulic and Krautz[39] tried to bridge the gap between the two hypotheses by the hypothesis of a "second adsorbed layer". They argue that a second adsorbed atom on the top of the first one can still possess some binding energy (i.e. his calculation gives B.E$\sim$ 0.02 ev for He). As this is small, it cannot bind the second He atom permanently, but can certainly bind it long enough to increase enormously the probability of ionization (as a result of the increased dwelling time).

Rendulic and Krautz hypothesis assumes a complete accommodation of the gas atoms to the tip temperature. In fact, accommodation is not complete[29, 35]. But the author feels that Rendulic and Krautz hypothesis is broadly equivalent to Forbes' hypothesis, since instead of dealing with many mobile gas atoms in the right position to be ionized (i.e. Forbes' hypothesis of gas concentration), Rendulic and Krautz hypothesis deals with a single second layer atom staying long enough to be ionized.

2.3 Field Adsorption

2.3.1 Field Adsorption and the dipole - dipole interaction

In the early days of Field Ion Microscopy, an emitter surface subjected to high positive electric field (i.e. between 40 to 60 V/nm) was believed to be atomically clean, despite the presence of about 1 mTorr

of inert imaging gas.

The weak binding energy due to London dispersion forces[40] (approximately 10 meV) is incapable of adsorbing inert-gas atoms permanently on the surface, because it is comparable with the thermal vibrational energy of adsorbed atoms, even at liquid-nitrogen temperature ($k \times 80K \simeq 7$ meV). The induced long-range polarization potential, due to the presence of high field around the emitter tip, was held to cause a hopping motion of imaging-gas atoms, rather than permanent adsorption[41].

The first experimental indication of field adsorption was promotion of helium ionization when it is used as imaging gas, by introducing a small quantity of hydrogen. This was explained as due to the invisible adsorption of hydrogen between the widely spaced atoms of the emitter surface[42].

An observed improvement of imaging conditions by adding a small quantity of neon to the helium[41] was assumed to be due to the enhanced thermal accommodation of the hopping helium atoms when they collide with temporarily adsorbed neon atoms rather than heavier metal atoms. The invention of the atom-probe provided the first real evidence of helium field adsorption; in 1969 Müller[43] noticed complex helium ions and molecular ions containing helium coming off the emitter surface after the application of a desorption pulse. Ions such as W He^{+++}, were observed, and the argument was that such ions could not be formed in the gas phase, so the helium must physically have been present at the surface in the first place.

The first published theory of field adsorption was put forward by Müller and Tsong[14] in 1970. They suggested that adsorption results from a short-range field-induced dipole - dipole interaction, which drastically modifies the electric field in the vicinity of the kink-site metal surface atom. They suggested that there was a field-induced short-range binding energy ΔB(conv.) at a binding site above a kink-site atom, given by:

$$\Delta B \text{ (conv.)} = \tfrac{1}{2} b_A (f_A - 1)(F^{ext})^2 \qquad \ldots\ldots 2.8$$

where b_A is the polarizability of the inert gas atom;

f_A is an enhancement factor due to field induced dipole - dipole interaction;

F^{ext} is the "applied" or "external" electric field.

The enhancement factor f_A is obtained from:

$$f_A^{\frac{1}{2}} = [1 + 2b_E/4\pi\varepsilon_o S^3]/[1 - 4b_A b_E/(4\pi\varepsilon_o S^3)^2] \qquad \ldots\ldots 2.9$$

where b_E is the polarizability of the metal emitter surface atom; ε_o is the electric constant; and S is the separation of the emitter and adsorbate atoms.

(In writing down these formulae, we have converted the formulae originally given into an SI form, and have used our own notation rather than that of the original papers).

Using simple calculations, Müller and Tsong[14] found that the binding energy was largest when the inert-gas atom is situated at the apex of a surface metal atom, and suggested that field adsorption occurs at the apex of the metal surface atoms rather than at the inter-atom position as is the case for ordinary adsorption (i.e. if there is no applied field).

The repulsive potential between neighbouring field-adsorbed atoms was found to be of the order of 0.01 eV, and turned out to be negligible compared to a ten times or more dipole - dipole interaction. Short-range binding energies calculated by Tsong and Müller[14], directly above kink-site atoms on a tungsten (110) plane, at the best imaging voltage F_{BIV}, were found to be: 0.13 eV for a He atom at F_{BIV} = 45 V/nm; 0.14 eV for a Ne atom at F_{BIV} = 37.5 V/nm; and 0.15 eV for A_r atom at F_{BIV} = 22 V/nm.

Later, Tsong and Müller[15], by examining statistical considerations and expressing the probability of adsorption in terms of experimental

parameters available using the atom-probe, showed the dependance of adsorption probability on temperature and field, and thence experimentally inferred the short-range binding energy to be 0.23 eV for He on W(114) at a holding field of F = 49 V/nm, and to be 0.28 eV for Ne on W(322) at a holding field F = 50 V/nm.

Simultaneously, Forbes[18] suggested an alternative mechanism to explain field adsorption. He represented the charged metal surface by discrete positive charges, and calculated the short-range adsorption binding energy of He on W to be of the order of 0.1 eV. This may not be large enough by itself to explain the adsorption phenomenon, but there is also doubt as to the validity of the method used.

These arguments seemed to demonstrate the existence and the theoretical plausibility of field adsorption. Field adsorption was also believed to enhance the local image contrast significantly, either by enhancing the ionization rate-constant as argued by Tsong and Müller[14], or by enhancing the field variation above the tip surface, and hence enhancing the gas-concentration variation as argued by Forbes[37].

The point that the enhanced field variation could be the cause of image contrast effects was made earlier by Forbes[44]. To explain the hopping bright spots[45, 46, 47, 48] appearing when introducing a small quantity of a heavier inert gas (like Ne) to the chamber containing the lighter imaging gas atoms (He usually), we could assume that Ne atoms replace adsorbed He atoms, and so enhance the field even more, and hence enhance the gas-concentration above them. In consequence, the neon atoms enhance the local ion current J, which gives brighter image spots. A similar effect would of course be achieved if the adsorbed atom enhanced the ionization rate-constant[47, 49].

It has been assumed in the above disussion that helium atoms are adsorbed as neutrals. An alternative suggestion was put forward by

Röllgen and Beckey[50], that helium and other inert gas atoms are adsorbed on surface as ions. But it seems to be a very remote possibility that there would be sufficient field penetration into the metal for the ionic state to become the ground state for these adsorbed imaging gas atoms[51], certainly for the lighter atoms.

2.3.2 Models of Field Adsorption

As explained above, Tsong and Müller[14] based their calculation on the interaction of two parallel dipoles representing a single emitter atom and adsorbed inert-gas atom in an applied electric field F^{ext}; this model was later called by Forbes the "isolated-dipole pair (IDP)" model. This is represented mathematically by equations (2.8) and (2.9).

Tsong[52] later attempted to develop the (IDP) model to deal with the case of adsorbed atom (represented by single dipole) sitting on a substrate of metal surface atoms, represented by an array of dipoles. This model was based on a new analysis of the field-induced dipole - dipole interaction between two atoms. Equation (7) in ref. (52), when expressed in scalar form, implies that the short-range interaction energy $\Delta\varepsilon$ between two dipoles is:

$$\Delta\varepsilon = 2\, P_E\,(ad)\, P_A\,(ad)/4\pi\varepsilon_o S^3 \qquad \ldots\ldots\ 2.10$$

where P_E (ad) and P_A (ad) are the SI dipole moments of the emitter atom and the adsorbate atom in the "as adsorbed" state, and S is the separation between the dipoles.

However, the above Tsong formula was contested by Forbes[53] for two reasons. First, on grounds of classical electrostatics: for polarizable dipoles the full expression for the short-range interaction energy should be:

$$\Delta\varepsilon = \left[P_A\,(ad) - P_A\,(ext) + P_E\,(ad) - P_E\,(ext)\right] F^{ext} +$$

$$2\,P_A\,(ad)\,P_E\,(ad)/4\pi\varepsilon_o\,S^3 \qquad \ldots\ldots\ 2.11$$

Obviously, Tsong's formula (eq. 2.10) ignores the first term of (eq. 2.11). Second, Tsong implicitly identifies the electrostatic interaction between classical dipoles ($\Delta\varepsilon$), with the field-induced binding energy component ΔB^{el}. This is true in the case of atoms with permanent dipole moments, but not true in the case of polarizable atoms, since part of the interacting energy is converted into internal electronic energy as given by the following equation:

$$\Delta B^{el} = \Delta\varepsilon - \Delta V \qquad \ldots\ldots\ 2.12a$$

where ΔV is the increase in internal electronic energy.

Forbes also argued[53] that there is a fault in the conventional[14,15] treatment of the (IDP) approximation, in that the "change (ΔU_s) in the internal energy of the source of the field acting on the adsorbate atom" has not been taken into account. Thus the electric component (ΔB^{el}) of the binding energy is related to the conventional expression ΔB(conv.) by:

$$\Delta B^{el} = \Delta B(conv.) - \Delta U_s \qquad \ldots\ldots\ 2.12b$$

In the IDP approximation, this correction is of the order of 5 - 10%.

In an attempt to bridge the ideas of Müller and Tsong on the one hand, and Forbes on the other, Rendulic and Krautz[39] argued that there exists a second mobile layer of adsorbed atoms on top of the first fixed layer of adsorbed atoms. These second-layer atoms have a high probability of ionization. To estimate the binding energy they extended the (IDP) model to include a second adsorbed atom on top of the first one. Calculated binding energies for helium in a field of 45 V/nm were about 0.02 eV.

All the above models are based on the interactions of pairs of atoms.

This type of model may be appropriate for a kink-site, but looks inappropriate for a crystallographic plane; array models seem likely to be better.

Attempts to calculate fields above a finite square array were made by Forbes[37] and by the present author[54]. These showed the existance of effects due to the finite size of the array, and suggested the use of infinite arrays, and hence the topic of this thesis. The first published discussion of the infinite array situation, however, is that of Tsong[52]. As a result of the work described in this thesis, deficiencies in this are now known to exist, and are discussed in chapters 6 and 7.

2.3.3 Summary

To conclude this section, we restate the main physical points concerning field adsorption. Field adsorption is an interaction that occurs between strongly positively charged metal surfaces and inert gas atoms. The adsorbed gas atom is bound to the apex of the metal surface atom because the binding energy maximises above the metal surface atoms, rather than inbetween them (as is the case in the absence of the field). Field adsorption differs from ordinary physisorption and chemisorption in that:

(1) the short-range binding energy is much larger than that due to dispersive forces (i.e. ten times or more);

(2) the nature of the short-range bonding energy is physical (i.e. mainly dipole - dipole interaction) rather than chemical (i.e. ionic or covalent bond). There is also a strong belief that field adsorption is the major factor in forming the image contrast in the FIM.

2.4 Charged Metal Surface Theory

2.4.1 Jellium-type models

All inter-atomic forces and metal surface forces originate from the electro-magnetic interactions of the nuclei and electrons comprising the system. The quantitative description of these forces (and of the charge distribution at the metal-vacuum surface), needs the use of quantum mechanical principles, and calculations must in principle be based on the mutual interactions of all entities making up the system. In practice, this task is too difficult to carry out. Even very limited attempts, like finding a formula for the charge distribution of a model of a 6 x 6 hydrogen-atom-like surface[55] by quantum-mechanical means, face so many complications that it is very difficult to find.

Convenient simplification and approximation, with the help of a suitable metal surface model (which may not necessarily represent reality well), have been most useful in investigating many problems. Surface forces have been treated implicitly in what we may call "Surface charge theory". The formalization of this theory started by the early work of Frenkel[56], who treated the surface problem from the standpoint of Thomas Fermi theory[57]. In this, free electrons at a metal surface were treated as a classical liquid; the electron density n(r) plays a central role.

This was followed by an important self-consistent work by Bardeen[5] on sodium. He formulated the base of the very widely used "Jellium" Surface model of the metal. In this the positive nuclear charges of the atoms are supposed to be smeared together, to form a rigid positively charged background (i.e. homogeneous positive charge at all $x' \leq 0$, where $x' = 0$ marks the surface). The electrons are assumed to spread out above

the background as a cloud, and the whole sum of positive and negative charges is zero. This picture of a metal surface was useful in calculating the work function, as the sum of two main contributions: the binding energy of electrons due to a volume (or "bulk") contribution; and the electrostatic energy required to move an electron through the electrostatic surface double layer. This included an attempt by Bardeen to include the effect of correlation (polarization).

During the following three decades, there was very little interest in tackling the problem of the metal surface[2]. One paper of particular interest was by Smoluchowski[58], who suggested that the variation in work function of tungsten as between different faces is due to the variation in the contribution of the double layer. Working on a surface model using S-polyhedra, he showed that there are two effects tending to cancel each other. The first is a smoothing of electron charges by moving between surface lattice cores; the second is due to the partial spreading of electron charges outwards towards the vacuum. These effects are responsible for the variations in work function.

Interest in surface theory revived in the early sixties. In particular, Kohn and colleagues[59, 60, 61] worked on the construction of a form of surface theory that was designed to deal with a system where the electron density was inhomogeneous and slowly varying, and to include the effects of exchange and correlation. As described below, this system was subsequently developed to deal with the existence of a weak external field.

2.4.2 Charged Surfaces and the Jellium model

With a neutral surface, the main objective of jellium-based calculations was to obtain values for quantities such as the work-function. At a charged surface a new problem arises: where is the "effective electrical

surface" of the metal? - i.e. the surface defined in such a fashion that (at large distances x from the surface) the electrostatic energy v of an electron is given by

$$v = eFx \qquad \ldots\ldots 2.13$$

where e is the elementary charge and F is the external field.

This problem is often discussed in terms of (so-called) "field penetration". Distance x measured from the electrical surface is related to distance x' measured from the jellium surface (see fig.2.2) by:

$$x = x' + \lambda \qquad \ldots\ldots 2.14$$

Thus v is given by:

$$v = eF(x' + \lambda) \qquad \ldots\ldots 2.15$$

The parameter λ is called the "effective field penetration length".

The determination of field penetration length is vital in studies of FIM, particularly those concerning ionic adsorption binding energy, field evaporation, and field ionization, because this length λ is not small compared with the distance of the adsorbed atom from the "surface" or the critical distance of field ionization x_c (inside which no auto-ionization could happen). For example, Müller calculates[7] x_c for Helium on tungsten as 0.45 nm and estimates λ as 0.05 nm.

The problem of field penetration length has been approached in various ways. It was first investigated by Rice[62], who assumed that the electrons were confined behind the jellium surface, and used degenerate Fermi statistics. Another approach[63] simply considers an exponential decay of field inside the metal surface. Gomer and Swanson[64] introduced the idea of field penetration length in their theory of field desorption.

Tsong and Müller[65] describe the field penetration effect in terms

of a change in work function, but follow in the footsteps of Rice by treating the metal surface electrons as a degenerate Fermi gas confined behind the jellium surface. The effect of a weak electric field was calculated by solving Poisson's equation with a suitable boundary condition. They estimate λ to be in the range 0.021to 0.1 nm.

Lang and Kohn[66] continued the development of metal surface theory in an important piece of work, by producing a profile of the surface charge induced in the presence of a weak external field. They apply a linear response formalism to the electron motion, the electrons being allowed to "spread" outside the jellium surface. They find that:

(1) The centre of mass of the induced charge is outside the jellium surface, by a distance that is independent of field but depends on the metal electron density. (Typical values lie in the range 0.06 to 0.08 nm).

(2) In the limit of large distances, the electrostatic potential energy of a point charge is proportional to distance measured from this centre of mass, and the correlation potential energy is given by the image potential, with distance measured from this centre of mass. Lang and Kohn call the plane passing through the centre of mass the "effective metal surface", but clearly it may be identified with the "metal's electrical surface", as defined here. Lang and Kohn also find that:-

(3) The classical turning point for electrons is outside the electrical surface, by a small distance (about 0.04 nm).

The significance of this result will become clear later.

An alternative approach to the charged surface problem was formulated by Theophilou and Modinos[67]. This was based on an approximately self-consistent calculation, that avoids any abrupt boundary condition at

$x' = 0$ (i.e. at the jellium surface). In contradiction to Tsong and Müller, and Lang and Kohn, Theophilou and Modinos find that the metal's electrical surface has a position that varies with the field strength, and may be inside or outside the jellium surface.

Thus at the present time, jellium models do not give a clear picture of "field penetration". The parameter λ as defined in eq.(2.14) may be positive, may be negative, and may or may not be independent of field - depending on what theoretical assumptions are made.

Apart from the above difficulties, use of a jellium-type model in the context of field-ion emission is problematical because it ignores the facts that a real surface is structured, and that this atomic structure is observed in a field-ion microscope. In a sense, there has always been a double standard in the theory of field-ion emission. In considering some physical phenomena (e.g. field evaporation) an unstructured jellium-type model has been used; but to discuss other problems (in particular field adsorption) structured models are employed. The merit of the self-consistent model originated by Forbes[68] and developed by the present author, that is described in the next two chapters, is that both types of problem can be dealt with in a unified treatment.

CHAPTER 3

DEVELOPMENT OF NEW THEORY

3.1 Objectives

As became clear in chapter 2, the consequence of the invention of the field-ion microscope in many ways demanded a new look at many theoretical aspects of charged metal surfaces, the imaging process, and field adsorption. However, existing treatments have been found not clear enough, not self-consistent and even not correct in many aspects of the theory and its applications, in our view. We think that by setting up the foundations of a new self-consistent theory, and by clarifying some past concepts, we can make a useful contribution to this field, that could pave the way to further steps.

In this chapter, we deal generally with conceptual aspects, leaving the algebraic aspects to the next chapter. We start by summarising the evidence that now exists concerning field adsorption, and go on to discuss a new charged surface model and develop a new treatment of field adsorption in sec.3.3. This leads on to careful definitions of field and polarizability in sec.3.4, 3.5 and 3.6. The concept polarizability has been a source of much confusion, and we devote particular attention to this in sec.3.5. Finally, a simple discussion of the binding energy and the effect on it of the repulsive forces is described in sec.3.7.

Much of the work in this chapter has been carried out and developed jointly with Dr. R.G. Forbes.

3.2 Evidence of field adsorption and the concept of binding energy

As already stated, the existence of field adsorption was first inferred experimentally by Müller[43] when metal-helium complex ions were detected by the atom-probe. Other experimental evidence came from imaging in a mixture of gases[45, 46, 47, 48], in the "hopping bright spot" phenomenon. But the strongest evidence probably comes from the measurement of field-ion energy distributions[69, 70, 71]. It is noticed that, when a second-species gas such as hydrogen is present the field-ion spectrum from helium contains a main peak (corresponding to ionization near the critical surface), and a low-deficit subsidiary peak corresponding to the energetic ions. The analysis of this subsidiary peak shows that those ions could only come from a field-adsorption site within the forbidden zone, and presumably result from the excitation by the impact of electrons from the second-species gas atoms.

All the above evidence leads to a strong belief that, at high fields as used in FIM, there exists a layer (or partial layer) of adsorbed inert gas atoms at the emitter surface. And theory suggests that each one of those atoms is strongly bonded to the apex of one of the metal surface atoms (see section 2.3 for details). There is almost total consensus as to the short-range nature of the binding process.

We may define the field-adsorption short-range binding energy ΔB as "the energy required (or work done) to remove an adsorbed atom from its adsorption site to a position in the external field F^{ext}." The total binding energy B of an individual field-adsorbed atom is the work needed to remove this atom to remote field-free space. This work can be split into two parts: a long-range part (i.e. $\frac{1}{2} b_A.(F^{ext})^2$), equal to the electric-field-induced binding energy of an isolated imaging gas atom in

the (approximately uniform) external field, acting somewhat above the surface; and the short-range part ΔB. The total binding energy at a specific bonding site above the emitter surface can thus be written as:

$$B = \tfrac{1}{2} b_A (F^{ext})^2 + \Delta B \qquad \ldots\ldots 3.1$$

where b_A (as before) is the SI polarizability of the adsorbate atom.

There are components in ΔB resulting from the different types of interaction between the field-adsorbed atom and its surroundings. These are:-

(1) London dispersion forces between atom and substrate[40];

(2) Repulsive "interpenetration" forces between atom and substrate[40];

(3) Lateral forces due to the above causes;

(4) "Indirect" lateral forces, mediated via the substrate[73];

(5) Field-induced forces.

Thus we may write:-

$$\Delta B = \Delta B^{disp} + \Delta B^{rep} + \Delta B^{lat} + \Delta B^{indir} + \Delta B^{elec} \qquad \ldots\ldots 3.2$$

The nature and sizes of the first four types of force will be discussed in more detail later. But in the context of field adsorption the dominant component is the electric-field-induced part (ΔB^{elec}).

Most attempts to calculate ΔB^{elec} have equated it with the "conventional" expression for binding energy, $\Delta B(conv.)$ given by:

$$\Delta B(conv.) = \tfrac{1}{2} b_A (F_A^{loc})^2 - \tfrac{1}{2} b_A (F^{ext})^2$$

$$= \tfrac{1}{2} b_A (\beta_A^2 - 1)(F^{ext})^2 \qquad \ldots\ldots 3.3$$

where F_A^{loc} is the self-consistent local field acting on the adsorbate

atom at the adsorption site, and β_A is the field ratio:

$$\beta_A = F_A^{loc}/F^{ext} \qquad \ldots\ldots 3.4$$

β_A^2 is sometimes written f_A, as in eq.2.8.

Forbes[53] has recently pointed out that the conventional conceptual treatment of field adsorption ignores an induced change in the internal energy of the source of electric field. A change ΔU_s is induced by the removal of the adsorbate atoms and consequently:

$$\Delta B^{elec} = \Delta B(conv) - \Delta U_s \qquad \ldots\ldots 3.5$$

The ΔU_s contribution is of the order of 5% for the IDP model for the He/W system[53], and is assumed to be of similar order for more complex systems.

At this point it should be made clear that the values calculated for ΔB and ΔB^{elec} will depend on the nature of the removal process involved. It would be possible to consider a process in which a complete layer of adsorbed atoms is: (a) removed <u>as a whole</u> from the surface into a region of space where the applied field is F^{ext} but atom-surface interactions are negligibly small; (b) dispersed laterally until atom-atom interactions are negligibly small. This process would define mean (or <u>integral</u>) values of short-range binding energy and ΔU_s.

But of more interest in the field-ion situation is the work needed to remove a <u>single</u> atom from the field-adsorbed layer to a position in the external field, with the other atoms remaining in their places in the layer. This process defines "<u>differential</u>" values of short-range binding energies and ΔU_s, and can also be seen as the work needed to create a <u>vacancy</u> in the field-adsorbed layer. In what follows we shall assume that ΔU_s and all ΔB-type symbols refer to this "differential" or vacancy-creation-type removal process.

In this context Forbes (private communication) has very recently proposed a generalised interpretation of eq.3.5. He argues as follows: "ΔB^{elec} is difficult to calculate because creating the vacancy reduces the symmetry of the situation and causes changes in the induced dipole moments in the vicinity of the vacancy. It is much easier to treat the situation in which the dipole moments of all the emitter and adsorbate-layer atoms (other than that of the vacancy-site atom) are taken as "frozen" at their complete-layer values during the removal process: the work relevant to this removal process may be denoted by $\Delta B(main)$. If the frozen moments are then allowed to relax, there is a change ΔU_s in the potential energy of the system. To obtain ΔB^{elec}, this quantity ΔU_s must be subtracted from $\Delta B(main)$."

The advantage of this interpretation of eq.3.5 is that the two terms in it both have physical rather than algebraic definitions. Forbes then argues that, strictly, $\Delta B(conv)$ as defined by eq.3.3 and $\Delta B(main)$ are not identical: "In principle $\Delta B(main)$ is obtained from the formula for the potential energy $U_{isol}(F)$ of an isolated atom in a field F, as

$$\Delta B(main) = U_{isol}(F^{ext}) - U_{isol}(F_A^{loc}) \qquad \ldots\ldots 3.6$$

This quantity $U_{isol}(F)$ is given by

$$U_{isol} = -\tfrac{1}{2} b_A F^2 - (\text{higher terms})$$

where the higher terms relate to hyperpolarizabilities and field-gradient polarizabilities[74] of the imaging-gas atom. Thus, in reality:

$$\Delta B^{elec} = \Delta B(main) - \Delta U_s \qquad \ldots\ldots 3.7$$

$$\Delta B(main) = \Delta B(conv) + (\text{higher terms}) \qquad \ldots\ldots 3.8$$

So $\Delta B(conv)$ as defined by eq.3.5 is, in the generalised interpretation of

eq.3.8, only the lowest in a series of terms that appear in ΔB(main) and hence should appear in ΔB^{elec}."

This generalised interpretation is of very recent origin, so we shall ignore the "higher terms" in eq.3.8 in the main part of this thesis, returning to consider them (in chapter 6) as a correction to our results. We thus concentrate on ΔB(conv).

To calculate ΔB(conv) we need a value for β_A, the field ratio at an adsorption site. And to derive this we need a specific model for a structured surface.

3.3 The "monopole-dipole" surface model

To avoid many difficulties arising from the jellium model, and from other inconsistent treatments of the metal surface, as described in chapter 2, Forbes[68] has suggested an alternative charged metal surface model.

This consists of a regular infinite planar array of superimposed dipoles and point positive charges (monopoles), together with a distant parallel array of charges of opposite polarity as shown in Fig(3.1). This model has been adopted in this thesis because we believe that the jellium model cannot any more represent an acceptable basis for the FIM theory, and that this alternative model can be a first step towards developing a more sophisticated quantum - mechanical model in the future.

The use of dipoles in the charged-surface model is simply an extension, to the infinite-planar-array situation, of their use in the IDP model. The introduction of monopoles perhaps needs some explanation.

Forbes argues that Müller and Tsong in their hypothesis of field adsorption did not explain the source of the external field (what they call the applied field). He thought of the external field as a logical consequence of an excess positive charge at the metal surface. The excess

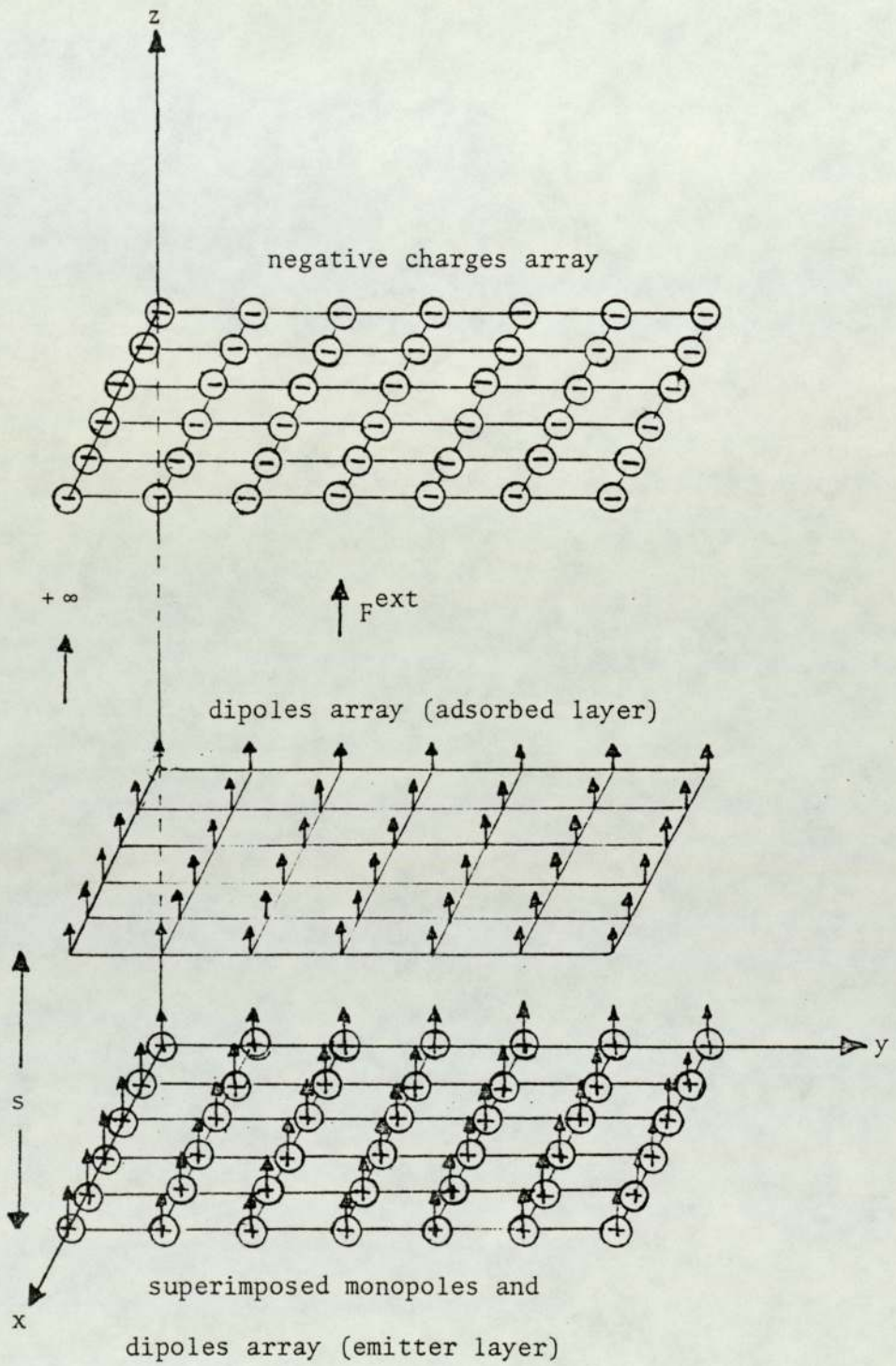

Fig.3.1

A schematic diagram of the monopole-dipole metal surface model

positive charge is due to the removal of some electrons from the metal surface. In reality the excess positive charge must be localized in a small volume surrounding the mean position of the nuclei of the metal surface atoms, and can be approximated by point charges. This model is applied to an infinite surface plane of a single crystal, so that the whole picture at this stage will look like an infinite planar array of positive point charges.

The assumption of an infinite array, though unrealistic, is necessary as a first approximation, and to overcome any unnecessary difficulties due to the edges effect and to unsymmetrical field and potential contributions[54].

For electrostatic self-consistency, the withdrawn electrons have to be placed in a capacitor configuration with the excess positive charge (i.e. the quantity of the negative charge on the "distant" plane shown in Fig(3.1) is equal to that of the positive excess charge). The argument is valid even when the negative charges array is at infinity.

If the excess positive charge is averaged, so that there is a charge quantity σ per unit area, then by applying Gauss' theorem the external field (well above the charged surface) is given by:

$$F^{ext} = \sigma/\varepsilon_o \qquad \ldots\ldots 3.9$$

Each of the planar arrays contributes a field component of magnitude $\frac{1}{2}\,\sigma/\varepsilon_o$ (or $\frac{1}{2}\,F^{ext}$). They add in the middle to give F^{ext}, but cancel each other outside the planes, as shown overleaf.

Forbes then argues that, in reality, at a charged metal surface, the electron distribution around each surface atom is not spherically symmetric. The true charge distribution at a structured surface is not known, but as a first approximation it can be represented by an array of dipoles superimposed on the array of point positive charges. (The need to include the dipole array was demonstrated in Ref.(68), where it was shown that binding energies calculated on the basis of a monopole array alone were not high enough to explain the existence of field adsorption).

The adsorbed inert gas atoms are also represented in the model by an array of dipoles. Each of those dipoles is positioned directly above a corresponding metal surface dipole.

The question then arises as to what strengths should be allocated to the dipoles. This leads on to questions concerning the definitions of fields and polarizabilities, which we now consider.

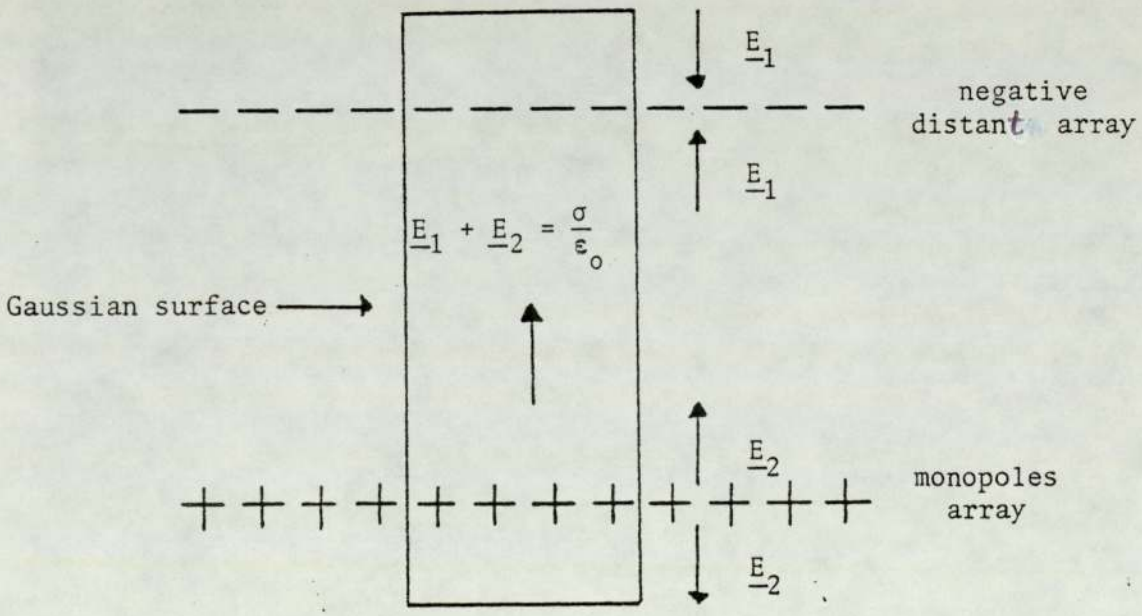

3.4 The electric field

Failure to distinguish between the self-consistent local field (F^{loc}), and the external field (F^{ext}) may lead to great error in the evaluation of the binding energy at a metal surface, since F^{loc} can be greater or less than F^{ext}.

An electric field can be produced either by applying a voltage to the emitter surface, which produces an excess charge, or/and by introducing a finite charge or dipole above the emitter surface, which induces a change in the charge distribution at the surface. The sum of the field created by the induction effect, and the original local applied field is called the self-consistent local field. This is defined by Forbes[53] as the "field that would act at the position of the nucleus of the atom, in the absence of the atom itself, but in the presence of any effects induced by the atom when itself present." The external field (F^{ext}) is the field that exists somewhat above the charged emitter surface, at a position where effects due to localisation of charge in the surface are negligible. F^{ext} can be evaluated by applying equation 3.9.

3.5 Polarizability

One of the largest confusions in the FIM literature is over the polarizability factor. Though this sub-section cannot be a perfect account of the main defaults associated with this term, it is hoped to be able to clarify much of the confusion, and to define the polarizability in a self-consistent manner.

The first three sub-sections are devoted to basic definitions and units concerning "proper SI polarizability", and this is followed by sub-sections discussing other quantities that have been called "polarizability" or "effective polarizability". We then discuss the conventional estimates

of surface-atom polarizability, and the defects of these. And finally we discuss better ways of estimating polarizability.

3.5.1 Basic definition

Strictly, polarizability is a term associated with the polarization of the positive and negative charge distribution of an atom or molecule, under the effect of an electric field. The polarizability b is given by:

$$p^{tot} = \mu + bF^{loc} + \text{higher terms} \quad \ldots\ldots 3.10$$

where p^{tot} is the total SI local dipole moment

b is the "proper" S I polarizability

μ is the SI dipole moment that would exist under the condition of zero local field.

The higher terms are terms associated with hyperpolarizabilities and field-gradient polarizabilities[73], and can be ignored as a first approximation. However, in field adsorption these terms cannot really be ignored, and we return to this point later.

3.5.2 Units of Polarizability

The SI unit for polarizability is C V^{-1} m^2 or J V^{-2} m^2. This is most easily seen from the binding-energy expression

$$U = -\tfrac{1}{2} b (F^{loc})^2 \quad \ldots\ldots 3.11$$

However, in the context of field-ion emission it is convenient to express energy U in eV and fields in V nm^{-1}. Thus a more convenient unit for polarizability is the eV V^{-2} nm^2, or the meV V^{-2} nm^2. These units have the same dimensions as the SI unit and the conversion factor is

$$1 \text{ meV } V^{-2} \text{ nm}^2 = 1.602189 \times 10^{-40} \text{ J } V^{-2} \text{ m}^2$$

3.5.3 SI Polarizability and Gaussian Polarizability

Equation 3.11 can also be written in the form :

$$U = -\tfrac{1}{2}(4\pi\varepsilon_o b_s)(F^{loc})^2 \qquad \ldots\ldots 3.12$$

where b_s ($= b/4\pi\varepsilon_o$) is the so-called "Gaussian polarizability" of the atom or molecule. The SI unit for Gaussian polarizability is m^3, but b_s is most commonly cited in $Å^3$. The numerical conversion factor between b and b_s is given by:

$$b/\text{meV V}^{-2}\text{ nm}^2 = 0.694456\ b_s/Å^3$$

It is to distinguish b from b_s that we call b the "SI polarizability".[75]

Most discussions of polarization in field-ion literature between 1960 and 1980 are in terms of a gaussian polarizability expressed in $Å^3$ and an SI field expressed in V/Å or V/nm. In effect a dimensionally-inconsistent equation, from which the $4\pi\varepsilon_o$ term has been omitted, has been used.

3.5.4 Polarizability and Polarization-energy coefficient

If we ignore μ and the higher terms in eq. 3.10 then this equation can be written in the form:

$$p = bF^{loc} = b\beta F^{ext} \qquad \ldots\ldots 3.13$$

where β is the field ratio F^{loc}/F^{ext}. Similarly, the polarization energy U is given by:

$$U = -\tfrac{1}{2}b(F^{loc})^2 = -\tfrac{1}{2}b\beta^2(F^{ext})^2 \qquad \ldots\ldots 3.14$$

Ignoring β in eq.3.13 and β^2 in eq.3.14 can lead to large error.

Forbes defines the "dipole-moment coefficient" g as:

$$g = \beta b \qquad \ldots\ldots 3.15$$

and the "polarization-energy coefficient" c as:

$$c = \beta^2 b \qquad \ldots\ldots 3.16$$

He further suggests (private communication) that in the literature the symbol α sometimes means $b/4\pi\varepsilon_o$, sometimes means $c/4\pi\varepsilon_o$ and may sometimes mean $g/4\pi\varepsilon_o$. This is why a new symbol (b) has been introduced for polarizability, to replace α, and why we call b the "proper SI polarisability".

3.5.5 The Polarization term in Field Evaporation

Muller[21] found it necessary to include a term in the evaporation activation energy equation, relating to the difference in the polarization of a neutral atom at the surface and that of the same atom when it becomes ionized during desorption. The polarization energy correction according to Muller in this case is given by:

$$U = \tfrac{1}{2}(\alpha_a - \alpha_i)(F^{ext})^2 \qquad \ldots\ldots 3.17$$

where α_a is the so-called "surface polarizability" of the neutral atom, and α_i is the so-called polarizability of the ion.

The idea of "surface polarizability" was introduced by Muller on the assumption that the metal surface atoms are partially immersed in the surface electron cloud. Hence α_a is different from the free space polarizability. Forbes (private communication) argues that this equation and approach need some correction, because it is assumed that both the atom and the ion are in the same environment field (F^{ext}); really one should consider the local fields at the position of the neutral atom, and at the position of the ion at the critical surface. He prefers to write the

polarization term in eq.3.17 in the form:

$$d_{eff} = (c_a - c_i) = (b_a\beta_a^2 - b_i\beta_i^2) \qquad \ldots\ldots 3.18$$

where β_a is the field ratio for the bonding site (atom present);

β_i is the field ratio for the critical surface (ion present);

d_{eff} is sometimes called "effective polarizability"

There is also a question as to whether b_a is the same for a (partially ionised) surface atom as it would be for the same atom (neutral) in free space. The present approach separates the issues of "what is β_a" and "what is b_a".

3.5.6 Charge-transfer Polarizability

In the preceding sections the terms "polarizability" and "polarization" have referred to the polarization of atomic orbitals. But these terms have also been used in literature[76] when an F^2 energy term arises in circumstances involving partial transfer of electron charge from a surface-adsorbed atom to the substrate. In these cases it is more appropriate to talk of "charge-transfer polarizability". The theory of charge-transfer polarizability has been reviewed by Tsong[52].

3.5.7 Effective Polarizability (Tsong and Muller, 1971)

Tsong and Muller[15] suggested that the apparent polarizability of an inert-gas atom close to a Tungsten surface would be less than the free-space value. By using a simplified quantum-mechanical method they derived an expression dependent on the penetration distance (λ) and the surface-to-adsorbate distance. Their argument is based on an assumed penetration of the electron charge clouds of the inert-gas atom inside the jellium surface, and there is doubt as to whether this is physically

reasonable.

3.5.8 Effective Polarizability (Forbes and Wafi, 1980)

Another use of the term "effective polarizability" is in connection with eq.3.10. For noble gases we may assume $\mu = 0$, but strictly we can not assume this for an emitter substrate atom. Within the framework of our metal surface model, this may be taken into account by substituting for the emitter-atom polarizability b_E an "effective" value $b_E(\text{eff})$ given by:

$$P_E^{tot} = b_E(\text{eff})\ F_E^{loc} = b_E(1 + \mu_E/b_E.F_E^{loc}) \qquad \ldots\ldots\ 3.19$$

where the term in brackets represents a correction factor. A reasonable estimation is that μ_E is of the order of 0.01 e.nm, and the correction factor can be up to (approximately) 1.3[77]. The size of the correction factor depends on the value of the local work function, and varies with the crystallographic orientation.

In practice, the error involved in using b_E rather than $b_E(\text{eff})$ is less than the uncertainty over the value of b_E itself, so it seems satisfactory to normally neglect the effects of any zero-field dipole moment. However, the correction is not really negligible and the figure here suggests that a more thorough treatment will eventually be required.

A similar approach in terms of an effective polarizability can in principle be used to deal with the "higher terms" in eq.3.10.

3.5.9 Conventional estimates of polarizability

There have been various attempts to estimate the "polarizability" of surface metal atoms. Within the framework of the jellium model, Muller (see Ref 7, p68) attempted to derive an expression for $c/4\pi\varepsilon_o$ by equating

the polarization energy of an atom to the polarization energy of the field, in the situation where field penetration occurs. But this treatment seems unconvincing.

The first experimental approach was to derive a value of $c/4\pi\varepsilon_o$ from measurement[78] of the field-sensitivity of evaporation rate-constant, assuming a charge-exchange mechanism of field evaporation. But Forbes[79] has shown that there is a mathematical flaw in the analysis of these measurements, and that the derived "polarizability" values are not valid.

An alternative approach[15] fitted a theoretical curve to an experimental field-adsorption isotherm, to give an adsorption binding energy, and then derived a gaussian polarizability $b/4\pi\varepsilon_o$ using the IDP model. This derivation is not valid because mutual depolarization of surface atoms has been neglected. Depolarization effects decrease the binding energy of the adsorbed atom to the surface, for a given assumed value of proper surface-atom polarizability, as will be seen later.

Yet another approach[76] was to derive a value of $c/4\pi\varepsilon_o$ from the average velocity of the directional walk of a tungsten adsorbed atom. $c/4\pi\varepsilon_o$ for a W adsorbed atom on W(110) plane was found to be 9.2 A^3, which is more than that obtained by field evaporation rate-constant experiments. However, the quantity derived from diffusion experiments is a charge-transfer polarizability, and it was suggested that this quantity is related to the electronic density of states of the adsorbed atom. This quantity is not necessarily relevant to a surface atom in a cystallographic plane.

Thus none of the conventional approaches provide a valid estimate of the proper polarizability of a surface metal atom.

3.5.10 Alternative Estimates of Polarizability

Theoretical estimates of the polarizabilities of various metal atoms

in free space were made by Thorhallson et al.[80], using a simple form of self-consistent-field quantum-mechanical calculation. Results in the units used here are tabulated in Ref.(75); for tungsten the value is 11.7 meV $V^{-2}nm^2$. In those cases where experimental data are available for comparison the Thorhallson et al values are approximately twice the experimental values, and this had led Miller and Bederson to suggest in their review[81] that all the Thorhallson et al. values should be "scaled" to give "best estimates" of free-space polarizability for materials where no experimental data is available for comparison. For tungsten this results in the value 7 meV $V^{-2}nm^2 \pm$ 50%. This value is somewhat higher than the polarizability values commonly stated in field-ion literature; we shall treat it as an upper limit for surface-atom polarizability.

Because a surface atom is in a different environment from an atom in free space, there is no good reason to suppose that the polarizabilities of a given species of atom in these two situations will be the same. No reliable theory relating the two polarizability values yet exists.

An alternative experimental method of determining a proper polarizability has recently been suggested by Forbes[82]. This is based on measurements of "anomalously low" helium ion energy deficits, carried out by Culbertson et al[71].

Ref.(82) shows that at a charged surface there is a work-function correction (negative if the external field is positive), associated with a polarized layer of atoms, given by:

$$\delta\phi^e = -\tfrac{1}{2}\, beF^{ext}/A\varepsilon_o M \qquad \ldots\ldots 3.20$$

where: A is the area per atom in the layer;

and M is a parameter with the role of a relative permittivity for the array. This parameter M depends on the structure of the array, and on the value of b, and its derivation is discussed in chapter 4.

Forbes argues that $\delta\phi^e$ can alternatively be thought of as a shift outwards in the effective electrical surface, from the plane of the superimposed monopole and dipole layer, by a distance d given by:

$$d = - \delta\phi^e / e F^{ext} \quad \ldots\ldots 3.21$$

If x' denotes distance as measured from the jellium surface, then for an adsorbed helium atom in contact with the jellium this is equivalent to the relationship:

$$d = (r_W + r_{He}) - (x'_{ad} + \lambda) \quad \ldots\ldots 3.22$$

where r_W and r_{He} are the known tungsten and helium-atom radii, and λ is the "field-penetration distance" as used in chapter 2. (Note that Refs. (71) and (82) use z_{ad} for x'_{ad} and λ^{-1} for λ).

The vital step was supplied by the work of Culbertson et al, where the value of $(x'_{ad} + \lambda)$ was empirically determined. This enables a value to be obtained for d, and by combining eqns.3.20, 3.21 and 3.22 we have:

$$d = \tfrac{1}{2} b / A\varepsilon_o M \quad \ldots\ldots 3.23$$

M contains b in this equation, but b is the only unknown, and hence the proper polarizability can be determined. The results are shown in table 3.1 below.

Table 3.1

Facet	$(x'_{ad} + \lambda)$/pm	b/meV V^{-2} nm^2
(111)	180	2.07
(112)	171	2.01
(011)	164	

Forbes suggests that values of polarizability derived by this method may still be on the small side. But he suggests that 2 meV V^{-2} nm^2 is an adequate choice for a "provisional working value". We shall treat this as

a lower limit for b.

Though the calculation of b is still dependent on a parameter apparently produced within the framework of a jellium model (i.e. $x'_{ad} + \lambda$), we believe that this does not disturb the self-consistency of the whole theory.

3.5.11 Polarizability - Summary

It may be helpful to summarise the last few subsections.

1) We have shown that "proper SI polarizability" should be defined in terms of the local field acting on an atom, and can be measured in meV V^{-2} nm^2 (or equivalent units).

2) We have distinguished between this "proper SI polarizability" and various other parameters called "polarizability" or "effective polarizability" in the literature.

3) We have argued that none of the conventional estimates of the proper polarizability of a tungsten surface atom is reliable.

4) We have described alternative theoretical and experimental methods of estimating tungsten surface-atom polarizability.

These last provide upper and lower estimates of 7 and 2 meV V^{-2} nm^2 respectively ($b/4\pi\varepsilon_o \simeq 10$ $Å^3$ and $3Å^3$ respectively).

3.6 Finite dipoles and higher moments

In the preceding discussion the polarized atom is being treated as a point dipole in a uniform field. In the normal mathematical treatment of dipole moment (see, for example, ref.(83)) it is necessary to expand

binomially in powers of ℓ/r (see figure below); the second, third, etc. terms of this expansion are then ignored. With a finite dipole this approximation is valid when $\ell/r \ll 1$, so that the higher terms are very small.

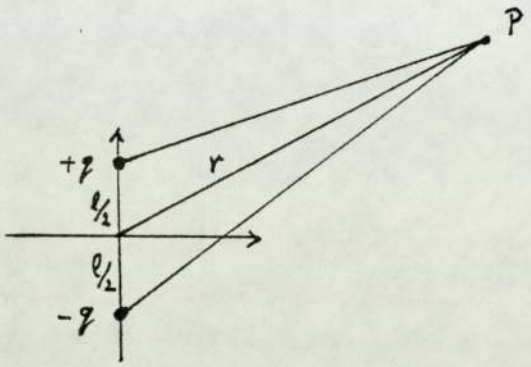

But this may not be the case in the field-adsorption situation. Let us compare the dipole length of the helium atom with the surface-atom/adsorbate-atom separation, s. For example, taking the field F = 45 V/nm, the polarizability for He = 0.143 meV V^{-2} nm^2, and the charge q = e = unit proton charge, then from:

$$p = bF \qquad \ldots\ldots 3.24$$

and

$$p = q\ell \qquad \ldots\ldots 3.25$$

we get

$$\ell = \frac{bF}{q} \simeq .0064 \text{ nm} \qquad \ldots\ldots 3.26$$

We may compare this with s for the He/W system, which is 0.259 nm. Thus $\ell/r \sim 0.03$. With this value one should perhaps expect the next term in the expansion to be small but not completely negligible.

This divergence between the mathematical expression and the physical situation of a polarized atom has another aspect, since Forbes[73] in a recent paper suggested that a full treatment should include other terms corresponding to the effect of higher moments, as well as correction terms to the simple dipole-moment expansion.

At the present time we do not fully understand the relationships between the assumption of a finite dipole and the inclusion of higher-moment terms. As the effects seem likely to be small we neglect them in a first approximation.

3.7 The Influence of Repulsive Forces on Binding Energy

Finally, in this chapter, we consider the influence of repulsive forces on binding energy. If we neglect effects due to lateral interactions as described in section 3.2, then the total potential energy U in which an adsorbate atom moves has the form:

$$U = U^{elec} + U^{disp} + U^{rep} \qquad \ldots\ldots 3.27$$

where the component potentials are due, respectively, to electric-field-induced, dispersive, and repulsive forces. The repulsive forces result from the interpenetration of electric charge clouds.

As a simple approximation, we may take the dispersive and repulsive potentials to go inversely as the sixth and twelfth powers of the separation s of adsorbate and substrate atoms, and may ignore the change in the "internal energy of the source" when considering U^{elec}. Then eq.3.27 can be written as:

$$U(z) = -\beta_A^2(z).\tfrac{1}{2}\, b_A.(F^{ext})^2 - C/z^6 + G/z^{12} \qquad \ldots\ldots 3.28$$

where C and G are constants.

At the adsorption equilibrium position (s) there is no resultant force acting on an adsorbate atom, so we must have:

$$dU/dz\big]_s = -\, d(\beta_A^2)/dz\big]_s.\tfrac{1}{2}\, b_A(F^{ext})^2$$

$$+ 6\, C/s^7 - 12\, G/s^{13} = 0 \qquad \ldots\ldots 3.29$$

By definition, the dispersive and repulsive contributions (B^{disp} and B^{rep}) to the total energy B are given by:

$$B^{disp} = - U^{disp}(s) = C/s^6 \qquad \ldots\ldots 3.30a$$

$$B^{rep} = - U^{rep}(s) = -G/s^{12} \qquad \ldots\ldots 3.30b$$

Hence it follows from eq.3.29 that:

$$B^{rep} = (s/12).d(\beta_A^2)/dz]_s.\tfrac{1}{2}\, b_A(F^{ext})^2 - \tfrac{1}{2}\, B^{disp} \qquad \ldots\ldots 3.31$$

Since dispersion-induced forces are relatively short-range, U^{disp} is equal to zero at positions in the external field somewhat above the emitter surface; consequently, B^{disp} is equal to ΔB^{disp}. Similarly B^{rep} is equal to ΔB^{rep}, and these substitutions can be made in eq.3.31. For purpose of discussion it is then possible to write this equation in the form:

$$\Delta B^{rep} = -\eta\, \Delta B(conv) - \tfrac{1}{2}\, \Delta B^{disp} \qquad \ldots\ldots 3.32$$

where η is given by

$$\eta = - (s/12).d(\beta_A^2)/dz]_s/(\beta_A^2 - 1) \qquad \ldots\ldots 3.33$$

If we continue to neglect lateral interaction and the change in the internal energy of the source, then ΔB^{elec} in eq.3.2 can be replaced by $\Delta B(conv)$, and substitution of eq.3.32 into eq.3.2 gives:

$$\Delta B \simeq (1 - \eta)\, \Delta B(conv) + \tfrac{1}{2}\, \Delta B^{disp} \qquad \ldots\ldots 3.34$$

Hence it may be seen that the effect of repulsive forces, in the approximation represented by eq.3.28, is to reduce the dispersion-induced component of the short-range binding energy by one-half, and to reduce the electric-field-induced component by a fraction η. An estimate of the component's contribution to the total short-term binding energy ΔB, to be described in later chapters, shows that the factor $(1 - \eta)$ is approximately equal to

one half in case of helium on tungsten, so the effect of repulsive forces cannot be neglected.

It should be noted though that calculated η-values will be a direct consequence of our assumption of an inverse twelfth-power low for U^{rep}. This assumption is a convenient first approximation; but a more careful treatment of the repulsive potential at a charged surface will eventually be required.

CHAPTER 4

ALGEBRIC ANALYSIS

4.1 Introduction

This chapter describes the mathematical formulation of our model of charged surfaces, and field adsorption. As a first step it is necessary to define some parameters and conventions that are used frequently in the theory.

Suffices: Parameters relating to the emitter layer will be labelled "E" and parameters relating to the adsorbed imaging gas layer will be labelled "A". An upper suffix indicates the type, and the source, that generates the parameter itself; and the lower suffix indicates the position where the parameter is acting. For example $F_A^{d,E}$ denotes the field component F, due to the dipoles d, in the emitter layer E, acting on the adsorbed layer A. Other labels may be added in brackets if found necessary, but the general trend will be to avoid any unnecessary labelling particularly where it is felt that the complete meaning of the parameter is clear to the reader.

Lattice parameters: consider a surface lattice unit cell, as a rectangle of particular surface lattice parameters a_x, and a_y

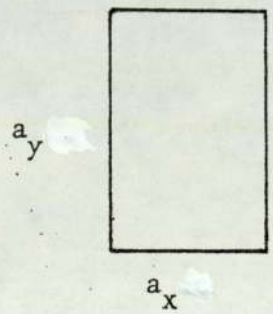

We can write a_x, and a_y in terms of a more general parameter, namely a distance c, as:

$$a_x = d_x.c$$

$$a_y = d_y.c \qquad \ldots\ldots 4.1$$

d_x, and d_y are two scaling parameters in the a_x and a_y directions. c will normally be chosen as the space-lattice parameter of a cubic lattice, but other choices are in principle possible. Since there are four lattice points, each contributes one fourth to the rectangle, so the area per lattice point (A) is:

$$A = d_x d_y c^2 \equiv A_c.c^2 \qquad \ldots\ldots 4.2$$

The quantity A_c defined by $A_c = A/c^2$ we call the "lattice characteristic". Clearly, for a primitive lattice cell $A_c = d_x d_y$. For a centred cell $A_c = d_x d_y/2$.

Distance Parameters: If we choose an arbitrary reference point "O" in the emitter surface plane as origin, then we can write a real distance $\underline{R}$ from the origin as:

$$\underline{R} = \underline{r}.c \qquad \ldots\ldots 4.3$$

where $\underline{r}$ is a dimensionless parameter and c is the same standard distance as used before. Also, we can write R in terms of its components, perpendicular (R_z), and parallel (R_n) to the plane thus:

$$R^2 = R_z^2 + R_n^2 \qquad \ldots\ldots 4.4$$

and write

$$R_z = z.c$$

$$R_n = n.c \qquad \ldots\ldots 4.5$$

z, and n are dimensionless parameters corresponding to the R_z and R_n directions.

Dimensionless Parameters: The quantities r, z, n etc. are "dimensionless distances". It is mathematically convenient and the results are more general if fields, potentials, and certain other parameters are also in a dimensionless form; thus the field (F) will be expressed in terms of a dimensionless parameter (β) defined as:

$$\beta = F/F^{ext} \qquad \ldots\ldots 4.6$$

where (F^{ext}) is the external field. The electrostatic potential Φ will be expressed in terms of a dimensionless parameter V, defined by:

$$V = -\Phi/c.F^{ext} \qquad \ldots\ldots 4.7$$

This V is of course a dimensionless potential for a negative charge, and is used for historical reasons.

Summation factors: From the laws of electrostatics, the electric field due to a single point positive charge, E^{m+}, at a distance R from the charge is given by:

$$\underset{\sim}{E}^{m+} = (q/4\pi\varepsilon_o)\ \frac{\underset{\sim}{R}}{|\underset{\sim}{R}|^3} \qquad \ldots\ldots 4.8$$

The component of this in the z-direction, E^{m+}, is given by:

$$E^{m+} = (q/4\pi\varepsilon_o)\ \frac{R_z}{R^3} \qquad \ldots\ldots 4.9$$

Using dimensionless distance parameters, this becomes:

$$E^{m+} = (q/4\pi\varepsilon_o c^2)\ \frac{z}{r^3} \qquad \ldots\ldots 4.10$$

If we now consider a planar array of equal charges, then the z-component F^{m+} of the total field $\underset{\sim}{F}^{m+}$ is obtained by summing over all individual charges, thus:

$$F^{m+} = (q/4\pi\varepsilon_o c^2) \cdot z \cdot \Sigma \frac{1}{r^3}$$

which may be written

$$= (q/4\pi\varepsilon_o c^2) \cdot z \cdot S_1 \qquad \ldots\ldots 4.11$$

where S_1 denotes the sum over all individual charges

$$S_1 = \sum_{\substack{\text{all} \\ \text{charges}}} \frac{1}{r^3} \qquad \ldots\ldots 4.12$$

The quantity S_1 is dimensionless, and is here called a "summation factor".

Similarly, the z-component of the electric field due to a point dipole, of moment p, aligned along the z-axis, at distance R from the dipoles is given by:

$$E^d = (P/4\pi\varepsilon_o).\left[\frac{3R_z^2}{R^5} - \frac{1}{R^3}\right] \qquad \ldots\ldots 4.13$$

Using dimensionless distance parameters, this becomes

$$E^d = (P/4\pi\varepsilon_o c^3).\left[\frac{3z^2}{r^5} - \frac{1}{r^3}\right] \qquad \ldots\ldots 4.1.15$$

If we consider a planar array of equal point dipoles each of dipole moment P, then the z-component F^d of the total dipole field $\underset{\sim}{F}^d$ is:

$$F^d = (P/4\pi\varepsilon_o c^3).\left[3z^2 \Sigma \frac{1}{r^5} - \Sigma \frac{1}{r^3}\right] \qquad \ldots\ldots 4.14$$

This we can write in the form:

$$F^d = (P/4\pi\varepsilon_o c^3).\left[3z^2 S_2 - S_1\right] \qquad \ldots\ldots 4.15$$

$$F^d = (P/4\pi\varepsilon_o c^3).S_3 \qquad \ldots\ldots 4.16$$

where

$$S_2 = \sum_{\substack{\text{all} \\ \text{dipoles}}} \frac{1}{r^5} \qquad \ldots\ldots 4.17$$

$$S_3 = 3z^2 S_2 - S_1 \qquad \ldots\ldots 4.18$$

The summation factor S_2 is evaluated over all dipoles in the array.

Structure Factors: It is also helpful to define some other parameters relating to special cases of S_1, S_2 and S_3; these parameters we call "Structure Factors".

The structure factor T_1 represents the value of the summation factor S_1 in circumstances when:

(1) The origin of R is taken at a lattice point;

(2) c is taken as the space-lattice parameter;

(3) the value of z is taken as zero;

(4) the summation is taken over all points except the origin (this is indicated by the prime on the summation sign).

Thus: $$T_1 = \Sigma' (R_n/c)^{-3} = \Sigma' (1/r_n)^3 \qquad \ldots\ldots 4.19$$

A closely analogous quantity is Toppings's[84] structure factor K_1, used by Tsong in his calculations[52], which is defined by

$$K_1 = \Sigma' (R_n/a)^{-3} \qquad \ldots\ldots 4.20$$

where a is the interatom distance in the surface lattice.

We define T^m as a structure factor associated with monopoles, representing the value of the summation factor S_1, evaluated at the position "A" of the nucleus of an adsorbed atom. If the separation between the adatom, and the nearest emitter atom is s, then $z_A = s/c$, and

$$T^m = S_1 \ (z_A = s/c) \qquad \ldots\ldots 4.21$$

Similarly we define T^d, a structure factor associated with dipoles, as

$$T^d = S_3 (z_A = s/c) \quad \ldots\ldots 4.22$$

T^d is analogous to the structure factor K_2, used by Tsong in ref(52), except that it uses c instead of a (i.e. $K_2 = S_3 (z = s/a)$).

4.2 Self-induced depolarization and local field

Consider a layer of atoms (L), of proper polarizability (b_L), forming a regular planar lattice. If an electric field F_L^{imp}, normal to the plane of the array, is impressed on each atom in the layer by charge distributions outside the layer, then the self-consistent local field (F_L^{loc}) on each atom in the layer is given by the sum of the impressed field (F_L^{imp}), and the field due to all other atomic dipoles in the layer ($F_L^{d,L}$) :

$$F_L^{loc} = F_L^{imp} + F_L^{d,L} \quad \ldots\ldots 4.23$$

The field $F_L^{d,L}$ is calculated by summing over all the other dipoles in the layer. If each of these has dipole moment P_L, then

$$F_L^{d,L} = \Sigma' (- P_L/4\pi\varepsilon_o . r_n^3 . c^3) \quad \ldots\ldots 4.24$$

$$F_L^{d,L} = - T_1 P_L/4\pi\varepsilon_o c^3 \quad \ldots\ldots 4.25$$

where T_1 is the structure factor defined by equation 4.19. The whole term represents a "depolarising field" acting at every atom in the layer, so as to reduce the field acting on the atom. If we assume that there is no zero-field dipole moment, then the dipole moment P_L is given by

$$P_L = b_L F_L \qquad \ldots\ldots 4.26$$

Then, by substituting eq.4.26 into eq.4.25 and then eq.4.24 into eq.4.23, and re-arranging we get:

$$F_L^{loc} = M_L^{-1} F_L^{imp} \qquad \ldots\ldots 4.27$$

where $$M_L = 1 + \frac{b_L}{4\pi\varepsilon_o c^3} T_1 \qquad \ldots\ldots 4.28$$

The parameter M_L plays the role of "relative permittivity" for the layer, as has been pointed out by MacDonald and Barlow[85].

If we apply this to the emitter layer (E), taking into our consideration the condenser configuration of the emitter surface, explained in sec.3.2, then the impressed field F_E^{imp} is given by

$$F_E^{imp} = \sigma/2\varepsilon_o = \tfrac{1}{2} F^{ext} \qquad \ldots\ldots 4.29$$

Then: $$F_E^{loc} = \tfrac{1}{2} M_E^{-1} F^{ext} \qquad \ldots\ldots 4.30$$

and a dimensionless quantity β_E can be defined as follows

$$\beta_E = F_E^{loc}/F^{ext} = \tfrac{1}{2} M_E^{-1} \qquad \ldots\ldots 4.31$$

β_E represents the field ratio at the position of an emitter atom, where the effect of the atom itself is excluded.

Note that the last part of this derivation, from eq.4.29 onwards, assumes that the emitter layer is present by itself. If an adsorbed layer is also present then a different expression must be used for F_E^{imp}. This case is discussed in section 4.4.

4.3 Field above plane emitter surface

Consider a layer of emitter atoms (E), forming a regular planar array extending to infinity in all directions. In the context of our model, the emitter atoms are represented by dipoles, superimposed on monopoles (i.e. point positive charges). There is also a negative charge distribution, stationed above the emitter surface at infinite distance, forming with the monopoles a condenser configuration as shown in fig(4.1).

The field acting at a point P, some distance R_Z = z.c above the emitter layer can be written as:

$$\underline{F}^{E} = \underline{F}^{m} + \underline{F}^{d,E} \qquad \ldots\ldots 4.32$$

where $\underline{F}^{m}$ is the field due to positive monopoles and the negative charge distribution, and $\underline{F}^{d,E}$ is the field due to the dipoles in the emitter layer.

All terms in eq.4.32 can be resolved into components perpendicular and parallel to the array plane, but at symmetry points, such as points situated above a lattice point or above a mid point between four lattice points, all parallel components cancel each other. We will confine our study to these symmetry points, since they are of direct interest in our investigations both of the field-adsorption binding energy and of field-ion image contrast.

With reference to field adsorption, note that any adsorbed atom temporarily situated above an "asymmetrical" point on the emitter plane will be driven by the resultant force towards a "symmetrical" position above the nearest emitter surface atom, where the binding energy will be a maximum.

It is much easier to carry out analysis and calculations for symmetrical positions, since eq.4.32 will be reduced to the perpendicular

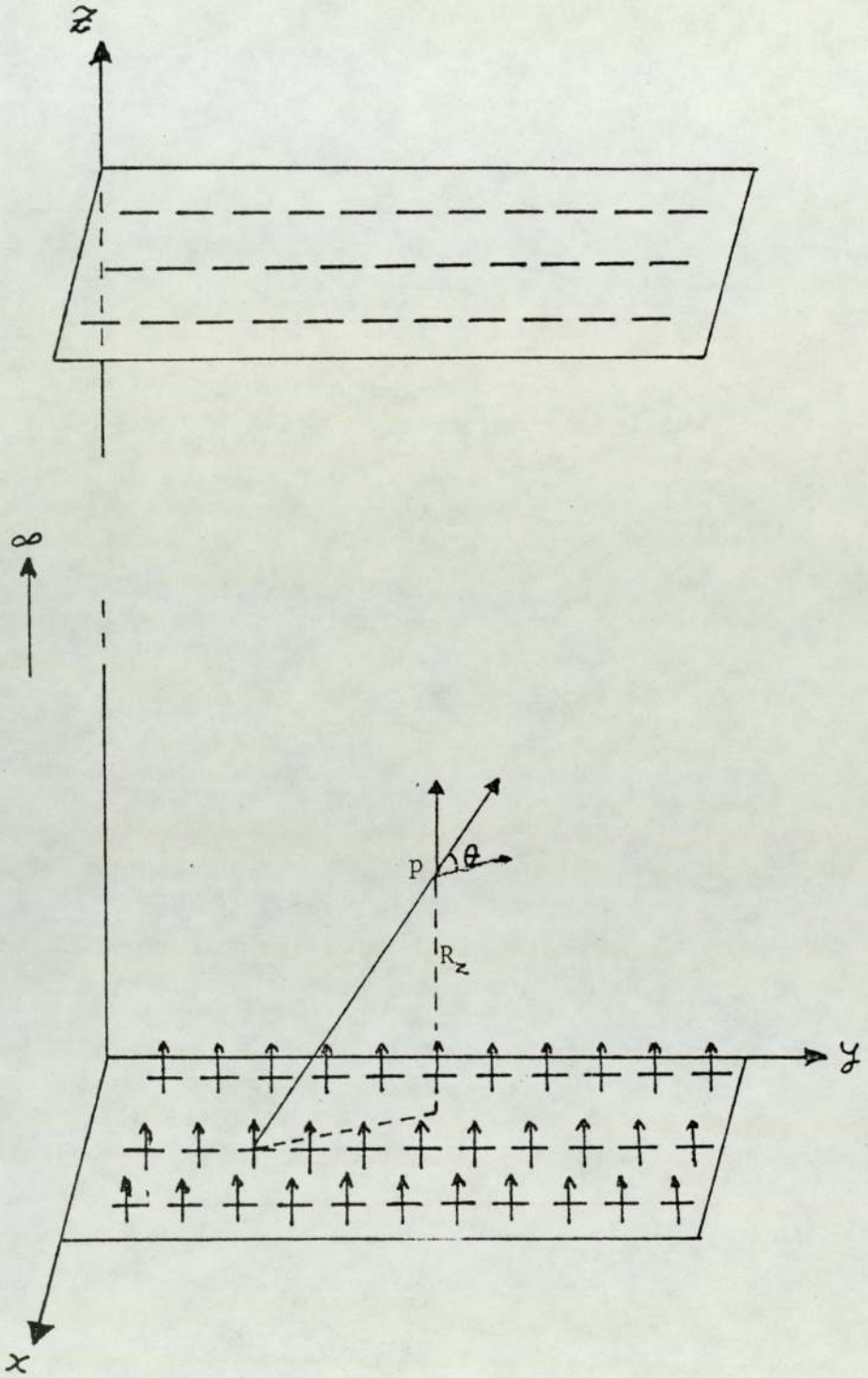

Fig.4.1

A field point p above the array plane

component terms only and in effect becomes a scalar equation. Hence all following calculations will be performed in scalar form. Nevertheless, it should be borne in mind that they represent the perpendicular component only.

4.3.1 The monopole contribution to the field (F^m)

The field due to the positive monopole contribution with conjunction to the negative charge distribution contribution can be written as:

$$F^m = F^{m+,E} + F^{m-,\infty} \qquad \ldots\ldots 4.33$$

Each plane of charge gives rise to a field of magnitude $(\sigma/2\varepsilon_o)$ on either side (somewhat away from the array planes, where local field variation vanishes), σ being the mean charge per unit area in the array. The application of Gauss theory shows that the contribution of both positive and negative charges adds in the middle between the two planes, so that at sufficient distances from the array, the total field is normal to the array plane and we have:

$$F^m = F^{ext} = \sigma/\varepsilon_o \qquad (\text{for } R_z >> c) \qquad \ldots\ldots 4.34$$

At a distance from the emitter plane comparable to c, local variations in the field due to the localised positive charges can not be ignored, and eq.4.34 is not valid. In this case we write:

$$F^m = \sigma/2\varepsilon_o + F^{m+,E} \qquad \ldots\ldots 4.35$$

The first term is equal to $\frac{1}{2} F^{ext}$ as is clear from eq.4.3. As we are working at symmetry positions the second term is identical with the field F^{m+} discussed in sec 4.1, and so:

$$F^{m+,E} = \frac{q.z}{4\pi\varepsilon_o c^2} S_1 \qquad \ldots\ldots 4.36$$

where S_1 is the summation factor defined by eq.4.12.

The monopole charge q can be expressed in terms of external field, and the surface charge density σ as:

$$\sigma = q/A \qquad \ldots\ldots 4.37$$

where A is the area per charge, given by $A_c.c^2$ in eq.4.2, therefore we have:

$$F^{ext} = \sigma/\varepsilon_o = q/A_c.c^2.\varepsilon_o$$

$$\text{or} \quad q = A_c.c^2.\varepsilon_o.F^{ext} \qquad \ldots\ldots 4.38$$

By substituting eq.4.38 into eq.4.36, and then eq.4.36 into eq.4.35, we obtain:

$$F^m = \tfrac{1}{2} F^{ext} + (A_c/4\pi).\mathbf{z}.S_1 F^{ext} \qquad \ldots\ldots 4.39$$

Hence we define the dimensionless field ratio β^m as:

$$\beta^m = F^m/F^{ext} = \tfrac{1}{2} + (A_c/4\pi).\mathbf{z}.S_1 \qquad \ldots\ldots 4.40$$

4.3.2 The dipole contribution to the field

As above, we consider the field at symmetry positions above the array. In this case, we have from eq.4.16 that the dipole contribution to the total field is given by:

$$F^{d,E} = (P_E/4\pi\varepsilon_o c^3) S_3 \qquad \ldots\ldots 4.41$$

Substituting P_E by $b_E F_E^{loc}$, where F_E^{loc} is, as before, the self-consistent

local field acting on an emitter atom, and then writing $F_E^{loc} = \beta_E F^{ext}$:

$$F^{d,E} = (b_E/4\pi\varepsilon_o c^3)\, \beta_E\, S_3\, F^{ext} \qquad \ldots\ldots 4.42$$

Then we define:

$$\beta^{d,E} = F^{d,E}/F^{ext} = (b_E/4\pi\varepsilon_o c^3)\, \beta_E\, S_3 \qquad \ldots\ldots 4.43$$

4.3.3 The total field above single emitter layer

Finally the total monopole and dipole contribution to the field due to a single emitter layer can be produced by substituting eq.4.42 and eq.4.39 into eq.4.32, thus:

$$F^E = \left[\tfrac{1}{2} + (A_c/4\pi)\,.\,\mathbf{z}\,.\,S_1 + (b_E\beta_E/4\pi\varepsilon_o c^3)S_3\right] F^{ext} \qquad \ldots\ldots 4.44$$

The corresponding dimensionless field ratio is given by:

$$\beta^E = \tfrac{1}{2} + (A_c/4\pi).\mathbf{z}.S_1 + (b_E\beta_E/4\pi\varepsilon_o c^3)S_3 \qquad \ldots\ldots 4.45$$

Note that in all the above formulae, if the single layer is present physically by itself then β_E is given by $\tfrac{1}{2} M_E^{-1}$, as in eq.4.31. If an adsorbed layer is also present then β_E must be derived self-consistently as in the following section.

4.4 Self-consistent fields for the emitter-adsorbed-layer system

We now move on to consider a "field adsorption situation" represented by the positively charged array of emitter atoms, analysed in the previous section, and a similar layer of inert gas atoms situated above it (i.e. each adsorbed atom is situated directly above the corresponding emitter atom). For convenience we will drop the suffix "loc" and refer to the

self-consistent local field at the position of adsorbed atom as F_A, and to that at the position of emitter atom as F_E. The adsorbed-atom dipole moment P_A can be expressed as in eq.4.26 as:

$$P_A = b_A F_A \quad \ldots\ldots 4.46$$

If we define a dimensionless field ratio factor β'_A as

$$\beta'_A = F_A/F^{ext} \quad \ldots\ldots 4.47$$

Thus by substituting eq.4.47 into eq.4.46, we get

$$P_A = b_A \beta'_A F^{ext} \quad \ldots\ldots 4.48$$

Similarly, for the emitter layer:

$$P_E = b_E F_E = b_E \beta'_E F^{ext} \quad \ldots\ldots 4.49$$

Using the results in the first part of section 4.2, but replacing "L" by "A", we can write the self-consistent local field F_A, in terms of the field impressed on the adsorbate layer from sources outside it, and the depolarising field due to the dipoles of the adsorbed layer atoms itself, as follows:

$$F_A = M_A^{-1} F_A^{imp} \quad \ldots\ldots 4.50$$

with

$$F_A^{imp} = F_A^m + F_A^{d,E} \quad \ldots\ldots 4.51$$

F_A^m is the field due to the monopole distribution, as explained in section 4.3.1, and the relation represented by eq.4.40 can be easily modified to suit the field adsorption situation, as follows:

$$\beta_A^m = \tfrac{1}{2} + (A_c/4\pi)\ z_A\ T^m \quad \ldots\ldots 4.52$$

τ_A is given by s/c, where s is the separation of the layers, and T^m is the structure factor given by eq.4.21. Then:

$$F_A^m = \beta_A^m F^{ext} \quad \ldots\ldots 4.53$$

$F_A^{d,E}$ is the field due to the emitter atom dipoles, and eq.4.43 can be easily modified to suit the field adsorption situation, as follows:

$$\beta_A^{d,E} = \frac{b_E \beta'_E}{4\pi\varepsilon_o c^3} \cdot T^d$$

$$= \gamma_A^{d,E} \beta'_E \quad \ldots\ldots 4.54$$

where T^d is the structure factor defined by eq.4.22. $\gamma_A^{d,E}$ is a dimensionless coefficient (corresponding to dipole characteristics) defined by eq.4.54; this coefficient gives the field acting on the atoms in the adsorbate layer, due to the dipoles in the emitter layer †. Thus eq.4.54 can also be written in the form

$$F_A^{d,E} = \gamma_A^{d,E} F_E \quad \ldots\ldots 4.55$$

We then have that

$$F_A^{d,E} = \gamma_A^{d,E} \beta'_E . F^{ext} \quad \ldots\ldots 4.56$$

Thus, combining eqs. 4.56, 4.53 and 4.51, we get:

$$F_A^{imp} = (\beta_A^m + \gamma_A^{d,E} \beta'_E) F^{ext} \quad \ldots\ldots 4.57$$

Hence, from eqs.4.50, 4.57 and by dividing by F^{ext} we get:

$$\beta'_A = M_A^{-1} [\beta_A^m + \gamma_A^{d,E} \beta'_E] \quad \ldots\ldots 4.58$$

As discussed in section 4.2, M_A is a factor acting as a relative permittivity for the layer A, and is defined by:

$$M_A = 1 + T_1 \, b_A / 4\pi\varepsilon_o c^3 \qquad \ldots\ldots 4.59$$

We may treat the field acting at the position of an emitter atom in an exactly analogous way. Because of the symmetry of the situation, we can get the result by exchanging "A" and "E" wherever they occur to give:

$$\beta'_E = M_E^{-1} \left[\beta_E^m + \gamma_E^{d,A} \, \beta'_A\right] \qquad \ldots\ldots 4.60$$

where M_E is a factor acting as a relative permittivity for the layer E and defined as:

$$M_E = 1 + T_1 \, b_E / 4\pi\varepsilon_o c^3 \qquad \ldots\ldots 4.61$$

Note that the same quantity T^d appears in the definition of $\gamma_E^{d,A}$ as in the definition $\gamma_A^{d,E}$ in eq.4.54, because S_z is symmetrical function of z.

Finally by substituting β'_E in eq.4.60 into eq.4.58 and solving for β'_A, we get:

$$\beta'_A = \frac{M_A^{-1} \, \beta_A^m + M_A^{-1} \, \gamma_A^{d,E} \, M_E^{-1} \, \beta_E^m}{1 - M_A^{-1} \, \gamma_A^{d,E} \, M_E^{-1} \, \gamma_E^{d,A}} \qquad \ldots\ldots 4.62$$

A similar formula can be deduced for β'_E by replacing A by E wherever it occurs in eq.4.62, and vice versa.

Interpretation. A rough physical interpretation of eq.4.62 can be made as follows:

(1) the term $M_A^{-1} \, \beta_A^m$ represents a contribution to β_A resulting from the monopole charge distribution, reduced as a result of the mutual depolarization influence of the adsorbate layer atoms.

(2) the second term in the numerator represents a contribution from the emitter atom dipoles, similarly reduced.

(3) the denominator represents an enhancement effect due to the influence of the adsorbate-layer dipoles on the emitter-layer dipoles.

---

† It should be noted that Forbes, in his recent paper[73] made an important correction to the dimensionless coefficient γ^d, by including the effects due to higher moments; thus for example the total effect can be written in principle as: $\gamma_E^A = \gamma_E^{d,A} + \gamma_E^{q,A} + \ldots$. where $\gamma_E^{d,A}$ and $\gamma_E^{q,A}$ are the dimensionless coefficients corresponding to dipole and quadrupole ..... etc. characteristics. The new coefficient may replace the old in all our previous treatments.

4.5 Fields above emitter-adsorbed layer

The local field above the emitter-plus-adsorbed layer can be found by extending the method of section 4.3. First we need to define the distances. Let the distance from the emitter layer to a chosen point P, in dimensionless units, be z. The dimensionless distance z* of point P from the adsorbate layer is given by:

$$z^* = z - s/c \qquad \ldots\ldots 4.63$$

where s is the real layer separation, as before.

The field F at point P is obtained by adding contributions due to the two layers, so:

$$F = F^E + F^A \qquad \ldots\ldots 4.64$$

or, in terms of dimensionless factors:

$$\beta = \beta^E + \beta^A \qquad \ldots\ldots 4.65$$

β^E is given by eq.4.45, but with β_E replaced by β'_E.

The field due to the adsorbed layer is the field due to the adsorbed atom dipoles only; thus

$$F^A = F^{d,A} \qquad \ldots\ldots 4.66$$

or:

$$\beta^A = F^A/F^{ext} = (P_A/4\pi\varepsilon_o c^3).S_3^*/F^{ext} \qquad \ldots\ldots 4.67$$

$$\beta^A = (b_A/4\pi\varepsilon_o c^3).\beta'_A.S_3^* \qquad \ldots\ldots 4.68$$

where, if S_3 denotes a structure factor evaluated for some distance z, S_3^* denotes the structure factor evaluated at distance z* given by eq.4.67.

If we now substitute eqs.4.45 and 4.68 in eq.4.65 we get finally

$$\beta = \left[\tfrac{1}{2} + (A_c/4\pi).z.S_1 + (b_E\beta'_E/4\pi\varepsilon_o c^3).S_3 + (b_A\beta'_A/4\pi\varepsilon_o c^3).S_3^*\right] \quad \ldots\ldots 4.69$$

Note that in this formula the parameters β'_E and β'_A relate to the self-consistent fields existing in the emitter-plus-adsorbed-layer situation, as discussed in section 4.4.

4.6 Self-consistent field for emitter-double-adsorbed-layer system

Some FIM literature (i.e. for example ref.(39)), views the imaging process in terms of a second mobile layer of adsorbed imaging gas atom(s). We find it interesting to explore this possibility using the same method as before. Naming the second adsorbed layer of inert gas atoms B, the local field at the position of an atom in the E-layer is

$$F_E^{loc} = M_E^{-1}\left[F_E^m + F_E^{d,A} + F_E^{d,B}\right] \quad \ldots\ldots 4.70$$

The field $F_E^{d,A}$ is given in terms of the local field F_A^{loc} acting on the A-layer by:

$$F_E^{d,A} = \gamma_E^{d,A}\, F_A^{loc} \quad \ldots\ldots 4.71$$

where $$\gamma_E^{d,A} = (b_A/4\pi\varepsilon_o c^3)\, T_E^{d,A} \quad \ldots\ldots 4.72$$

Because there are now three inter-layer interactions involved it has been necessary to add suffices to the structure-factor symbol, T^d.

The structure factors used in this section are thus defined by:

$$T_E^{d,A} = T_A^{d,E} = S_3 \ (z = \rho_A + \rho_E) \qquad \ldots\ldots 4.73$$

$$T_B^{d,A} = T_A^{d,B} = S_3 \ (z = \rho_A + \rho_B) \qquad \ldots\ldots 4.74$$

$$T_E^{d,B} = T_B^{d,E} = S_3 \ (z = \rho_E + 2\rho_A + \rho_B) \qquad \ldots\ldots 4.75$$

As shown below in the figure, the quantities ρ_E, ρ_A, ρ_B are the dimensionless radii of the atoms composing the three layers

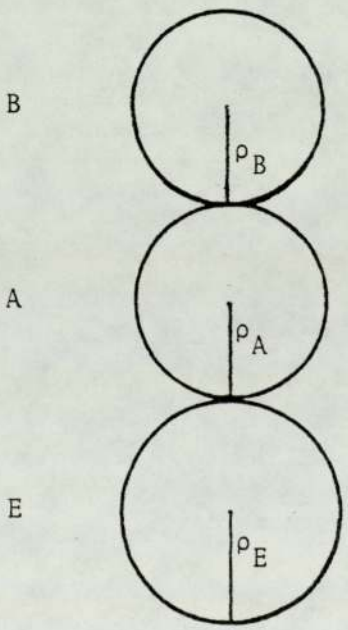

Other fields analogous to $F_E^{d,A}$ may be defined in a manner analogous to eqs.4.71 and 4.72.

Substituting into eq.4.70 then gives:

$$F_E^{loc} = F_E^m + \gamma_E^{d,A} F_A^{loc} + \gamma_E^{d,B} F_B^{loc} \quad \ldots\ldots 4.76$$

And on dividing through by F^{ext} we obtain

$$\beta_E'' = M_E^{-1} [\beta_E^m + \gamma_E^{d,A} \beta_A'' + \gamma_E^{d,B} \beta_B''] \quad \ldots\ldots 4.77$$

The double-primes indicate that the β-factors refer to the self-consistent local fields in the situation where there are <u>two</u> adsorbed layers.

Following the same procedure as above, we get finally:

$$\beta_A'' = M_A^{-1} [\beta_A^m + \gamma_A^{d,B} \beta_B'' + \gamma_A^{d,E} \beta_E''] \quad \ldots\ldots 4.78$$

$$\beta_B'' = M_A^{-1} [\beta_B^m + \gamma_B^{d,A} \beta_A'' + \gamma_B^{d,E} \beta_E''] \quad \ldots\ldots 4.79$$

where $$M_A = 1 + (T_1 b_A / 4\pi\varepsilon_o c^3) \quad \ldots\ldots 4.80a$$

$$M_B = 1 + (T_1 b_B / 4\pi\varepsilon_o c^3) \quad \ldots\ldots 4.80b$$

$$M_E = 1 + (T_1 b_E / 4\pi\varepsilon_o c^3) \quad \ldots\ldots 4.80c$$

Re-arranging eqs.4.77, 4.78 and 4.79 as:

$$M_A \beta_A'' - \gamma_A^{d,B} \beta_B'' - \gamma_A^{d,E} \beta_E'' = \beta_A^m$$

$$\gamma_B^{d,A} \beta_A'' + M_B \beta_B'' - \gamma_A^{d,E} \beta_E'' = \beta_B^m$$

$$\gamma_E^{d,A} \beta_A'' - \gamma_E^{d,B} \beta_B'' + M_E \beta_E'' = \beta_B^m$$

Then the field ratio can be deduced by using the determinant rules, as follows:

$$\beta''_A = \frac{C_{11}\,\beta_A^m + C_{21}\,\beta_B^m + C_{31}\,\beta_E^m}{C_{11}\,M_A - C_{21}\,\gamma_B^{d,A} - C_{31}\,\gamma_E^{d,A}} \quad \ldots\ldots 4.81$$

$$\beta''_B = \frac{C_{12}\,\beta_A^m + C_{22}\,\beta_B^m + C_{32}\,\beta_E^m}{-C_{12}\,\gamma_B^{d,A} + C_{22}\,M_B - C_{32}\,\gamma_E^{d,B}} \quad \ldots\ldots 4.82$$

$$\beta''_E = \frac{C_{13}\,\beta_A^m + C_{23}\,\beta_B^m + C_{33}\,\beta_E^m}{-C_{13}\,\gamma_E^{d,A} - C_{23}\,\gamma_E^{d,B} + C_{33}\,M_E} \quad \ldots\ldots 4.83$$

where

$$C_{11} = M_B\,M_E - \gamma_E^{d,B}\,\gamma_B^{d,E} \quad \ldots\ldots 4.84a$$

$$C_{21} = \gamma_A^{d,B}\,M_E + \gamma_E^{d,B}\,\gamma_A^{d,E} \quad \ldots\ldots 4.84b$$

$$C_{31} = \gamma_A^{d,E}\,M_B + \gamma_A^{d,B}\,\gamma_B^{E} \quad \ldots\ldots 4.84c$$

$$C_{12} = \gamma_B^{d,A}\,M_E - \gamma_E^{d,A}\,\gamma_B^{d,E} \quad \ldots\ldots 4.84d$$

$$C_{22} = M_A\,M_E - \gamma_E^{d,A}\,\gamma_A^{d,E} \quad \ldots\ldots 4.84e$$

$$C_{32} = \gamma_B^{d,E}\,M_A + \gamma_B^{d,A}\,\gamma_E^{d,A} \quad \ldots\ldots 4.84f$$

$$C_{13} = M_B\,\gamma_E^{d,A} + \gamma_E^{d,B}\,\gamma_E^{d,A} \quad \ldots\ldots 4.84g$$

$$C_{23} = \gamma_E^{d,B}\,M_A + \gamma_B^{d,B}\,\gamma_E^{d,B} \quad \ldots\ldots 4.84h$$

$$C_{33} = M_A\,M_B - \gamma_B^{d,A}\,\gamma_A^{d,B} \quad \ldots\ldots 4.84i$$

It is clear that by putting $M_B = 1$ and $\gamma_E^{d,B} = \gamma_A^{d,B} = 0$, the field ratio formulae reduce to the formal single-adsorbed-layer formulae.

4.7 The Calculation of the Potential

4.7.1 Initial Problems

In the context of field-ion theory there is sometimes a need to know the difference between the electrostatic potential of a point (P say) outside the emitter surface and the mean potential level in the interior of the emitter. A quantity of this type is needed, for example, when determining the position of the critical surface.

In the context of our surface model, this potential difference must be interpreted as the potential Φ_p at point P relative to a point behind the emitter surface plane at position $-\infty$. (That is, $z = -\infty$ represents deep inside the emitter).

In principle this elecrostatic potential can be written as follows:

$$\Phi_p = \Phi_p^m + \Phi_p^d \qquad \ldots\ldots 4.85$$

where Φ_p^m is potential at point P, relative to $-\infty$, due to the monopoles contribution; and Φ_p^d is the potential at point P, relative to $-\infty$, due to the dipoles contribution. The monopole contribution can in turn be expressed as a sum of positive and negative contributions, thus:

$$\Phi_p^m = \Phi_p^{m-,\infty} + \Phi_p^{m+,E} \qquad \ldots\ldots 4.86$$

But hereby lies a difficulty, since both terms are infinite, though of opposite signs. For example, the evaluation of $\Phi_p^{m-,\infty}$ involves the contribution of the negative charge distribution stationed at $+\infty$ in our model, that gives rise to uniform field equal to $\frac{1}{2} F^{ext}$ (see section 4.3.1

for details). $\Phi^{m-,\infty}$ is evaluated in terms of the work done to move a unit positive charge from the chosen point behind the emitter surface at $-\infty$ to point P and is thus infinite, since $\Phi_p^{m-,\infty} = -\frac{1}{2} F^{ext} \times +\infty$.

A general procedure for avoiding this is to choose some standard reference point M as shown in fig.(4.2) and then write the potential Φ_p^m as a sum of two parts,

$$\Phi_p^m = \Phi_M^m + \Delta \Phi_{MP}^m \qquad \ldots\ldots 4.87$$

Φ_M^m is the potential due to the monopoles contribution at the reference point M (relative to $-\infty$), and needs to be calculated once, or once for a given x-y coordinate. $\Delta \Phi_{MP}^m$ is the potential difference (due to the same source) between point M and point P, and we need to calculate it for every chosen value of z. Φ_M^m is evaluated as follows. Consider a point, say P', at large negative distance behind the emitter surface plane. Then Φ_M^m can be expressed in terms of an approximate expression represented by the potential difference between point M and point P' ($\Delta \Phi_{P'M}^m$). The correct value is obtained by extending point P' to $-\infty$, i.e.

$$\Phi_M^m = \lim_{P' \to -\infty} \Delta \Phi_{P'M}^m = -\lim_{P' \to -\infty} \Delta \Phi_{MP'}^m \qquad \ldots\ldots 4.88$$

In practice, as will be shown in chapter 6, it is sufficient to take P' at about 1000.c from the emitter surface plane. The choice of a suitable position for the reference point M proved troublesome, and for some time constituted an obstacle in solving the problem correctly. Various approaches have been considered.

The initial approach was to put the reference point in the plane of the emitter array. But hence a problem arises. In evaluating the contribution of the "distant charge" outside the "counting circle" (see section 5.2), it is possible to derive an exact formula for the difference in potential between two points on the axis of the counting circle. For this

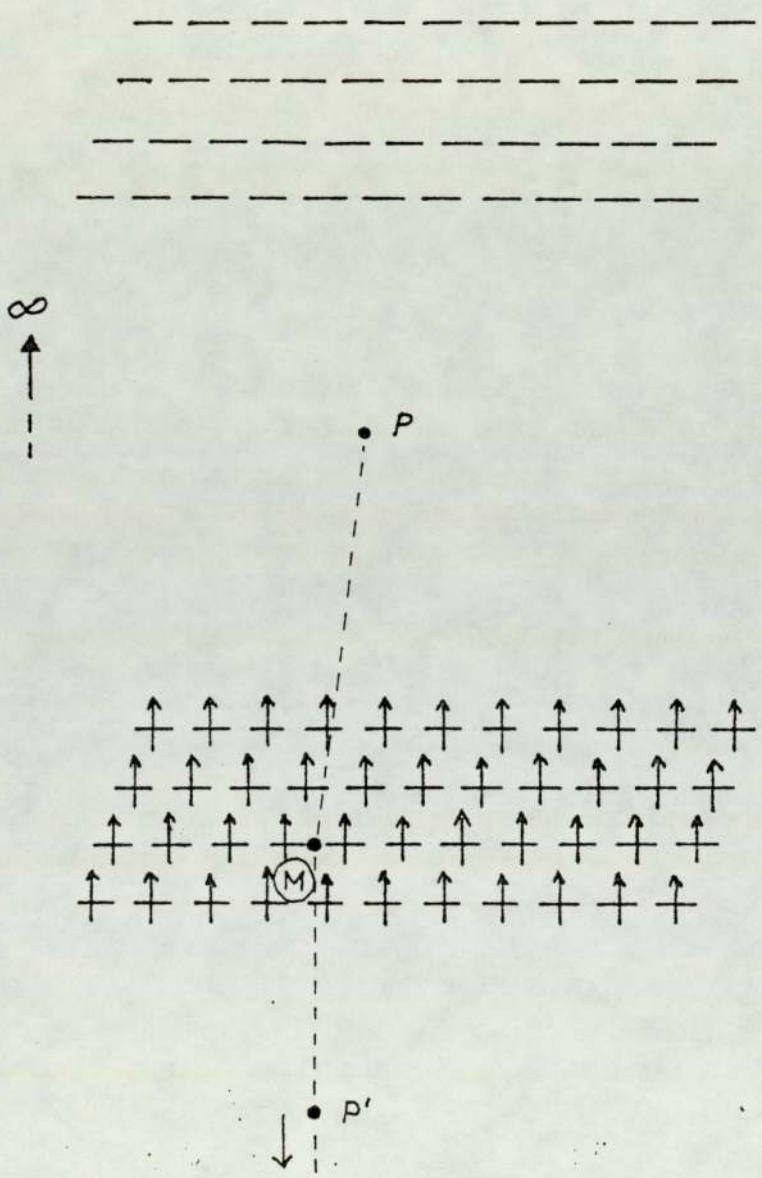

Fig.4.2

To illustrate a possible general relation between points p, M and p'

reason it is convenient to put M at the same X-Y coordinates as P. However, this means that when P is directly above a lattice point then M is located at a surface charge, and in this case both $\Delta \Phi^{m}_{P'M}$ and $\Delta \Phi^{m}_{MP}$ contain one infinite term, resulting from this charge.

The two approaches initially used to get round this difficulty were:

(1) To keep M at a fixed position in the emitter array plane, and develop approximate formulae for the difference in potential between M and P, due to the distant charge, when these have different X-Y coordinates.

(2) To keep M with the same X-Y coordinates as P, but to arrange for the troublesome infinite term to be dropped from the summations involved in evaluating both $\Delta \Phi^{m}_{P'M}$ and $\Delta \Phi^{m}_{MP}$ when M is at a lattice point. This approach was employed for sometime in the writer's programs.

A third approach, which seems to solve the problem, was subsequently developed out of the second approach, by Chibane[86]. He located the reference point M at a short distance below the emitter surface plane. This approach has now been incorporated in the writer's computer program as a final general solution.

The second approach discussed above can be seen as a special case of this third approach. What we shall therefore describe in this section is the final mathematical derivations of the monopole and dipole contribution to the potential through this last approach.

4.7.2 The Potential Contribution due to Monopoles

To determine the monopole contribution, the essential problem is to derive an expression for $\Delta \Phi^{m}_{MP}$. We shall take M to be at a position behind the emitter plane, with dimensionless coordinates (x, y, z'), as shown in Fig(4.3). This z' is a negative number, and the actual distance

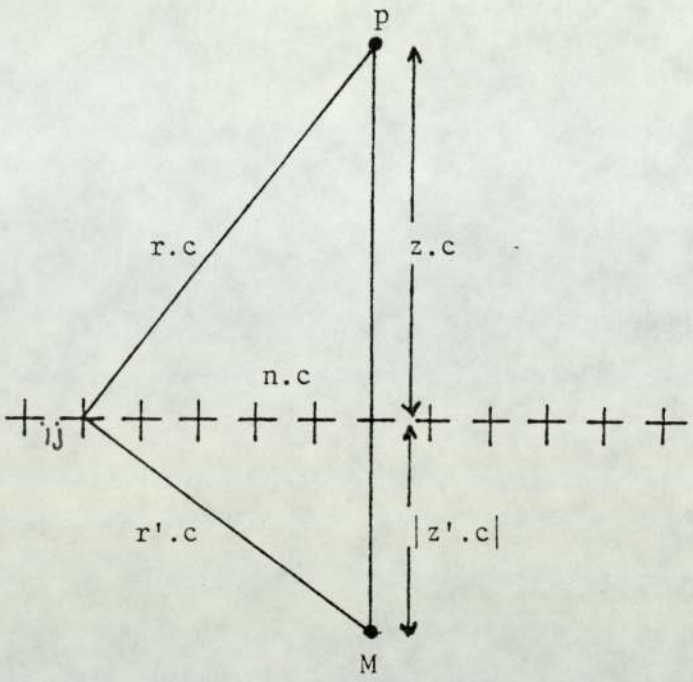

Fig.4.3

To illustrate actual position chosen for point M

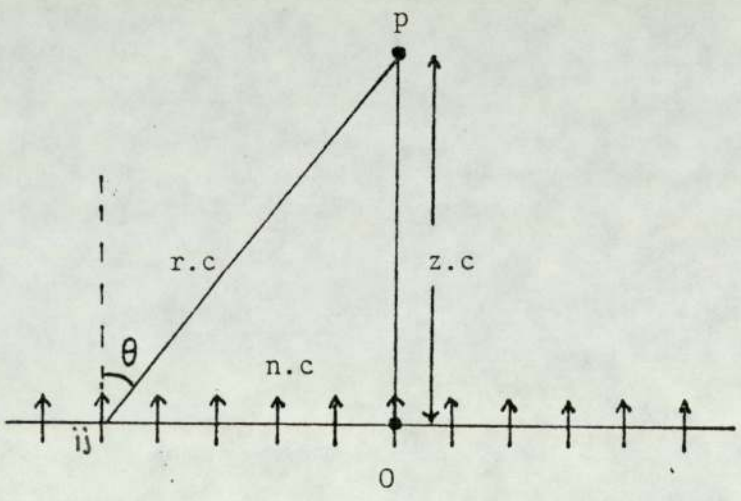

Fig.4.4

To illustrate the calculation of the potential due to the dipoles

of M behind the plane is $|z'.c|$.

$\Delta \Phi^{m}_{MP}$ can be expressed in terms of positive and negative components.

$$\Delta \Phi^{m}_{MP} = \Delta \Phi^{m+}_{MP} + \Delta \Phi^{m-}_{MP} \qquad \ldots\ldots 4.89$$

To obtain the negative contribution, we remember that the field due to the distant negative charge is $\frac{1}{2} F^{ext}$. Hence

$$\Delta \Phi^{m-}_{MP} = - \tfrac{1}{2} F^{ext} . (z - z').c \qquad \ldots\ldots 4.90$$

To obtain the positive contribution consider the monopole charge ij shown in Fig.(4.3). This is at a distance r.c from P and r'.c from M. Thus the potential difference between M and P due to the monopole (ij), of charge q, is:

$$\Delta \Phi^{m+}_{MP} (ij) = \frac{q}{4\pi\varepsilon_o c}\left[\frac{1}{r} - \frac{1}{r'}\right]$$

$$= \frac{-q}{4\pi\varepsilon_o c}\left[\frac{1}{r'} - \frac{1}{r}\right] \qquad \ldots\ldots 4.91$$

where $r = (z^2 + n^2)^{\frac{1}{2}}$, and $r' = (z'^2 + n^2)^{\frac{1}{2}}$.

Remembering from eq.4.38 that $q = A_c . c^2 . \varepsilon_o F^{ext}$, we obtain:

$$\Delta \Phi^{m+}_{MP} (ij) = - \frac{A_c.c}{4\pi}\left[\frac{1}{r'} - \frac{1}{r}\right] F^{ext} \qquad \ldots\ldots 4.92$$

The contribution due to all monopoles in the plane is produced by summing over them all, thus:

$$\Delta \Phi^{m+}_{MP} = - \frac{A_c.c}{4\pi} \sum_{ij}\left[\frac{1}{r'} - \frac{1}{r}\right] F^{ext} \qquad \ldots\ldots 4.93$$

Defining S_o as a summation factor associated with potentials as:

$$S_o = \sum_{\substack{\text{all} \\ \text{monopoles}}} \left[\frac{1}{r'} - \frac{1}{r}\right] \qquad \ldots\ldots 4.94$$

Then $$\Delta \Phi^{m+} = - \frac{A_c . c}{4\pi} S_o F^{ext} \qquad \ldots\ldots 4.95$$

Thus the total monopole contribution is the sum of eqs.4.90 and 4.95:

$$\Delta \Phi^m_{MP} = - \left[\frac{z-z'}{2} + \frac{A_c}{4\pi} S_o\right] c F^{ext} \qquad \ldots\ldots 4.96$$

Or in terms of the dimensionless potential difference defined analogously to eq.4.7 by:

$$\Delta V^m_{MP} = - \Delta \Phi^m_{MP}/c.F^{ext} \qquad \ldots\ldots 4.97$$

We have

$$\Delta V^m_{MP} = \frac{z-z'}{2} + \frac{A_c}{4\pi} S_o \qquad \ldots\ldots 4.98$$

The dimensionless potential V^m_M at M is then derived as:

$$V^m_M = - \lim_{z \to -\infty} \left[\frac{z-z'}{2} + \frac{A_c}{4\pi} S_o\right] \qquad \ldots\ldots 4.99$$

(Note S_o is a function of z). And we then have the monopole contribution to the dimensionless potential at M given by:

$$V^m_P = V^m_M + \Delta V^m_{MP} \qquad \ldots\ldots 4.100$$

The formulae initially used by the present writer are recovered by setting z' = 0 and r' = n.

4.7.3 The Dipole Contribution to Potential

For determining the dipole contribution to the potential at P, it is best to consider a reference point in the plane of the array (see Fig(4.4)), because it is a well-known fact that this plane is an equipotential plane. Denote a reference point in this plane by "O".

The potential at a point (P) above the emitter, relative to this point (O), due to the dipole (ij), can be written as follows:

$$\Delta \Phi_{OP}^{d,E} (ij) = \frac{P_E}{4\pi\varepsilon_o} \frac{\cos\theta}{r^2 c^2} \quad \ldots\ldots 4.101$$

where P_E is the dipole moment of this (ij) dipole, and θ is the angle shown in the figure, given by:

$$\cos\theta = \frac{z}{r} \quad \ldots\ldots 4.102$$

Then eq.4.102 can be written as

$$\Delta \Phi_{OP}^{d,E} (ij) = \frac{P_E}{4\pi\varepsilon_o c^2} \frac{z}{r^3} \quad \ldots\ldots 4.103$$

Assuming that all dipoles have equal polarizability, and hence equal dipole moments, the total contribution from all emitter dipoles is:

$$\Delta \Phi_{OP}^{d,E} = \frac{P_E z}{4\pi\varepsilon_o c^2} \sum_{\substack{\text{all} \\ \text{dipoles}}} \frac{1}{r^3}$$

$$= \frac{P_E z}{4\pi\varepsilon_o c^2} S_1 \quad \ldots\ldots 4.104$$

S_1 is the same as previously, because there is a dipole associated with every monopole.

If we substitute for P_E using $P_E = b_E \beta_E F^{ext}$, then:

$$\Delta \Phi_{OP}^{d,E} = (b_E \beta_E z/4\pi\varepsilon_o c^2) S_1 F^{ext} \quad \ldots\ldots 4.105$$

In terms of a dimensionless potential as used earlier, we have:

$$\Delta V_{OP}^{d,E} = -\Delta \Phi_{OP}^{d,E}/cF^{ext} = \frac{-b_E \beta_E z}{4\pi\varepsilon_o c^3} S_1 \quad \ldots\ldots 4.106$$

The dipole contribution to dimensionless potential of point P relative to $-\infty$ can now be written:

$$V_P^{d,E} = V_O^{d,E} + \Delta V_{OP}^{d,E} \quad \ldots\ldots 4.107$$

where the first term on the right hand side represents the potential of "O" relative of $-\infty$. This can be obtained from :

$$V_O^{d,E} = -\lim_{z\to-\infty} \Delta V_{OP}^{d,E} = \frac{b_E \beta_E}{4\pi\varepsilon_o c^3} \lim_{z\to-\infty} \{zS_1\} \quad \ldots\ldots 4.108$$

When the distance z is very large compared with the interdipole spacing, the array of discrete dipoles can be replaced by a uniform layer of dipoles (see Fig.(4.5)) and hence we have:

$$V_O^{d,E} = \frac{b_E \beta_E}{4\pi\varepsilon_o c^3} \lim_{\substack{z\to 0 \\ \varepsilon\to 0}} \{\int_\varepsilon^\infty \frac{z}{(n^2+z^2)^{3/2}} \cdot \frac{dN}{dA} dA\} \quad \ldots\ldots 4.109$$

dN/dA is the number of charges per unit area $= 1/A_c.c^2$, dA is an element area. Then:

$$dA = c^2 \int_o^{2\pi} d\theta\, ds = 2\pi n\, dnc^2 \quad \ldots\ldots 4.110$$

Solving the integral gives:

$$V_O^{d,E} = -\frac{b_E \beta_E}{4\pi\varepsilon_o c^3} \frac{2\pi}{A_c} \quad \ldots\ldots 4.111$$

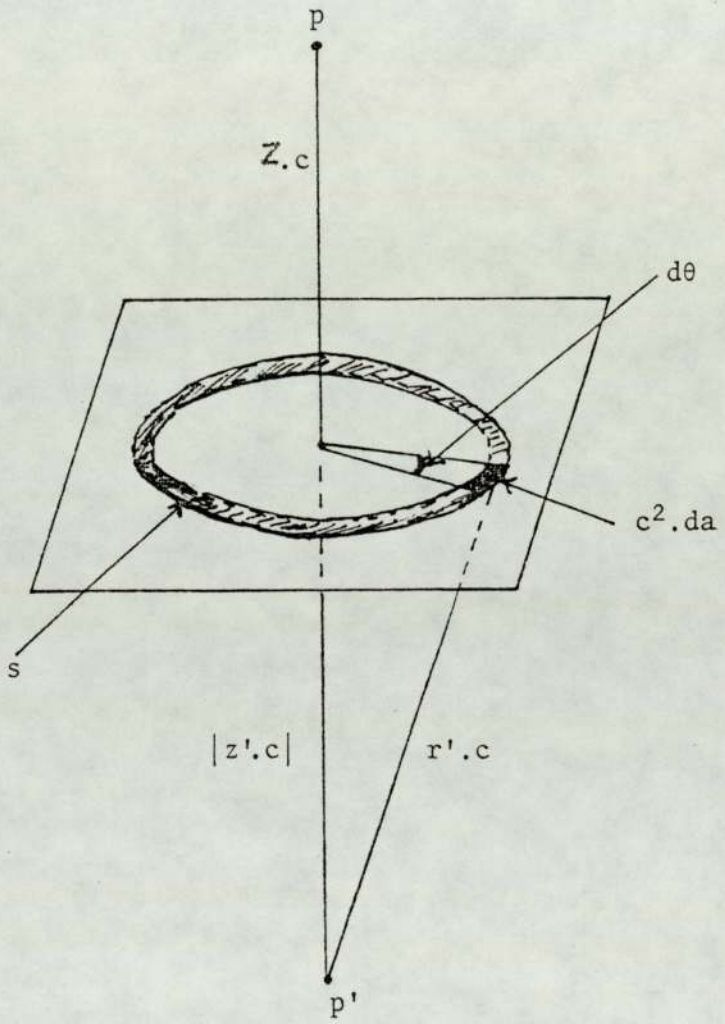

Fig.4.5

To illustrate integration over a uniform layer of dipoles

Putting eq.4.106 and eq.4.111 into eq.4.107 we have finally:

$$V_P^{d,E} = - \frac{b_E \beta_E}{4\pi\varepsilon_o c^3} \left[z S_1 + \frac{2\pi}{A_c} \right] \quad \ldots\ldots 4.112$$

4.7.4 The Potential due to the adsorbed layer of dipoles

The potential due to an adsorbed dipole layer (if present) can be expressed by a formula similar to eq.4.112 :

$$V_P^{d,A} = - \frac{b_A \beta'_A}{4\pi\varepsilon_o c^3} \left[z^* S_1^* + \frac{2\pi}{A_c} \right] \quad \ldots\ldots 4.113$$

where z^* is the dimensionless distance from the adsorbate layer to the chosen point above the emitter, and S_1^* is the corresponding summation factor. Note also that, if the adsorbed layer is present, then the quantities β'_A and β'_E as defined in section 4.4 should be used in eqs.4.105 to eq.4.112.

4.7.5 Total Potential

Finally, the total dimensionless potential of point P relative to $-\infty$ is given by:

$$V_P = V_P^m + V_P^{d,E} + V_P^{d,A} \quad \ldots\ldots 4.114$$

CHAPTER 5

COMPUTATIONAL PROCEDURES

5.1 Objectives

In order to make use of the field, potential and binding energy formulae derived in chapter 4, we need first of all to evaluate the summation factors S_o, S_1, S_2 and S_3, or/and the structure factors T_1, T^m and T^d. But except in a very specific case, the above factors are not being calculated. As far as we know, Topping[84] evaluated the factor K_1, (which is equivalent to the structural factor T_1 in our calculations as described in sec.4.1) for a square and hexagonal lattice array using analytical method, while Tsong[52] considered the factor K_2 (which is equivalent to T^d in our calculations). We conclude, that except in two very specific cases, where the structure factors are known, the effects of the crystallographic structure of the emitter have either to be ignored or approximated. In our view, that may lead to a big error in calculating quantities such as binding energy, as we shall see in chapter 6.

Rather than attempting to find some general analytical method to calculate those factors, we devised procedures for evaluating any desired summation or structure factor. We use computational methods to carry out mathematical summation to some reasonable limit, beyond which analytical approximation methods can be used. A comparison study shows that the values calculated using our technique have a margin of error comparable with or better than general analytical methods, as we shall see later in this chapter.

5.2 External Contributions and the Summation Circle

Obviously, when evaluating summation factors for an infinite planar array, we cannot carry on the summation to infinity. The trick being used is to carry on the numerical summation from a suggested "central point" to some limit, away from the central point, beyond which the summation is approximated by solvable integrals. Calling these the "internal" and "external" contributions, we thus have for each summation factor:

$$S = S(\text{int}) + S(\text{ext}) \qquad \ldots\ldots 5.1$$

It was originally thought that it would be easiest to carry out the "internal" summation over a square array. Hence some weeks were spent trying to obtain an analytical expression for fields and potentials above a plane of charge with a square cut from it. However the integrals involved have no analytical solution, and this approach was abandoned when it was realised that the corresponding integrals for a disc of charge are solvable.

The approach then adopted was to take a lattice point as the central point, and define a "summation circle" of fixed radius R_{CNT} ($= n_{CNT}.c$) about it, as shown in Fig(5.1). The dimensionless distance n_{CNT} is termed the "counting radius". The internal contribution is obtained by summing over all points inside the summation circle. The external contribution is obtained by replacing the lattice points outside the summation circle by a continuous distribution of the same mean surface density, and evaluating the relevant integral.

Take the evaluation of T_1 as an example. In this case $z = 0$, and the external contribution is evaluated from

$$T_1(\text{ext}) = \int \frac{1}{n^3} \frac{dN}{dA}\, dA \qquad \ldots\ldots 5.2$$

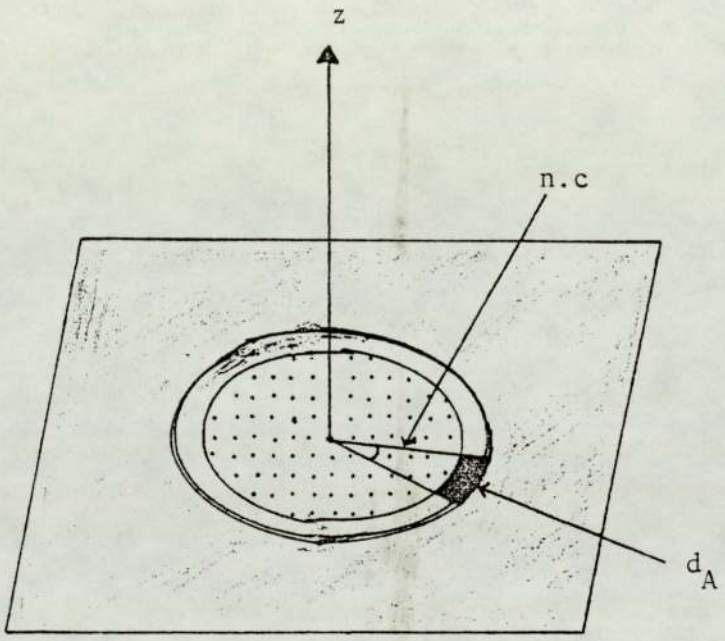

Fig.5.1

To illustrate the summation circle of radius R_{CNT}, and the continuous distribution outside it

As before, we write $\frac{dN}{dA} = \frac{1}{A_c . c^2}$. From Fig(5.1) it is clear that

$$dA = 2\pi nc \; . \; cdn \qquad \ldots\ldots 5.3$$

So:

$$T_1 \text{ (ext)} = \frac{2\pi}{A_c} \int_{n_L}^{\infty} \frac{1}{n^2} \, dn \qquad \ldots\ldots 5.4$$

$$= \frac{2\pi}{A_c . n_L}$$

where n_L is the radius of the circular disc excluded from the continuous distribution, and is termed the "calculation radius".

Initially, n_L was taken as equal to the counting radius. It was subsequently realised that the correct procedure would be to choose n_L such that the disc of charge excluded was exactly equal in magnitude to the amount of charge counted inside the counting circle. If the number of points inside the summation circle is N (CNT in the computer program), then we must have

$$2\pi n_L^2 \, c^2 = N \; . \; \frac{dA}{dN} = N \; . \; A_c . c^2 \qquad \ldots\ldots 5.5$$

$$n_L = (N \; . \; A_c / 2\pi)^{\frac{1}{2}}$$

Choosing the correct procedure for determining n_L was found to result in a very small correction.

In our preliminary tests we used a square lattice, and took c equal to the interatom spacing a. This provides an estimate of the quantity K_1 used by MacDonald and Barlow[85] and Tsong[52]. We then investigated how the estimate of K_1 varied with the choice of counting radius. The results of this are shown in Fig(5.2). It would seem that the larger the summation circle the more precise the results, but, of course, the greater

the number of points that have to be included in the summation and the longer the program takes to run. We settled on a counting radius of around 70·a as a suitable compromise.

An analytical determination of K_1 for square and hexagonal lattices was carried out by Topping[84] many years ago. These values and our computer-predicted values are shown in Table (5.1). Our values are within the limits of error predicted by Topping for his values, and we may take this agreement as evidence that our procedures are working satisfactorily.

Table 5.1

Array type	K_1 (Topping)	K_1 (computed)
Square	9.033623 ± 0.000006	9.033622
Hexagonal	11.034177 ± 0.000007	11.034176

5.3 Analytical Forms for the External Contributions (On axis)

5.3.1 The external contribution to S_1

We now must derive analytical expressions for the external contributions to the various summation factors. In this and the following sections it is assumed that the field point is on the axis of the defining circle.

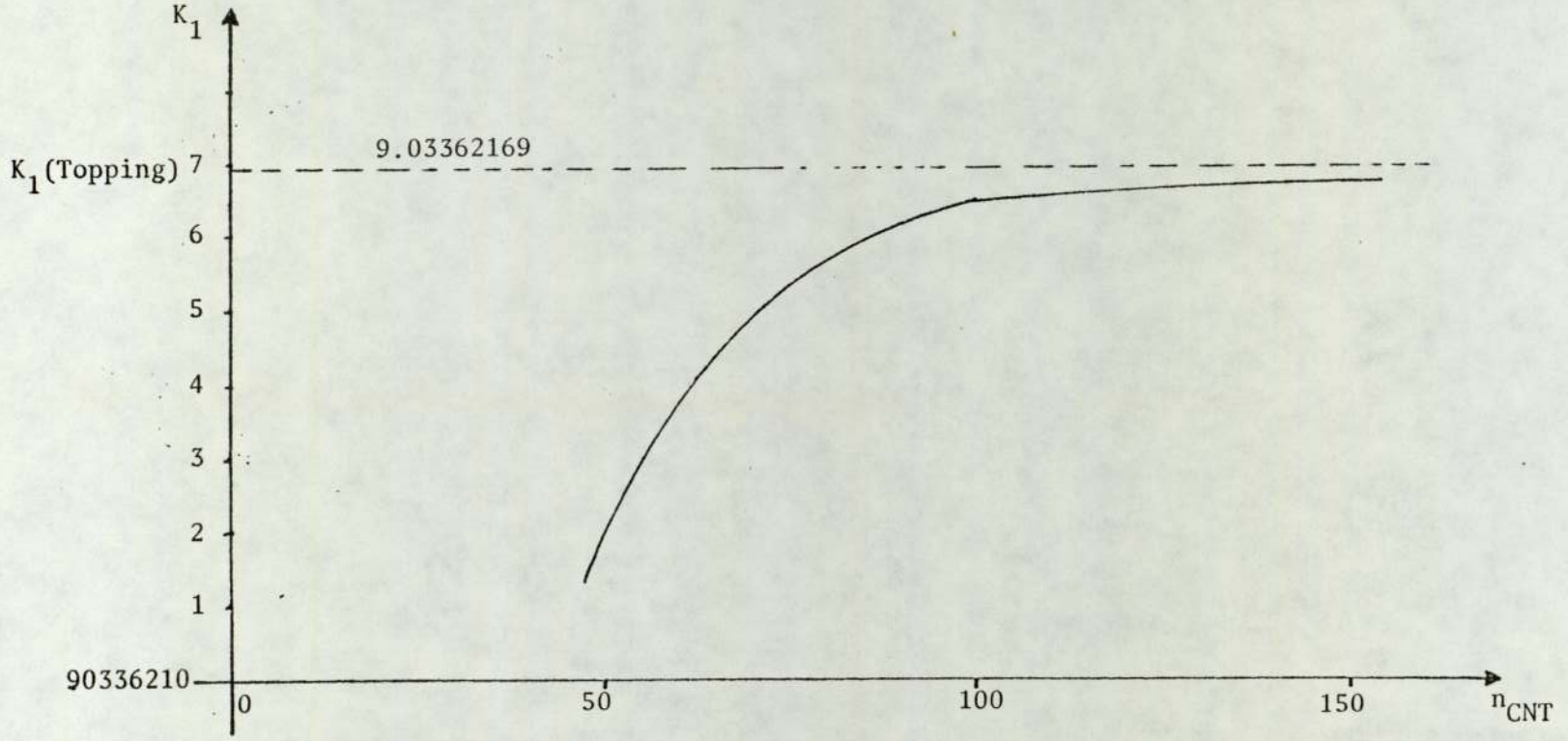

Fig.5.2

A graph shows the variation of the calculated summation factor K_1 with the counting radius n_{CNT}

The quantity S_1 is defined as:

$$S_1 = \Sigma \frac{1}{r^3}$$

Thus the external contribution is given by:

$$S_1 \text{ (ext)} = \frac{2\pi}{A_c} \int_{n_L}^{\infty} \frac{n}{r^3} \, dn \qquad \ldots\ldots 5.6$$

In writing this integral down, we have assumed the results given by equations 5.2, 5.3 and 5.4 in section 5.2.

Remembering that:

$$r^2 = (n^2 + z^2)$$

We have:

$$S_1 \text{ (ext)} = \frac{2\pi}{A_c} \int_{n_L}^{\infty} \frac{n}{(n^2 + z^2)^{3/2}} \, dn \qquad \ldots\ldots 5.7$$

$$S_1 \text{ (ext)} = \frac{2\pi}{A_c} \cdot \frac{1}{[n_L^2 + z^2]^{\frac{1}{2}}} \qquad \ldots\ldots 5.8$$

5.3.2 The external contribution to S_2

S_2 is defined by:

$$S_2 = \Sigma \frac{1}{r^5}$$

By an integration similar to that carried out above, we get:

$$S_2 \text{ (ext)} = \frac{2\pi}{A_c} \cdot \frac{1}{3} \cdot \frac{1}{[n_L^2 + z^2]^{3/2}} \qquad \ldots\ldots 5.9$$

Note that:

$$S_2 \text{ (ext)} = S_1 \text{ (ext)} \cdot \frac{1}{3.[n_L^2 + z^2]} \qquad \ldots\ldots 5.10$$

5.3.3 The external contribution to S_o

S_o is defined by

$$S_o = \Sigma \left[\frac{1}{r'} - \frac{1}{r}\right]$$

The external contribution is given by

$$S_o\,(ext) = \frac{2\pi}{A_c} \int_{n_L}^{\infty} n.\left[\frac{1}{r'} - \frac{1}{r}\right] dn \qquad \ldots\ldots 5.11$$

To carry out the above integral, we choose a point M at a distance beyond the lattice plane as shown in Fig(5.3). The above integral can be written as

$$S_o\,(ext) = \frac{2\pi}{A_c} \int_{n_L}^{\infty} n.\left[\left(\frac{1}{n} - \frac{1}{r}\right) + \left(\frac{1}{r'} - \frac{1}{n}\right)\right] dn \qquad \ldots\ldots 5.12$$

Remembering that $r = (n^2 + z^2)^{\frac{1}{2}}$, and $r' = (n^2 + z'^2)^{\frac{1}{2}}$, then by substituting in the above equation and integrating we get

$$S_o\,(ext) = \frac{2\pi}{A_c} \left[(n_L^2 + z^2)^{\frac{1}{2}} - (n_L^2 + z'^2)^{\frac{1}{2}}\right] \qquad \ldots\ldots 5.13$$

(A suitable choice of z' value is taken to be - 3.a, usually).

5.4 Evaluating the Internal Contribution

With the internal contribution the essential problem is to decide the order in which the summation over lattice points is to be conducted. At each lattice point the contribution to each of the summation factors is then determined in sequence, and added into the running totals. It is possible in many cases to take advantage of mirror plane symmetries to reduce the number of program steps. We shall first describe a systematic procedure for "visiting" every point inside the summation circle.

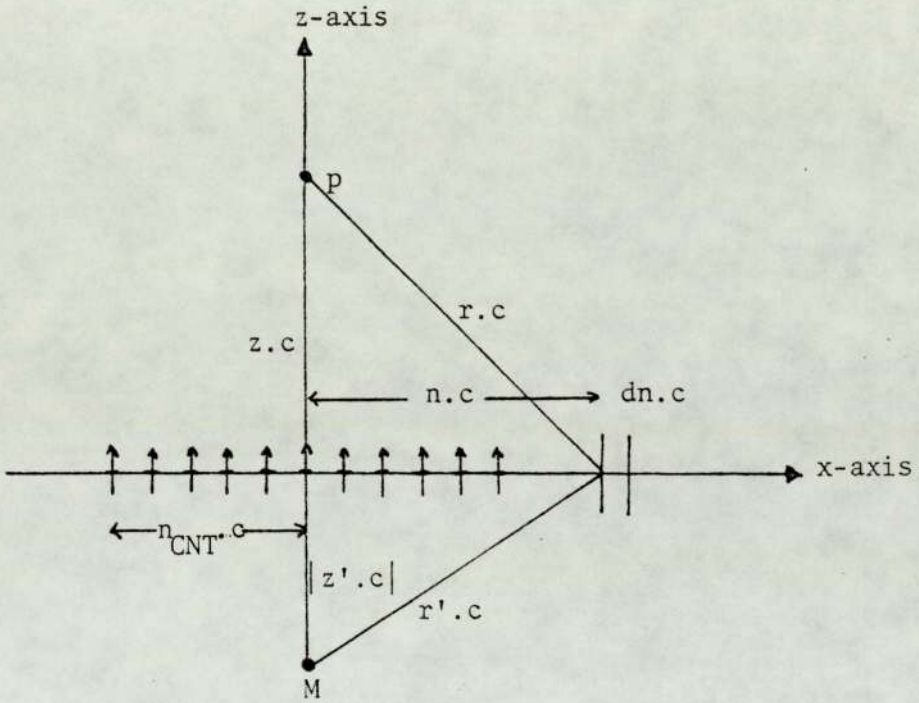

Fig.5.3

To illustrate the calculation of S_o

Initially we shall assume that the field point P at which fields and potentials are to be evaluated is directly above an array point, (which we shall label "O"). This is certainly the case in the calculations concerning field adsorption. We shall consider the summation circle as centred at "O" and having radius 70.0001 . d_x . c; that is, the summation circle has a radius just greater than 70 times the unit cell dimension in the x-direction. By taking 70.0001, rather than 70 exactly, we ensure that no array point lies exactly on the summation circle; this will avoid any difficulties in deciding, during program execution, whether a given array point lies inside the circle.

In general, in our work, we need to deal with a centred rectangular lattice. Take the point O as having coordinates (0,0). Points that have coordinates that are integral multiples of d_x.c and d_y.c may be designated "corner points"; points with half-integral coordinates are designated "centre points" as shown in Fig(5.4a). We first evaluate the summation factors over all the "corner" points, and then proceed with the "centre points" (if these are present).

Considering just the corner points (shown by blacked circles in Fig.(5.4a), we exclude the central point O and divide the summation circle into four "quadrants". In the program there is a subroutine that deals with evaluation over a quadrant. In quadrant I, this works as follows:

(1) The procedure starts at the innermost corner of the quadrant.

(2) Keeping the X-coordinate fixed, the summation works up the Y-axis until the counting circle is reached.

(3) The X-coordinate is then increased by d_x, and then summation then works up the next line of points.

(4) The procedure stops when the X-coordinate exceeds the counting radius.

The arrows in Fig(5.4a) illustrate this process, and show that the visiting

Fig.5.4a

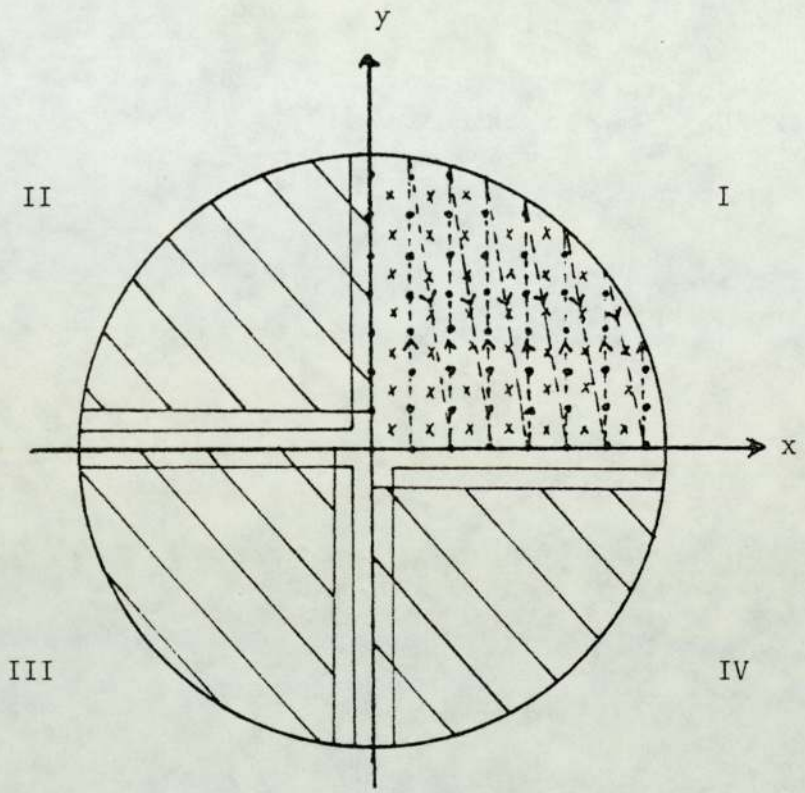

A schematic diagram shows the process of the visiting procedure of the computer program

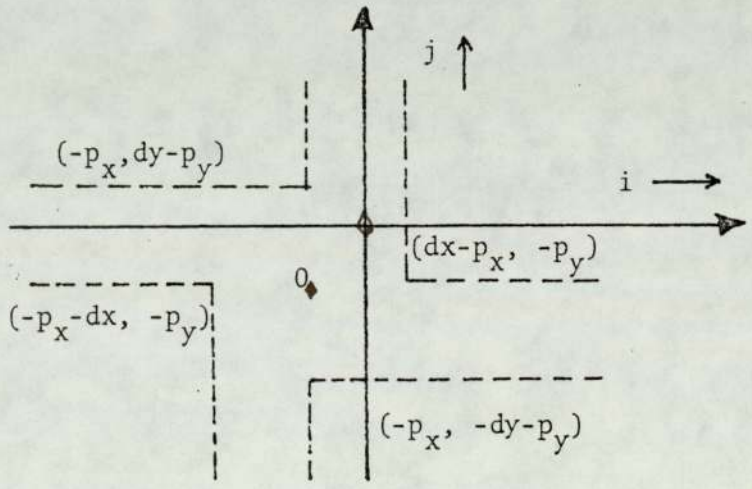

Fig.5.4b

A magnified scale of a region near the centre of the summation circle

sequence in this quadrant can basically be described as "vertically upwards".

The way in which this is implemented in the programming is illustrated in the block diagram shown in Fig(5.5). Note that we have chosen to test whether each point is inside the circle, by a statement of the type: "Is $(x^2 + y^2) \geq (n_{CNT})^2$?"

The starting points and increments in the subroutine can be set, so this can be used to evaluate the contribution of each quadrant in turn, by "vertically upwards" or "vertically downwards" visiting sequences (as appropriate). If the array is "centred" then the four quadrants of centre points can be processed similarly. And, finally, the contribution of the central point "O" is added in, if appropriate.

5.5 More general calculation of summation factors

The weakness with the previous summation-factors analysis is that it deals only with points on the axis that passes through a single chosen point in the emitter array plane. Consequently all the information which can be extracted (e.g. binding energy and potential) is limited to the perpendicular line that passes through the chosen "central point".

Procedurally there are two methods of overcoming this difficulty. The first is to rewrite the computer program everytime information is needed for a chosen point other than the array point initially chosen as the central point. The second is to modify the computer program by introducing "field-point coordinates".

Initially we developed several slightly different programs to serve the first option, but we subsequently abandoned that option, and diverted attention towards developing a "general multipurpose computer program" that would be suitable for any symmetry point. Let us call the new field point P, and let the coordinates of the symmetry point, relative to the

array point originally taken as the centred point "O", be (p_x.c, p_y.c, z.c).

It is straightforward to derive an expression for the quantities $\frac{1}{r^3}$ that are needed for the evaluation of summation factors. But there is a problem, or at any rate a choice, in deciding how the "internal" and "external" contributions are to be defined. The two main alternatives are:

(1) To keep the summation circle centred on the original array point O. In this case the "visiting" process remains the same as before, but it is necessary to develop new expressions for "off-axis" external contributions. (It turns out that there is no simple analytical expression, and approximations have to be made).

(2) To move the centre of the summation circle to the point (p_x.c, p_y.c, O), directly below the point P. In this case the external contribution is given by the same formula as before, but care has to be taken to get the limits of the "visiting" process correct; there is also the possibility of small artefact errors due to asymmetries in the counting process just inside the summation circle, as between opposite sides of the circle.

At one stage of the research, when interest centred on the calculation of fields, alternative (1) was adopted. Expressions for "off-axis" values of S_1 (ext) and S_2 (ext) were obtained, the results being

$$S_1 \text{ (ext)} \simeq \frac{2\pi}{A_c} \left[\frac{1}{n_L} - \frac{r^2}{2.n_L^3}\right] \quad \ldots\ldots 5.14$$

$$S_2 \text{ (ext)} \simeq \frac{2\pi}{A_c} \left[\frac{1}{3.n_L^3} - \frac{r^2}{2.n_L^5}\right] \quad \ldots\ldots 5.15$$

Derivations of these results are given in Appendix (A). Alternative (1) was subsequently used by Forbes (unpublished work) to produce a set of programs for the calculation of fields and potentials.

At a later stage, however, it seemed better to change to alternative (2). Partly this was due to the program philosophy we were using, but it was also wished to avoid the approximations inherent in equations 5.14 and 5.15 above. It was also realised that for points P on a symmetry axis there would be no artefact errors as mentioned above; so alternative (2) might in principle be more accurate than alternative (1).

With alternative (2) particular care has to be taken in choosing the limits of the "visiting" process, and we now look at this in more detail. We first consider the summation over the "corner points" as defined in section 2. Fig(5.4b) shows, on a magnified scale, a region near the centre of the array considered previously. The central point O is shown, and the four counting sectors previously used are marked with dashed lines. The centre of the new summation circle, at $x = p_x$, $y = p_y$ (relative to O), is marked with a diamond, and the axes of the new summation circle are shown as full lines. If we let dimensionless distances relative to these new axes be i, j, then clearly dimensionless coordinates in the new and old systems are related by:

$$i = x - p_x \qquad \ldots\ldots 5.16$$

$$j = y - p_y \qquad \ldots\ldots 5.17$$

In the new approach the array points in each sector are still visited in a vertical upwards or vertically downwards sequence, as before, but now the "D O" loops in the program have the form:

FOR i = "i-start" STEP "$\pm d_x$" UNTIL "$\pm n_{CNT}$" DO...

FOR j = "j-start" STEP "$\pm d_y$" UNTIL "$\pm n_{CNT}$" DO.

- the appropriate choice of plus or minus signs being made according to sector. The coordinates (i, j) of the "starting points" for each sector are shown in Fig(5.4b).

A generally similar argument applies to the starting points for the "centre points" when present.

In the program the procedure SUM (L1, L2, L3, L4, INC 1, INC 2) is used to evaluate the contribution of each sector to the various summation factors. This procedure has six parameters, corresponding to the parameters in the "DO" loop. For example, the contributions of sector 1 of the "corner point" are added in by means of the instruction:

SUM (DX - PX, CNTR, - PY, CNTR, DX, DY)

(CNTR is the program representation of the counting radius of the summation circle).

In the program, the evaluation of the summation factors for a given field point is carried out by a procedure EVAL. This calls SUM four times for a primitive lattice (eight for a centred lattice), and also has instructions that ensure that the contribution due to point O is included in the summation factors where relevant.

The heart of the programming has been the development of these two procedures. These procedures must now be incorporated into a complete program.

5.6 Description of the Computer Program

The main purposes of the computer program are of course: the calculation of field adsorption binding energy, for different emitter surface atoms and inert gas adsorbed atom(s) systems; the determination of the position of the critical surface; and the investigation of the field and potential variation above an emitter surface. Many byproduct variables can be

evaluated also, like number of lattice points inside the counted circle, the radius of the counted circle, the value of the summation and structure factors, the components of field and potential appearing in their specific formulas like M_A, M_E, $\gamma_A^{d,E}$ ... etc, and the repulsive force ratio (η).

The program is designed to work for optional choice of any crystallographical surface array structure, with or without the existence of adsorbed layer (i.e. for single or double layer). Fig(5.5) shows the flow chart of the program, whilst a standard copy of the actual program is reserved in appendix (B). It is divided into four parts; each part is designed for a specific purpose.

Part 1 - The data:- This part is the beginning of the program. Its first half is designated for the data needed to be fed each time we run the program (i.e. input data). Those are:

(1) some information about the species of metal and adsorbed atom in question (i.e. atom radius and polarizability)
(2) value of external field
(3) value of lattice parameter
(4) values of surface array parameters
(5) values of chosen point coordinates
(6) surface structure type (i.e. face-centred or primitive)

The second half contains some useful fixed data like the value of $(4\pi\varepsilon_o)$, some convenient counting circle radius (CNTR) value, and a convenient chosen reference point (W_z) for the purpose of potential calculation later in the program, beside few simple calculations to evaluate some fixed variables needed later in the program.

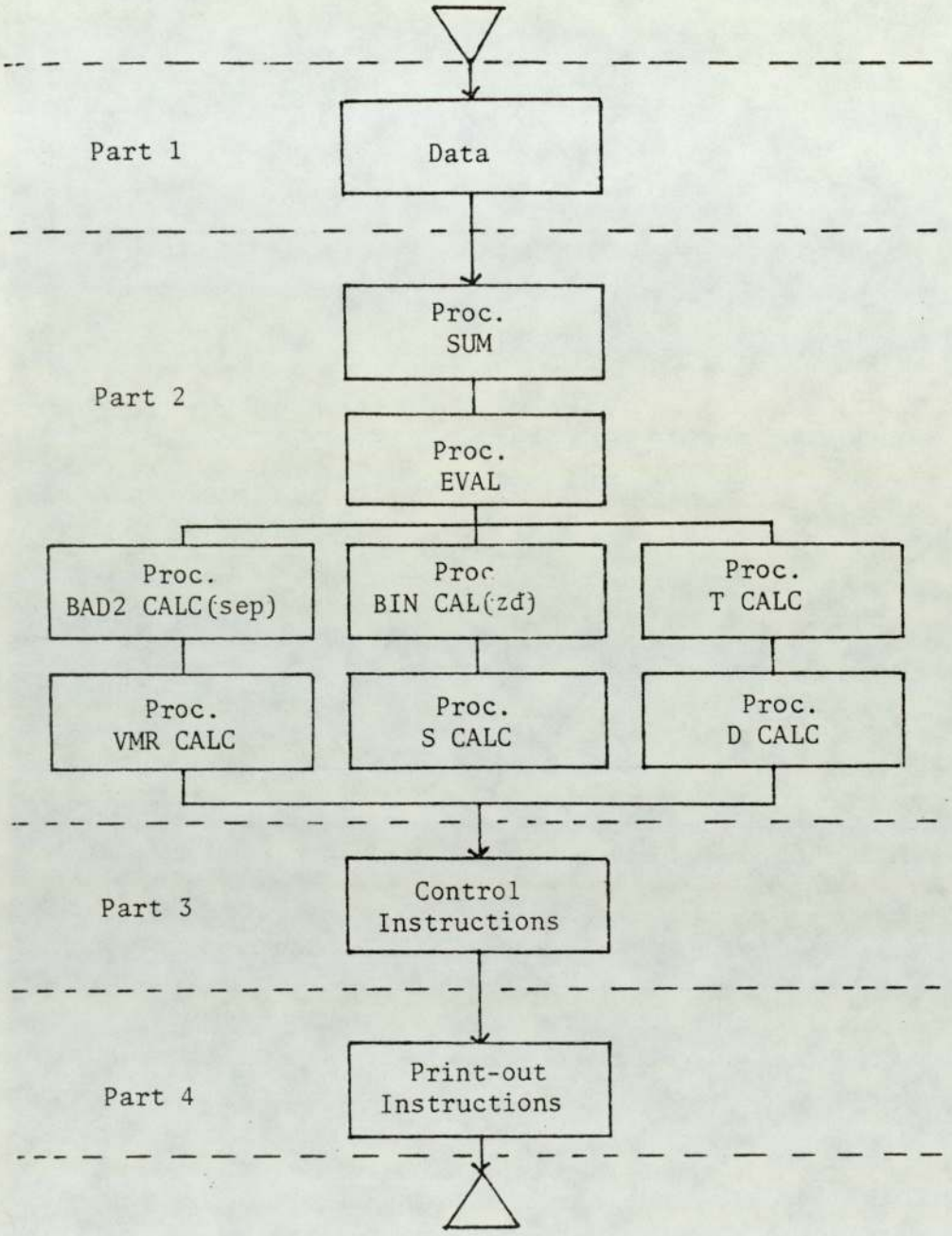

Fig.5.5

The flow chart of the computer program

Part 2 - The Procedures:- This constitutes the main part of the program, and contains eight procedures; each one is dedicated for the evaluation of particular variables. Including the two procedures just described in detail, these are:

(1) Procedure SUM:- This evaluates quadrant summation factors S_o, S_1, S_2 and S_3 in one of the four summation-circle quarters designated by the next procedure.

(2) Procedure EVAL:- Its purpose is: (i) to evaluate the total summation factors in the four quarters of the circle by repeated calling on procedure Sum, with suitable argument for each quadrant and type of lattice point; also central point if appropriate; (ii) it works out the calculated radius (n_L, or CALR); (iii) it calculates the external contribution to the summation factors, and adds this in to the summation factors.

(3) Procedure BAD2 CALC (SEP):- For specific separation of the E-A layers provided by the argument (SEP), the procedure evaluates the square of the field ratio for a double layer at the position of an adsorbed atom, $(\beta'_A)^2$, and various related parametres (e.g. β'_E can be also calculated with this procedure).

(4) Procedure BIN CALC (ZD):- For a specific E-A layer separation distance provided by the argument (ZD), this procedure evaluates the conventional binding energy (BIN CONV), the repulsive potential ratio (ETA), and hence the corrected binding energy (BINCORR).

(5) Procedure T CALC:- This calculates the structure factors T_1, T^m and T^d.

(6) Procedure VMRCALC:- This calculates the monopole reference point potential.

(7) Procedure S CALC:- This calculates the field ratio β and the potential ratio V from their monopole and dipole contributions for a single layer, presenting these as the variables BSL and VSL.

(8) Procedure D CALC:- This calculates the field ratio and the potential ratio from their monopole and dipole contribution for a double layer, presenting these as the variables BDL and VDL.

Part 3 - Control Instructions:- This part gives instructions for the desired calculations, which can be easily carried out by calling on the procedures.

Part 4 - Print-out instructions:- Calculated variables are printed out in a form appropriate to the investigation in question.

CHAPTER 6

RESULTS AND DISCUSSION: FIELDS AND POTENTIALS

6.1 Applications of the Array model

We shall now apply our model in a practical situation mainly to investigate the two groups of scientific problems reviewed in earlier chapters: first, those associated with fields and potentials above the emitter surface, and hence the shape and location of the critical surface (and the effect of field variations in the critical surface upon the field-ion imaging processes); second, those associated with calculating field-adsorption binding energies. This chapter deals with the first group of problems; chapter 7 with the second.

As an exemplary system we have chosen one of the most common field-adsorption situations known in FIM. That is tungsten (W) as an emitter, and helium (He) as the adsorbed layer of inert gas atoms.

Mathematically, our model can be applied to any crystallographic face with a face-centred or simple rectangular structure. But it needs to be recognised that our model is limited to one emitter-atom layer, namely the outermost surface plane layer. Any physical contribution of the second and inner layers of the emitter has been ignored. (This avoids complexities associated with the state of charge distribution as between, for example, the first and second-layer atoms). Thus, to use our model in a realistic way, we must confine our studies to surface structures where the second, third .... etc. layer atoms are adequately shielded by the surface layer atoms.

In our view there are two requirements for "adequate shielding". First that the facet in question be relatively close-packed, or nearly so. This requirement reveals itself in our calculations through high values of the structure factor T_1. Second, that the second-layer atoms be

suitably recessed into the surface.

Careful study of the pictures in Nicolas' atlas of crystal models[87] suggests that only seven of the surface array planes satisfy (or nearly so) the above two conditions. These are listed in table 6.1 with some other useful information. One of those array planes, namely the (111) plane, is used extensively in this chapter as a paradigm situation for our charged metal surface model, and to compare our calculations and results to that of previous discussions. This (111) plane is hexagonal in structure, with smallest interatom spacing equal to $c\sqrt{2}$. For tungsten c = 0.3165 nm, $c\sqrt{2}$ = 0.4476 nm.

So for the sake of discussion, the case of field adsorption of helium (He) on this (111) plane of tungsten (W) is being chosen, and we assume that an infinite array of tungsten atoms is covered by a similar array of helium atoms, as assumed in chapters 3 and 4. To compare our model with previous treatments we shall also need to consider the following lattice structures:

(1) A square lattice, with surface lattice parameter (a) equal to the interatomic spacing in the (111) face of tungsten (i.e. a = 0.4476nm). We call this "model 1" (abbreviated as mdl 1).

(2) A square lattice having the same area per lattice point as the hexagonal (111) lattice (i.e. a = $(3^{\frac{1}{4}}/2^{\frac{1}{2}})$ x 0.4476 nm = 0.4165 nm). We call this "model 2" (abbreviated as mdl 2).

To derive structure factors and other parameters for these two models, we can make use of the fact that the 100 plane of a bcc crystal structure is a simple square array of side length c. Thus, for example, to derive a value of M_E for these models we insert the T_1 value for the 100 face into eq.4.28 and replace c by a. This results in the formula

TABLE 6.1

Values of the structure factors T_1, T^m, and T^d, and M_E for specified lattice structures

Facet	Lattice Parameter		A_c	F.C.	Structure factor			M_E for
(hkl)	dx	dy	= dx dy	*	T_1	T^m	T^d	$b_E = 2b°$
100	1	1	1		9.033621	7.880183	1.096680	1.8207451
110	1	$\sqrt{2}$	$\sqrt{2}$	*	15.037595	10.953974	0.62737	2.3662331
111	$\sqrt{2}$	$\sqrt{6}$	$2\sqrt{3}$	*	3.901170	4.857514	1.872235	1.3544388
210	1	$\sqrt{5}$	$\sqrt{5}$		3.720067	4.306036	2.571067	1.3379851
211	$\sqrt{2}$	$\sqrt{3}/2$	$\sqrt{3}/\sqrt{2}$		7.500860	6.667411	1.652951	1.6814868
310	1	$\sqrt{10}$	$\sqrt{10}$	*	5.035373	5.353430	1.936465	1.4574862
411	$\sqrt{2}$	3/2	$3/\sqrt{2}$	*	8.266720	7.461686	1.178546	1.7510687

b^θ = 1 meV V^{-2} nm^2

$$M_E = 1 + \frac{b_E T_1 (100)}{4\pi\epsilon_o a^3} \qquad \ldots\ldots 6.1$$

We now must consider the choice of polarizability values.

The SI polarizability of helium $b_{(He)}$, is taken as 0.143 meV $V^{-2}nm^2$ [75]. But for the SI polarizability of tungsten surface atom, three values are used:

(1) $b(W_T)$ = 3.19 meV $V^{-2}nm^2$, which is the value used by Tsong and Müller; this will enable comparisons to be made between the present results and previous work.

(2) $b(W_{MB})$ = 7 meV $V^{-2}nm^2$, which is the "upper limit" discussed earlier (sec 3.5); and

(3) $b(W_{SF})$ = 2 meV $V^{-2}nm^2$, which is the lower limit discussed earlier. The Gaussian polarizabilities corresponding to the above SI quantities are, respectively: 0.206Å^3, 4.6Å^3, 10Å^3, and 2.9Å^3

6.2 The depolarization effect

One of the basic characteristics of a layer of dipoles (as in the emitter or adsorbed layer) is that each of these dipoles exerts an electric field on its neighbouring dipoles: this tends to reduce the local field acting on them (i.e. the field that passes through a dipole normal to the surface of the emitter), and hence creates a depolarization effect. This effect was ignored in the IDP model (see refs [15, 52]), but - as we shall see later - has to be taken into consideration.

The depolarization effect is represented mathematically by the parameter M, which plays the role of a relative permittivity for a layer (see sec 4.2). The depolarization effect as illustrated by M_E is a function of the emitter surface atom polarizability b_E and the structure

factor T_1. The structure factor T_1 itself is a geometrical function that depends on the degree of close packing of the emitter surface (as expressed by area per atom), and on the lattice structure.

To demonstrate the above effects, we show in table 6.2 some typical value of M calculated for the lattice structures and polarizability values mentioned in sec 6.1. The IDP approximation has also been formally included by setting M equal to unity.

Inspection of the table shows clearly that choice of a square lattice equal in area per atom to the (111) unit cell (mdl 2) gives closer results than choice of a square lattice with equal inter-atom spacing (mdl 1), indicating that area per atom is the more significant factor. Obviously, also, increasing the polarizability increases the value of M_E.

We also show in table 6.1 values of M_E for tungsten (using $b = 2b^\theta$), for the various lattice structures.

6.3 Properties of the single layer

In this section we study the behaviour of potentials and fields (in terms of the dimensionless potential ratio V and field ratio β, as assumed in chapter 4) above a single emitter layer of tungsten atoms.

6.3.1 Potentials above the bare emitter layer

We show in figs. 6.1 to 6.5, for the paradigm case of the W(111) surface, the potential variation normal to the surface due to, first the monopole distribution, second the dipole distribution, and third the two distributions jointly. In the case of the dipoles, the two polarizability values $b = 2b^\theta$ and $b = 7b^\theta$ are used. [For brevity, we henceforth use the symbol b^θ to mean 1 meV $V^{-2}nm^2$, and $4\pi\varepsilon_o$ x 1.44 $\mathring{A}^3$]. Potentials are shown above an array point (i.e. above a surface atom) and above a point midway between array points (i.e. between surface atoms).

TABLE 6.2

Values of the parameter M, for specified lattice structures and polarizability values

Type of Lattice	a nm	$b(He)_{\theta}$ $0.143b_{\theta}$	$b(W_{S/F})_{\theta}$ $2.00b_{\theta}$	$b(W_T)$ 3.19b	$b(W_{MB})_{\theta}$ $7.00b_{\theta}$
Hexagonal	0.4476	1.025	1.354	1.565	2.240
Square (mdl 1)	0.4476	1.021	1.290	1.463	2.015
Square (mdl 2)	0.4165	1.026	1.360	1.574	2.260
IDP aprx.	0.4476	1.000	1.000	1.000	1.000

With the monopole distribution the above-atom potential approaches minus infinity as the plane of the surface nuclei is approached, whereas the between-atom potential tails off towards zero as the interior of the emitter is approached. Note that both potentials tend to the same straight line as distance from the surface increases, and that this straight line would pass through the origin of coordinates if projected back. Also, the gradient of the line is unity. Thus at large positive distances:

$$V^m \to z$$

or

$$v^m \to z.c.eF \ (= eFR_z) \qquad \ldots\ldots 6.2$$

where v is the electrostatic component of the potential energy of an electron, as discussed in section 4.1 and v^m is that part of it due to monopoles.

With the dipole distribution, the effect at large distances is clearly equivalent to a negative step in potential V (relative to the emitter interior), with the size of the step being larger as the assumed surface-atom polarizability gets larger. As before, the above-atom potential tends to minus infinity as the plane of the array is approached, whereas the between-atoms potential changes smoothly.

The potential due to the monopoles and dipoles together is shown in Figs. 6.4 and 6.5, and several points deserve notice. Obviously, as before, the potential tends towards a straight line of gradient unity, as distance increases. But, if projected back, the line now cuts the distance axis at a point $R_z = d$ (or $z = z_d$), and cuts the V-axis at a value $V = V^\circ$, with the numerical values of these intersection points depending on the surface-atom polarizability. This graph illustrates the points made by Forbes[82], which were: first, that if we were to think of the "surface" of the metal as the plane of the surface-atom nuclei, then the effect of

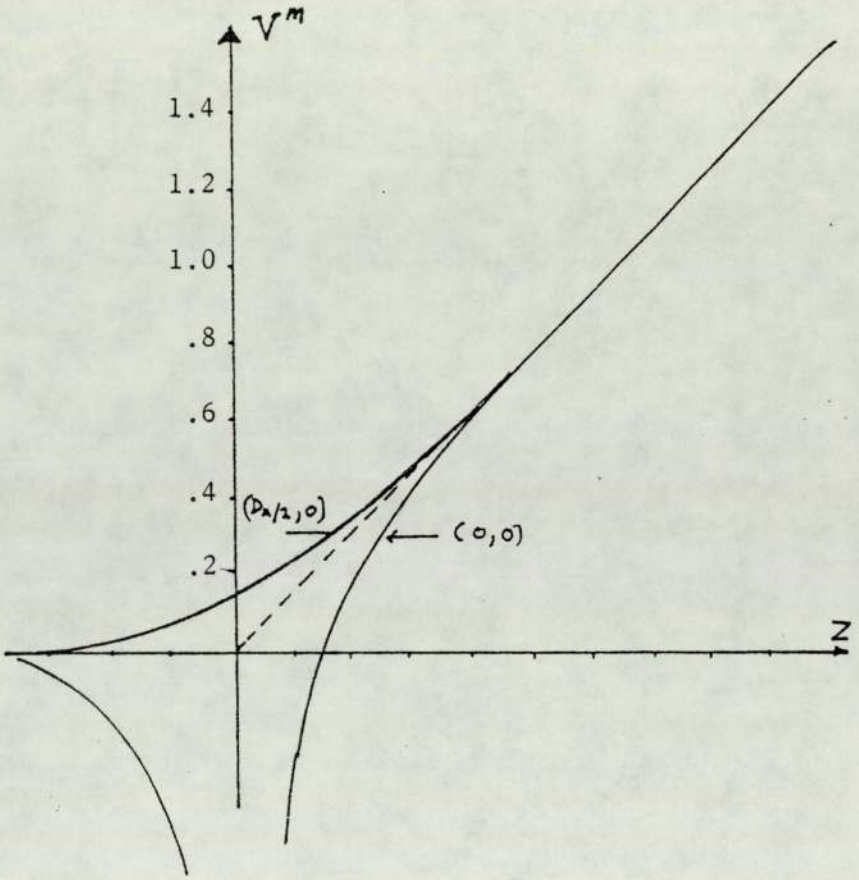

Fig 6.1

Variation of the monopole potential ratio V^m with the distance ratio z

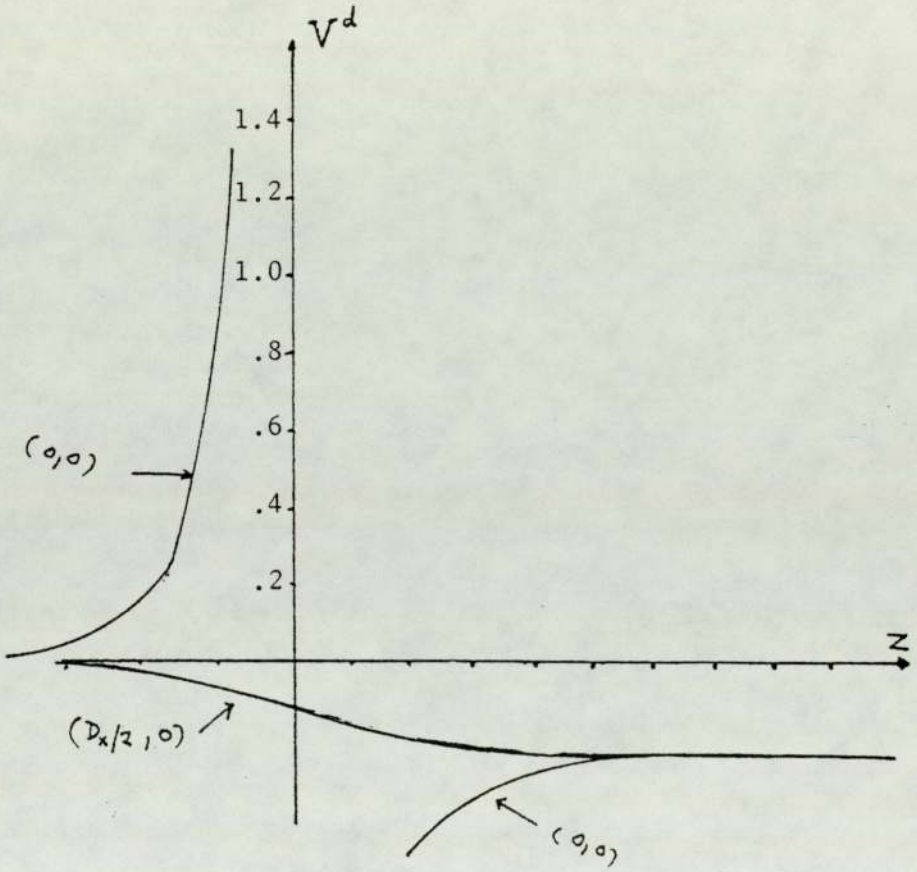

Fig 6.2

Variation of the dipole potential ratio V^d with the distance ratio, for $b_E = 2b^\theta$

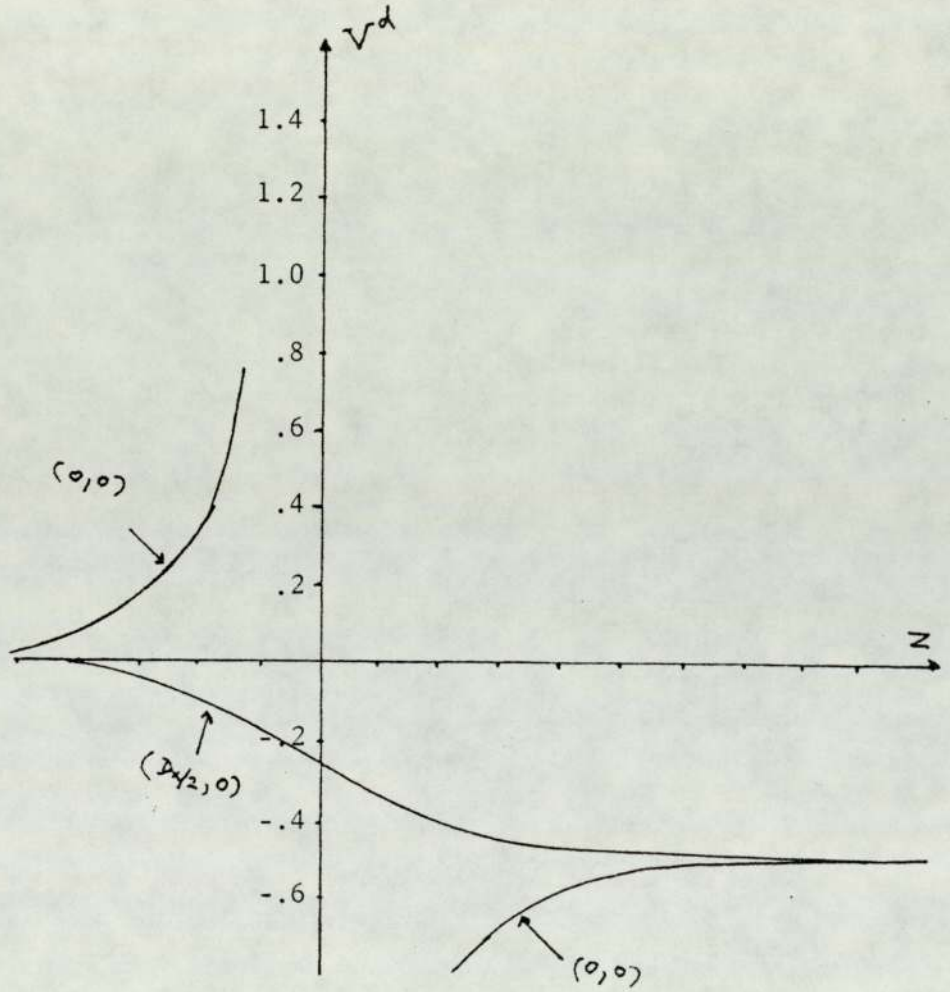

Fig 6.3

Variation of the dipole potential ratio V^d with the distance ratio z, for $b_E = 7b^\theta$

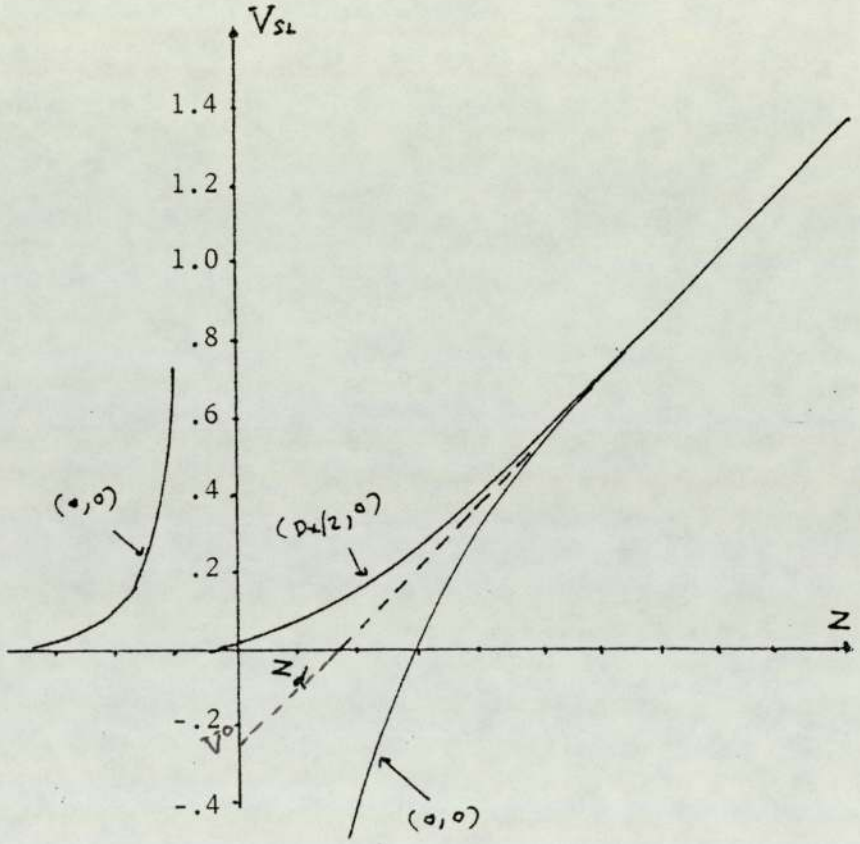

Fig 6.4

Variation of the potential ratio above a single layer V_{SL} with the distance ratio z, for $b_E = 2b^{\theta}$

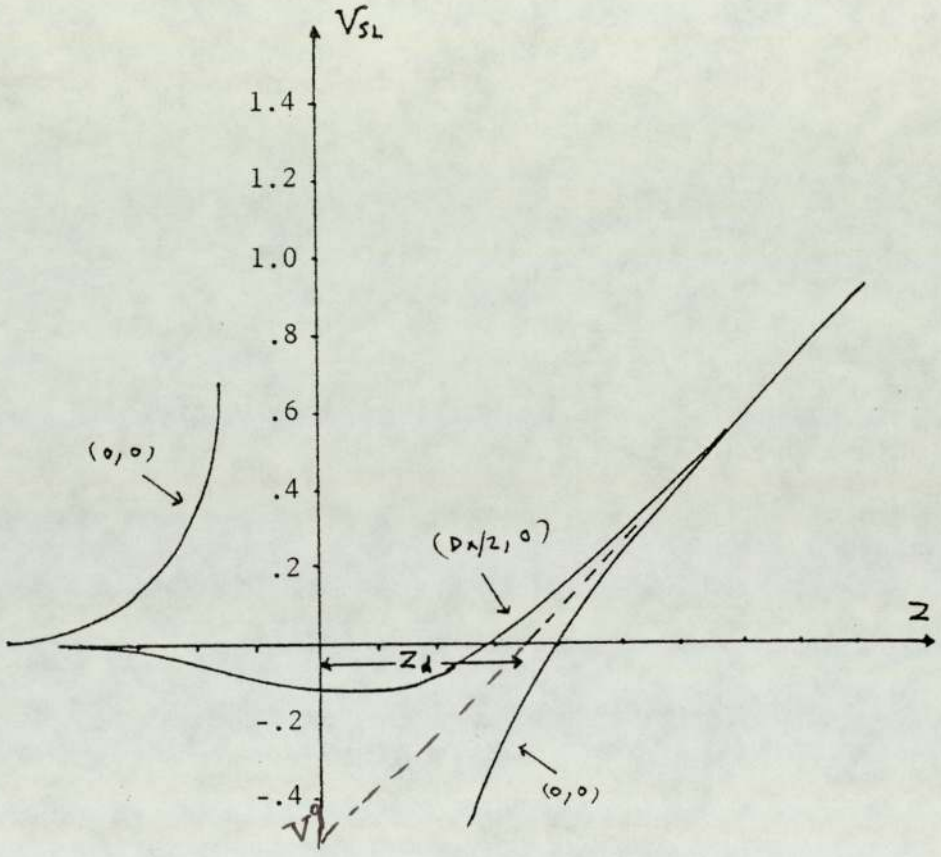

Fig 6.5

Variation of the potential ratio above a single layer V_{SL} with the distance ratio z, for $b_E = 7b^{\theta}$

the layer of polarized dipoles is to be interpreted as a "negative work function correction $\delta\phi^o$". Alternatively, we may interpret the effect of the layer of dipoles as a repulsion outwards of the electrical surface of the metal, by a distance d which we may term the repulsion distance.

It is straightforward to derive formulae for the above quantities from our earlier theoretical discussion. Thus we have:

$$\delta\phi^o = -\tfrac{1}{2} b_E e F^{ext}/A_c.c^2\varepsilon_o M_E \quad \ldots\ldots 6.3$$

$$V^o = -\tfrac{1}{2} b_E/A_c.\varepsilon_o c^3 M_E \quad \ldots\ldots 6.4$$

$$d = -\delta\phi^o/eF^{ext} = \tfrac{1}{2} b_E/A_c.\varepsilon_o c^2 M_E \quad \ldots\ldots 6.5$$

$$z_d = \tfrac{1}{2} b_E/A_c.\varepsilon_o c^3 M_E \quad \ldots\ldots 6.6$$

(In interpreting these formulae note that M_E is a function of b_E).

In these formulae V°, d and z_d are independent of the external field, but $\delta\phi^o$ is not. Thus, when working in real coordinates, it is better to think in terms of the repulsion-outwards effect, so, at large distances from the surface we write:

$$V \underset{z\to\infty}{\to} z - z_d$$

$$v \underset{z\to\infty}{\to} eF(R_z - d) \quad \ldots\ldots 6.7$$

It is then more convenient to define a new real coordinate normal to the array plane, and denoting this by $x^\dagger$, we have:

$$x = R_z - d \quad \ldots\ldots 6.8$$

which leads to the formulae:

$$v \underset{x\to\infty}{\to} eFx \quad \ldots\ldots 6.9$$

† This x has to be distinguished from the dimensionless coordinate in the plane of the array. In practice no confusion arises.

We call this x the "distance from the metal's electrical surface"

Obviously, formula 6.9 has the same form as eq.2.13 derived from the jellium model, as discussed in section 2.4.2. For practical purposes we may identify the variable x defined here with the variable x used there, and this gives the relationship between the two models. This relationship is illustrated partly in fig. 2.2 and partly in the figure below.

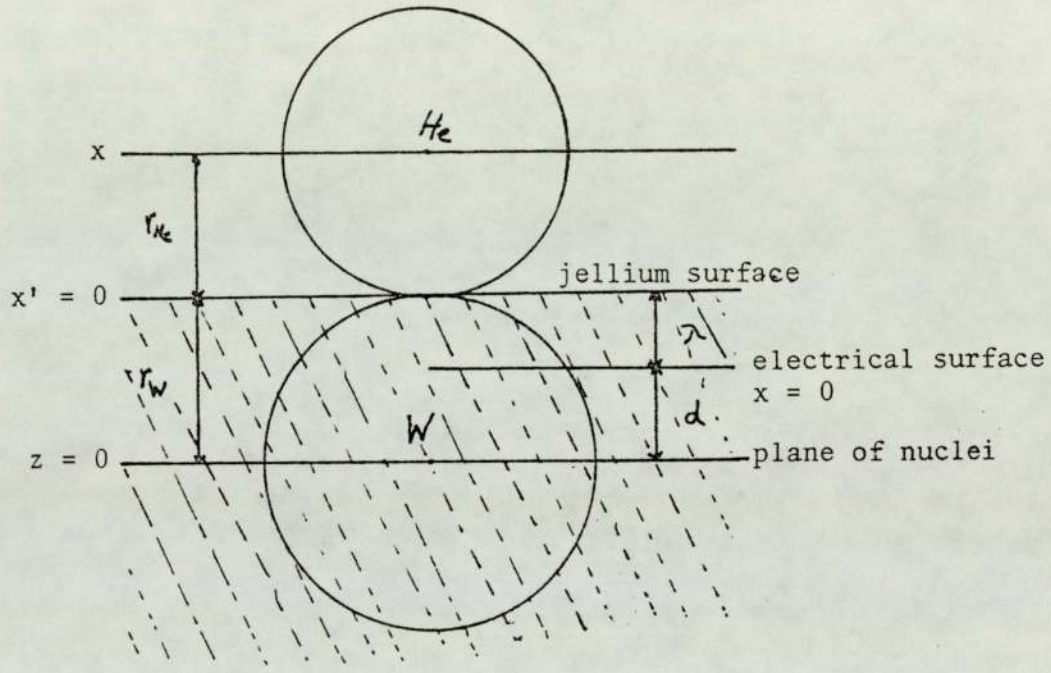

Two general points need to be made at this stage. First, the characteristics discussed above apply qualitatively to all the crystallographic surfaces, but there are numerical differences - for example, in the value of d, or in the rapidness with which the potential approaches the "straight-line value".

The second point relates to the physical validity of the calculated potentials. Our model of course uses point charges and dipoles, and the corresponding model potentials are electrostatically valid at all points in space. However, the charges and dipoles are meant to represent the charge distribution at a real surface. The model potentials will not be

valid at any point significantly inside the charge clouds of the emitter surface atoms: but outside the substrate charge distribution the Hellman-Feynman theorem will apply. That is, if the postulated distribution of monopoles and dipoles represents the actual charge distribution adequately, then - outside the substrate charge clouds - the real and model potentials and fields coincide.

6.3.2 Fields above the bare emitter layer

We show in figs. 6.6 to 6.8 for W(111), the field variation normal to the surface due to the monopole, dipole ($b_E = 2b^\theta$), and joint monopole-dipole distribution (jointly for both $b_E = 2b^\theta$ and $b_E = 7b^\theta$).

With the monopole distribution the above-atom field approaches infinity as the plane of the surface nuclei is approached, whereas the between-atom potential has a value of (½) at the surface. This is obvious since at a symmetrical point inbetween surface atoms the field components, due to the surface monopoles cancel each other and we only have the contribution (½) due to the distant negative charges. Both the above and inbetween atoms β-curves converge to unity rapidly. At distances from the surface comparable with the critical distance of elementary theory, the field difference $\Delta\beta^m$ as between above and between-atom positions is small, and, as will be seen later, this is important when discussing sources of the contrast in the process of image formation.

With the dipole field β^d, the above-atom field approaches infinity as the plane of the dipoles and positive charges is approached, whereas the inbetween-atoms field goes smoothly to a value of $\beta^d \sim -0.3$ (for $b_E = 2b^\theta$) for $z = 0$. With increasing R_z, the two curves converge to zero rapidly; so at sufficient distance from the layer, there are no dipole-induced field contributions. Again this point is important when discussing image contrast.

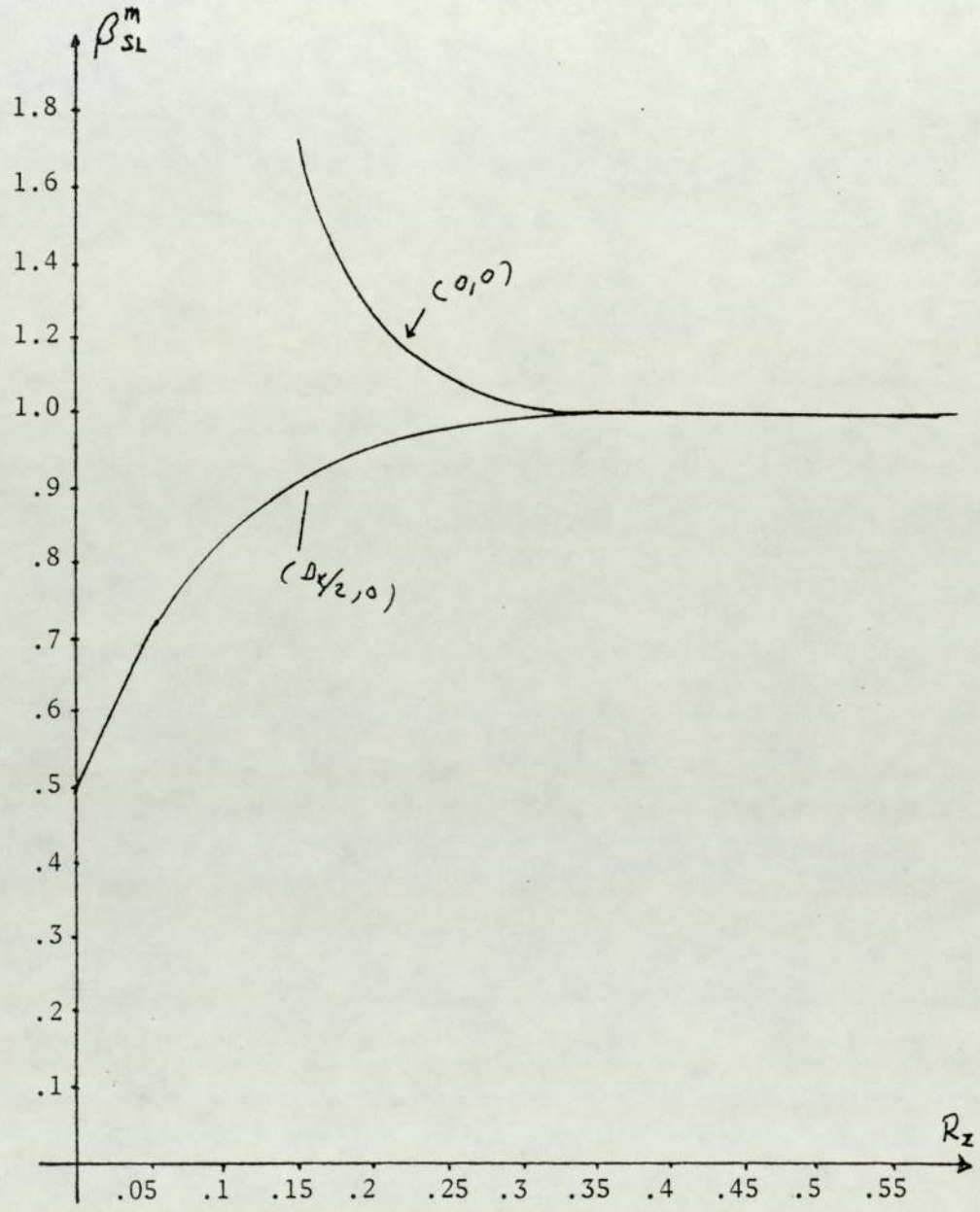

Fig 6.6

Variation of the monopole field ratio β^m_{SL} with the distance R_z

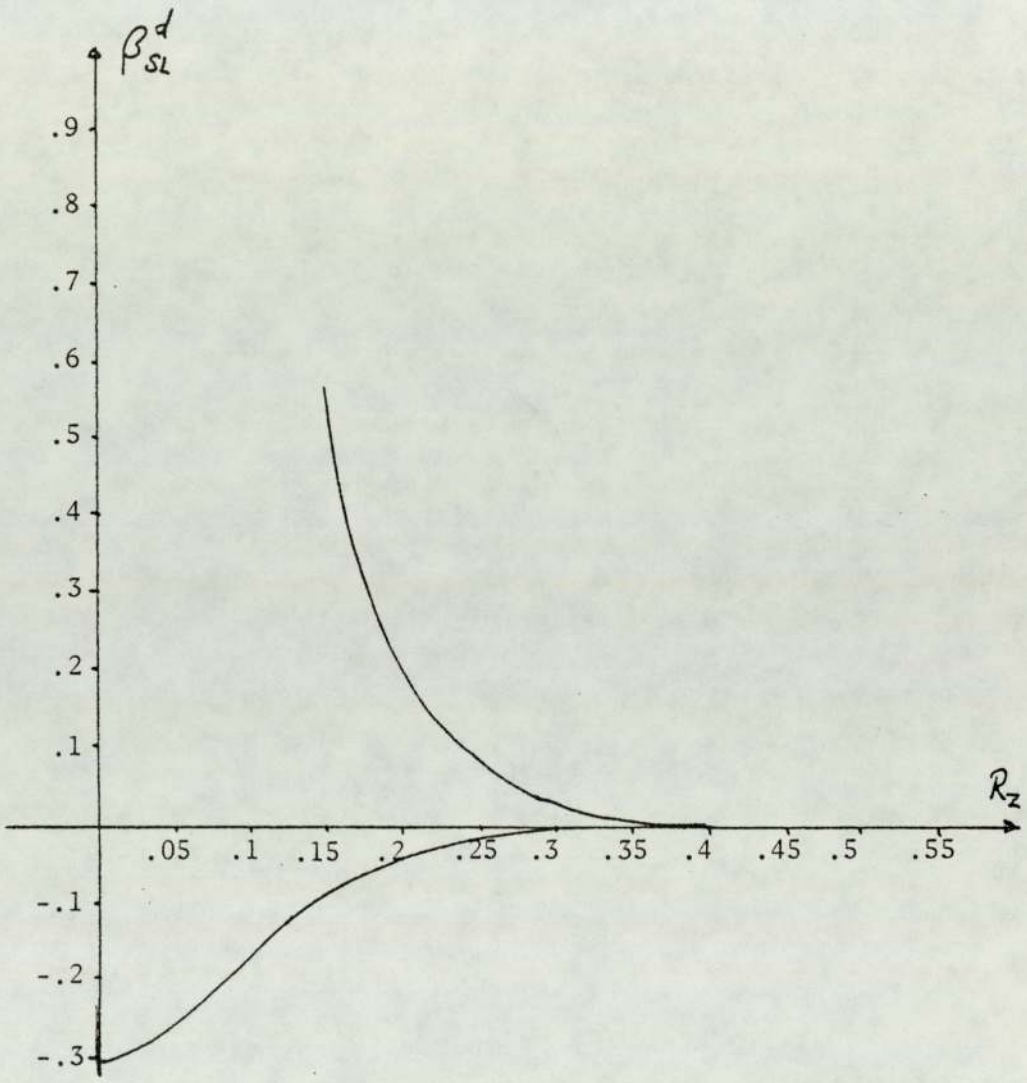

Fig 6.7

Variation of dipole field ratio above a single layer β^d_{SL} with the distance R_z, for $b_E = 2b^\theta$

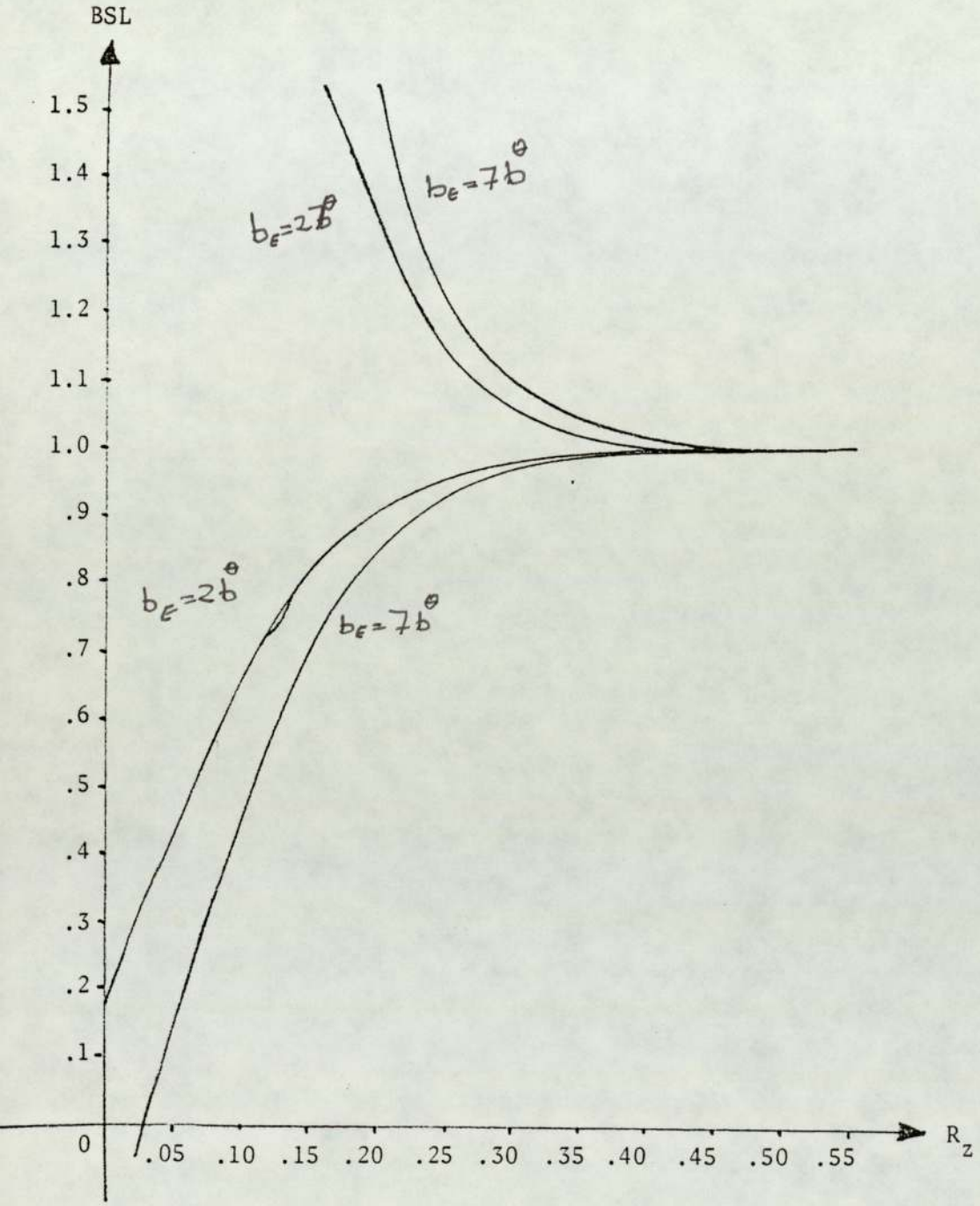

Fig 6.8

Variation of the field ratio above a single layer β_{SL} with the distance R_z, for $b_E = 2b^\theta$ and $b_E = 7b^\theta$

The combined monopole-dipole curves, drawn for both $b_E = 2b^\theta$ and $b_E = 7b^\circ$, show the same characteristics as the monopole curve, except that the field difference is much larger (e.g. for $b_E = 2b^\theta$, at the adsorption position $R_z = .259$ nm, $\Delta\beta^m \simeq .04$, $\Delta\beta \simeq .07$). The effect of using a higher polarizability value is, as can be seen from the $b_E = 7b^\theta$ curve, to increase $\Delta\beta$ even further, for given R_z.

The size of the field variations across the surface depends both on the crystallographic structure of the array and on the area per lattice point in the array, but chiefly on the latter. This is illustrated in table 6.3 where the values of β_A^m $\beta_A^{d,E}$ and β_A are compared for the W(111) surface and for models 1 and 2 discussed earlier. It is seen that the results for mdl 2, which has the same area per lattice point as does the (111) face, are much closer.

Also included in table 3, for comparative purposes, the data for the IDP model. In this case T^d is in effect defined by:

$$T^d = 2/|z|^3 \qquad \ldots\ldots 6.10$$

$\beta_A^{d,E}$ is higher for the IDP model (owing to the absence of depolarization effects), but β_A^m is less - essentially because the array-type models take the existence and localization of surface charge into account.

More generally, it deserves note that the field enhancement due to the localization of the charge, which is given by $(\beta_A^m - 1)$, is a significant component in the total enhancement factor β_A; the monopole contribution $(\beta_A^m - 1)$, however, is smaller than the dipole contribution $\beta_A^{d,E}$.

A comparison of β_A-values for the different faces of tungsten is also shown in table 6.3. It is clear that the area per atom in the face is the dominant geometrical factor in determining the magnitude of the field variations above the face in question.

Table 6.3

Values of the field ratio β_A^m, $\beta_A^{d,E}$ and β_A, and the short-range binding-energy component ΔB^*, for specified lattice structures

Lattice type	a/nm	β_A^m	$\beta_A^{d,E}$	β_A	ΔB^*/eV
hex. (111)	0.4476	1.048	0.063	1.111	0.034
md1 1	0.4476	1.067	0.074	1.141	0.044
md1 2	0.4165	1.050	0.063	1.113	0.035
IDP (aprx)	0.4476	1.000	0.3315	1.3315	0.112

For $b_E = 2b^\theta$ $\qquad$ $F^{ext} = 45$ V/nm

6.3.3 The binding potential

If certain small effects due to mutual induction between a single adsorbed atom and the emitter surface are ignored, then the field-induced component U^{pol} in the binding potential for this atom is given by:

$$U^{pol} = - \tfrac{1}{2} b_A \beta_A^2 (F^{ext})^2 \qquad \ldots\ldots 6.11$$

Plots of U^{pol} against R_z for the above-atom and between-atom positions, for helium and taking $b_E = 2b^{\theta}$, $F^{ext} = 45$ V/nm are shown in fig. 6.9, and illustrate a number of elementary features of adsorption.

As distance from the surface increases U^{pol} tends to the constant value $- \tfrac{1}{2} b_A (F^{ext})^2$. This is the long-range potential that can keep an imaging gas atom held in the vicinity of the emitter, even though it is not bound locally.

Starting from this constant level, and moving towards the surface, U^{pol} rises above the between-atom sites and falls above the atomic sites. This illustrates the existence of localised adsorption sites directly above the surface atoms. Note that the repulsive potential is neglected in this diagram - in reality this contribution would flatten the above-atom curve out and make it repulsive for distances $R_z < 0.259$ nm.

There is a general similarity of behaviour for all crystal faces, but the short-range binding-energy component ΔB^* given by:

$$\Delta B^* = \tfrac{1}{2} b_A (\beta_A^2 - 1)(F^{ext})^2 \qquad \ldots\ldots 6.12$$

is smallest for the closest-packed faces (i.e. those for which A_c is smallest). This point is illustrated in table 6.3.

Finally, note that for an adsorbed atom there is a barrier against diffusion, and the activation energy for diffusion is greater than that necessary to escape into the constant-potential region. Consequently, for a single atom on a charged surface, diffusion is a hopping process, not a direct lateral motion in space.

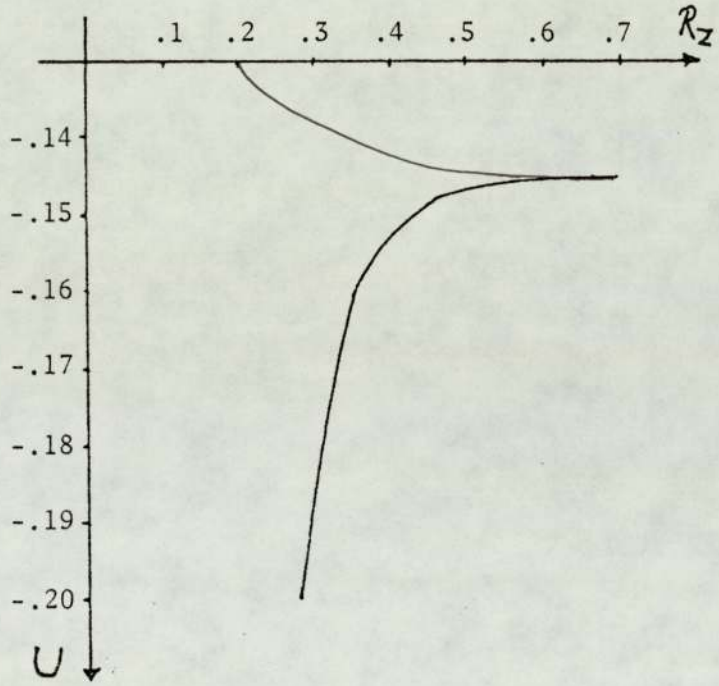

Fig 6.9

Variation of potential energy of a single atom with the distance R_z

6.4 Field and potentials above a double layer

We now look at the potential and field variations (in terms of the potential and field ratios V and β') above a layer of tungsten atoms (E) and an adsorbed layer of helium atoms (A), represented in our model by an array of monopoles and dipoles and a geometrically similar layer of dipoles above it. We shall assume that the tungsten-helium layer separation s is 0.259 nm[52]. The corresponding value in units of c is given by:

$$z = s/c = 0.5786 \qquad \ldots\ldots 6.13$$

As in the previous section, two polarizability values are used, but only the "total" V and β curves are drawn, since the separate monopole and dipole layer behaviours have been studied in the previous sections.

6.4.1 Potential above the double layer

We show in figs 6.10 and 6.11 the potential variation normal to the surface for a W(111)/He layer above a lattice point (or an atom) and at the midpoint between lattice points (or inbetween atoms).

Comparison of fig 6.4 and fig 6.10 shows that the effect of the adsorbed alyer on the potential variation can be roughly visualised as a shift in both the above-atom and between-atom curves outwards from the surface. As compared with the single-layer curves, there is - at any given distance greater than 0.259 nm - a slightly larger potential difference between the two curves; and a given value of V is reached at a slightly greater distance from the surface.

By extending backwards the straight line potential, valid at large distances, as in the previous section, we see that the extended straight line cuts the z-axis at a distance d' from the origin. As before d' can be interpreted as a shift outward (due to the dipole layer). Note that

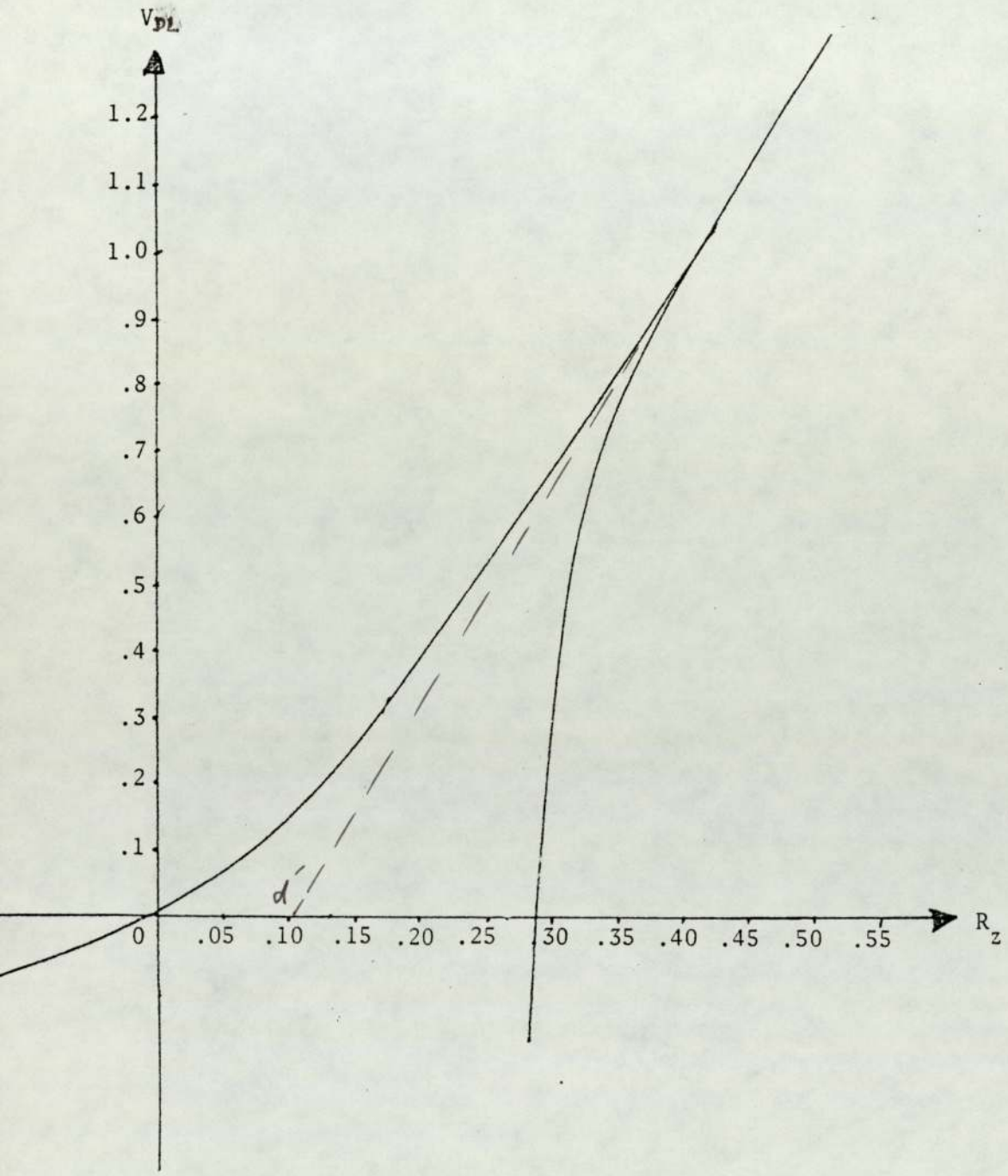

Fig 6.10

Variation of the potential ratio above a double layer V_{DL} with the distance R_z, for $b_E = 2b^{\theta}$

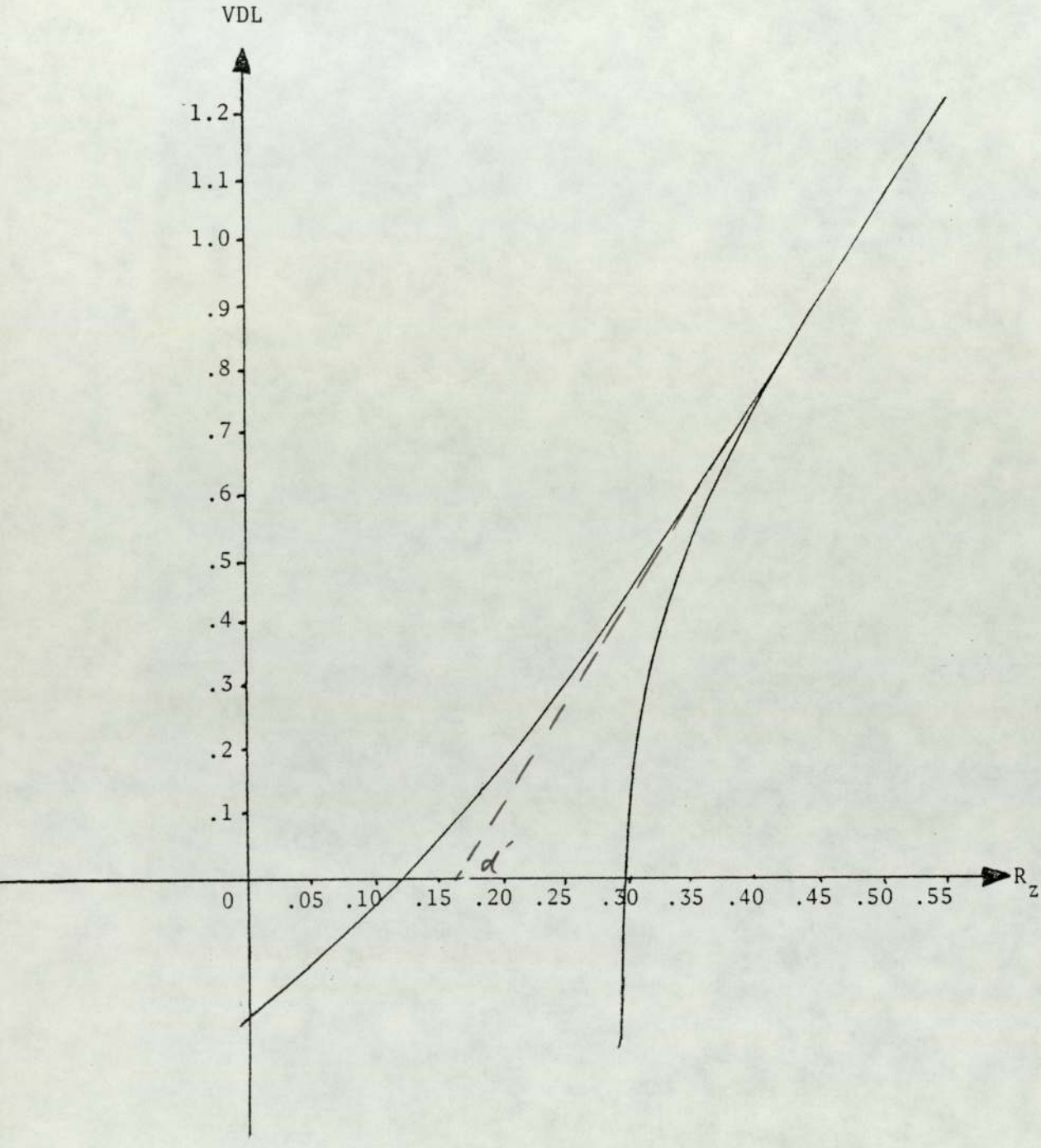

Fig 6.11

Variation of the potential ratio above a double layer V_{DL} with the distance R_z, for $b_E = 7b^{\theta}$

d' is slightly greater than d due to the effect of the adsorbed layer.

6.4.2 Field above the double layer

We show in fig 6.12 the field variation normal to the surface for W(111)/He, due to the monopole-dipole distribution jointly, for $b_E = 2b^\theta$ and $b_E = 7b^\theta$. The curves show the same characteristic shape as those for a bare surface (fig 6.8), with the difference that the curves corresponding to the above-atom field can be roughly visualised as having been shifted outwards from the surface by a distance equal to the diameter of the adsorbed atom.

At small distances above the adsorbate layer there has been a sharp increase both in the β-values above the adsorbate atoms, and in the field difference as between the above-atom and between-atom positions. For example, for $b_E = 2b^\theta$, at a distance 0.35 nm from the emitter layer, which corresponds to a distance of 0.0091 nm from the adsorbate layer, the value of $\Delta\beta$ is now 0.63 whereas for the single layer it was roughly 0.04. Although the field difference decreases rapidly as both curves converge to unity, it is believed that the sharp contrast of the FIM image can be attributed mainly to these enhanced field difference resulting from field adsorption, which causes high concentration of imaging atoms in a very small volume immediately above the adsorbed atoms, and consequently, higher ion current j, and brighter spots. This is discussed in more detail later.

6.5 Equipotentials and the Critical surface

6.5.1 Equipotential surfaces

The equipotentials above a real metal surface are not smooth planes (as would be the case for the jellium surface model). This is due to

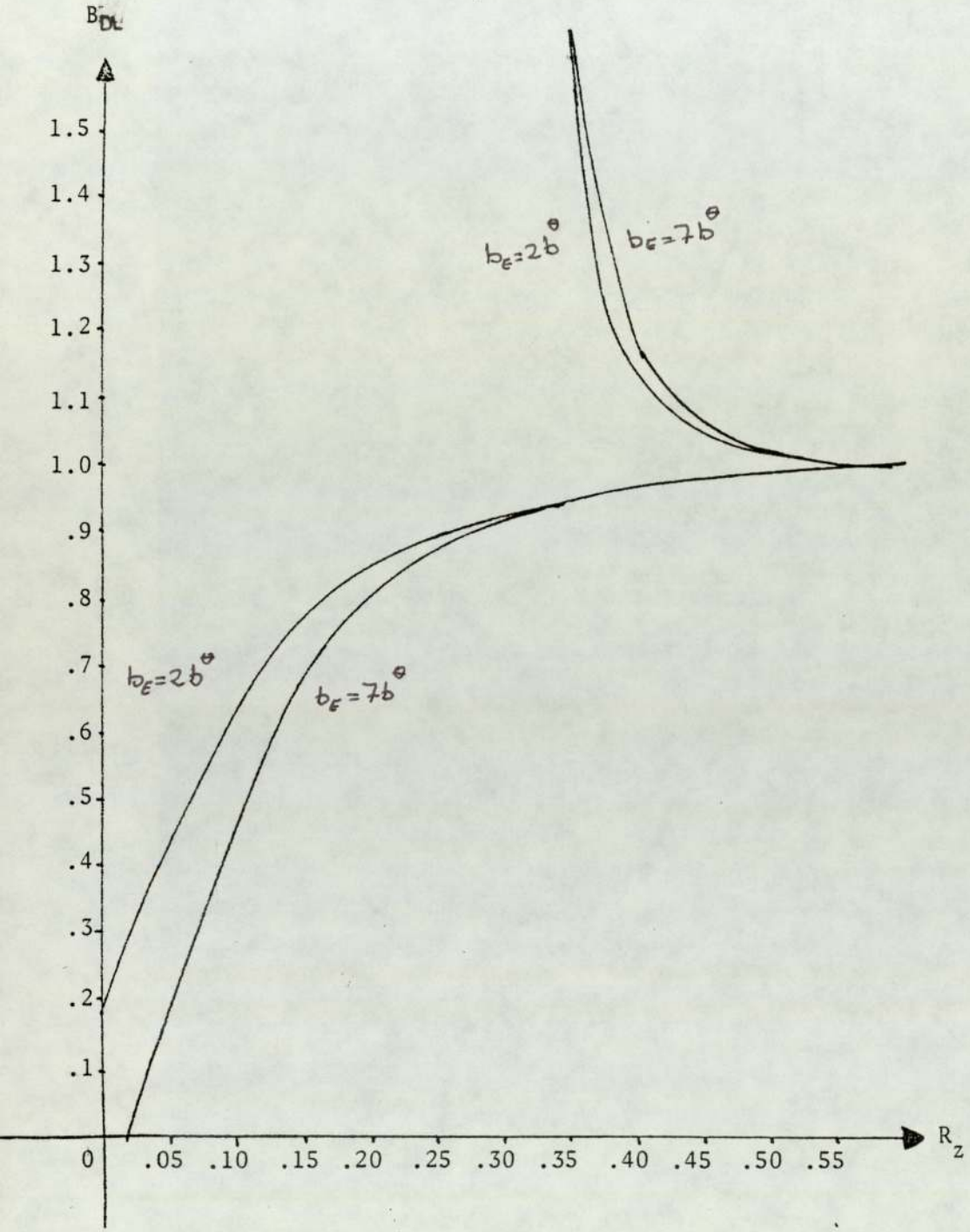

Fig 6.12

Variation of the field ratio above a double layer β_{DL} with the distance R_z, for $b_E = 2b^\theta$ and $b_E = 7b^\theta$

charge localisation at the metal surface, which force the equipotentials to assume a "rippled" or "egg-box " shape, with the equipotentials further from the metal surface above the atoms than they are above the between-atom position.

This variation above and inbetween atoms or "ripple" can be deduced graphically from the bare emitter surface potential curves (fig 6.4), by drawing a horizontal line parallel to the z-axes, at the required equi-potential value. The location of the equipotential is determined by the intersection with the potential curves. The ripple is small, and decreases gradually as we move away from the surface; it has effectively vanished by a few nanometres away from the surface.

Comparing fig 6.4 ($b_E = 2b^\theta$) and fig 6.5 ($b_E = 7b^\theta$) for the same equipotential value, shows that the effect of a higher polarizability value is to shift the equipotential surface outward.

Fig 6.10 for the double layer potential shows the same characteristic generally as the bare surface one, but the effect of the adsorbed layer (for positions outside it) is to increase the ripple and to shift the equipotential surface outward slightly.

6.5.2 The critical surface

The critical surface is (approximately) an equipotential surface above the charged emitter surface. Inside the critical surface ionization of imaging gas atoms (or a desorbed atom) in effect cannot happen, because imaging-gas atom electrons possess energy less than the Fermi level of the metal (below which nearly all electron energy levels are completely occupied), (see section 1.3.2). In the standard elementary treatment the critical distance X_c is given appromimately by :

$$X_c \simeq \frac{I - \phi}{e\, F^{ext}}$$

So according to the above equation the critical surface above a charged tungsten emitter, where F = 45 V/nm, I = 24.5 eV, and ϕ = 4.5 eV (ref [7]), is equal to 0.44 nm.

But the above equation has the weakness that it depends on the jellium model, which predicts a flat critical surface. To predict the critical surface using our surface model, we use the following procedure:

(1) Calculate the dimensionless potential or "critical V-value", V(crit) from the relationship:

$$V(crit) = \frac{I - \phi}{c.F^{ext}} \qquad \ldots\ldots 6.14$$

For F = 45 V/nm this has the value 1.40434. [It is useful to work with a precise value, though obviously the accuracy of this value is much less than its precision would suggest].

(2) Use our computer program to calculate the characteristic distance R_z^{char} for a certain position in the surface array, that gives a potential value equal to V(crit). The results, for He on W(111), for $b_E = 2b^\theta$ and $b_E = 7b^\theta$, are shown in table 6.4.

The general characteristics of the critical surface as obtained here are the same as those of equipotential surfaces, as already discussed. Table 6.4 demonstrates numerically the following things:

(1) In all cases R_z^{char} is greater above the surface atoms than between them, i.e. the critical surface is concave outwards above the imaged atoms.

(2) R_z^{char} is slightly greater in the double-layer situation, and is greater for the higher polarizability value.

(3) The "distance ripple" is greater in the double-layer case, but <u>smaller</u> for the higher polarizability value. In absolute terms

TABLE 6.4

Values of the field ratio and the field ratio difference, above and inbetween atoms, for a single and a double layer, and for polarizability values $2b^{\theta}$ and $7b^{\theta}$

b_E/b^{θ}	PX PY	R_z^{char} (SL) (nm)	R_z^{char} (DL) (nm)	β^{cr} (SL)	β^{cr} (DL)
2	0 0	0.52155	0.54028	1.00144	1.01002
	DX/2 0	0.52143	0.53948	0.99952	0.99085
	Differences	0.00012	0.00080	0.00192	0.01917
7	0 0	0.60743	0.62936	1.00058	1.00254
	DX/2 0	0.60738	0.62915	0.99981	0.99916
	Differences	0.00005	0.00021	0.00077	0.00338

$$V^{crit} = 1.40434$$

the ripple is fairly small in all cases.

With respect to fields, the tables demonstrate the following results:

(4) The above-atom fields are higher in the double layer case than in the single-layer ("bare emitter") case. This is a consequence of the fields due to the induced dipoles in the field-adsorbed layer.

(5) The critical surface fields are lower for the higher polarizability value, in both single-layer and double-layer cases; and the same is true for the difference $\Delta\beta^{cr}$ in field ratios as between above-atom and between-atom positions.

This last result was entirely unexpected, and has implications for imaging theory. Basically, it occurs because the fall-off in potential with distance is slower than the fall-off in field.

6.6 Imaging and Contrast

Since the ionization of imaging-gas atoms occurs in the vicinity of the critical surface, the fields in the critical surface have a specific importance in the theory of imaging and image contrast. Recalling eqns. 2.4 and 2.7, it is clear that the imaging process depends on the ionization densities in the ionization zones above protruding surface sites, (i.e. surface atoms), and contrast depends on the ratio of ionization densities as between points in the critical surface above and between neighbouring atomic sites.

This ratio of ionization densities is determined partly by the gas-concentration ratios, and this in turn is influenced by the field differences. If thermodynamic equilibrium exists, then we may write eq. 2.7 in the form:

$$C_A/C_M = \exp\left[\tfrac{1}{2}b_A(F^{ext})^2.2\Delta\beta^{cr}/kT\right]$$

There is a small approximation here, in that we have equated the average field with the external field, but this is not important for practical purposes.

We show in table 6.5 some values of C_A/C_M for the various cases considered above and for several different temperatures. Two results stand out. First, that the presence of the adsorbed layer markedly enhances the predicted gas-concentration ratio, second that in all cases the gas-concentration ratio corresponding to $b_E = 2b^\theta$ is much higher than that corresponding to $b_E = 7b^\theta$, which means that - contrary to our intuitive expectation - higher emitter surface-atom polarizability tends to reduce rather than enhance image-contrast. As already indicated, this is because the higher polarizability shifts the critical surface outwards, away from the dipoles in the field-adsorbed layer. Although the moments of these dipoles are increased by choosing a higher polarizability for the substrate atom, this increase is not enough to compensate for the outwards shift in the critical surface.

In discussing the influence of gas-concentration variations in contrast, it should be remembered that with a Raleigh criterion a ratio of 1.3 in the ionization densities is needed to explain contrast. Thus, if thermodynamic equilibrium were to exist, a ratio of 1.3 in the gas concentrations would be sufficient to explain contrast. On this basis, if $b_E \simeq 2b^\theta$, then contrast can be explained near 20K and below if no adsorbed layer is assumed present, but well above 80K if an adsorbed layer is assumed present.

In fact, the imaging gas is <u>not</u> in thermodynamic equilibrium with the emitter under imaging conditions[16, 26]. Duffell and Forbes[31] suggest that, as an approximation, we may assume the gas to be locally in equilibrium with itself, at some effective temperature T_{eff} above that of the emitter. They suggest that T_{eff} may be about four times the emitter temperature. On this basis, our results suggest that, to explain

the existence of resolved planes in the images of W(111), at emitter temperatures near 80K, the presence of a field-adsorbed layer has to be postulated.

Conversely, the results in table 6.5 confirm that, if the adsorbed layer is present, then gas concentration variations must be expected to have a significant role in imaging theory.

TABLE 6.5

Values of the gas concentration ratio above and inbetween atoms (C_A/C_M), at the critical surface, above a single and double layer, for polarizability values $2b^\theta$ and $7b^\theta$, at different temperatures

	b_E/b^θ	C_A/C_M (SL)	C_A/C_M (DL)
T = 5K	2	3.6	3.9×10^5
	7	1.7	9.7
T = 20K	2	1.4	25
	7	1.14	1.8
T = 80K	2	1.08	2.2
	7	1.03	1.15
T = 300K	2	1.02	1.24
	7	1.009	1.04

CHAPTER 7

RESULTS AND DISCUSSION: BINDING ENERGIES

7.1 Structure

We now turn to the discussion of short-range field-adsorption binding energies. The major part of this chapter deals with the calculation of binding energy ΔB for a complete layer, and we approach this in three stages: the calculation of the conventionally-defined component $\Delta B(conv)$; corrections necessary to obtain the full (differential) field-induced contribution ΔB^{elec}; and the further corrections necessary to obtain the total (differential) short-range binding energy ΔB. In the calculation of $\Delta B(conv)$ we compare our results with those of previous treatments.

The remainder of the chapter deals in a preliminary way with the calculation of binding energies for partially-occupied layers, and for a fully occupied second field-adsorbed layer.

7.2 The calculation of $\Delta B(conv)$

7.2.1 Comparison with previous treatments

To facilitate comparison of our treatment with those of Muller and Tsong[15, 52], we initially introduce some simplifications into our formulae. First, in eq. 4.62 we set $M_A^{-1} = 1$ and $\gamma_E^{d,A}$ (γ_E^A in the more general treatment) equal to zero. Physically, this is equivalent to ignoring the effects of the adsorbate-layer atoms on themselves and on the emitter-layer dipoles. Eq. 4.62 will then be reduced to

$$\beta'_A \simeq \beta_A^m + \gamma_A^{d,E} M_E^{-1} \beta_E^m \qquad \ldots\ldots 7.1$$

But the r.h.s. of this expression is just a formal version of the single

layer formula discussed in section 4.3, applied at the bonding point A. Thus we can write it more fully as:

$$\beta'_A \simeq \beta_A = \beta^m_A + \beta^{d,E}_A = \beta^m_A + b_E \beta^m_E T^d M_E^{-1}/4\pi\varepsilon_o c^3 \quad \ldots\ldots 7.2$$

Table 7.1 shows the results of calculations based on a simple square array. (We have in effect used the structure factors for the (100) face but have set c equal to the interatom spacing in the (111) face. This will give results for the geometry discussed in ref.(68). Various choices for the parameters in eq.(7.2) are given, together with the corresponding values of β_A, $(f_A - 1)$ and the binding-energy component $\Delta B(conv)$ as evaluated for an external field equal to 56 V/nm. We initially use the polarizability value 3.19 meV V^{-2} nm^2, which is equivalent to the value used by Tsong and Muller. The choices are as follows:

Choice 1: Apart from a very small correction factor, this is equivalent to the IDP approximation, represented in eq.2.8. Physically the choice disregards all interactions between the adsorbate atom and the highly charged-metal-surface atoms except that with nearest atom.

Choice 2: is equivalent to the unapproximated array equations given by Tsong[52]. It disregards the monopole effects in eq.4.62 (by putting $\beta^m_A = \beta^m_E = 1$), and gives the parameters M_E^{-1} and T^d values appropriate to a simple square dipole array. Physically this choice describes the interaction between a layer of neutral emitter atoms and a single adsorbed atom, isolated in free space in an applied field F^{ext}, and with mutual induction between the adsorbed atom and the layer ignored.

Choice 3: incorporates the fact that the emitter is an electrical conductor, by setting the impressed (monopole) field at the emitter surface equal to $\frac{1}{2} F^{ext}$ (i.e. $\beta^m_E = .5$), rather than F^{ext}. This is done because, in reality, the emitter - layer atoms form the surface of a charged conductor, and so they are in part the source of the external field.

TABLE 7.1

Values of specified field ratios and of the conventional short-range field-adsorption binding energy $\Delta B(\text{conv.})$, for a square lattice with a = 0.4476 nm, for specified choices of the parameters appearing in eq.7.2 and of β_A^m

	Choice					
	1	2	3	4	5	6
b_E/b^e	3.19	3.19	3.19	3.19	7.00	7.00
β_E^m	1.0	1.0	0.5	0.5	0.5	0.5
T^d	10.32	5.934	5.934	5.934	5.934	5.934
M_E^{-1}	1.000	0.6836	0.6836	0.6836	0.4962	0.4962
$\beta_A^{d,E}$	0.529	0.208	0.104	0.104	0.165	0.165
β_A^m	1.000	1.000	1.000	1.067	1.000	1.067
β_A'	1.529	1.208	1.104	1.171	1.165	1.232
$f_A - 1$	1.337	0.460	0.219	0.372	0.358	0.519
$\Delta B(\text{conv.})^b$	0.299	0.103	0.049	0.083	0.080	0.116

$\Delta b(\text{conv.})$ is evaluated for an external field of 56 V/nm, using the approximate value of the field-ratio shown, and is expressed in eV.

Choice 4: takes into account the enhancement of the field at the position of the adsorbate due to the localisation of the charges at the emitter surface, by setting β_A^m equal to 1.067 (our calculated value) rather than unity.

Choice 5: shows the effect of higher polarizability (i.e. putting $b_E = 7b^\theta$ rather than $3.19b^\theta$) on choices 3 and 4.

The sequence of choices from 1 to 4 represents a trend towards increasing realism in general mathematical and physical assumptions. It is shown clearly that the Tsong and Muller dipole-dipole theory (our IDP approximation, represented by choice 1) is not an adequate substitute for a full array calculation. With the data choice used here, the neglect of mutual depolarization amongst substrate-atom dipoles causes over-estimation of the binding energy by a factor of nearly three. The degree of over-estimation will depend somewhat on the values assumed for the lattice spacing and for the surface atom polarizability. The results here are incompatible with Tsong's statement, based on unpublished work mentioned in his review article[52], that the IDP aprox. leads to numerical results sufficiently accurate for comparing with experimental results.

A second point concerns the role of the field variations due to the discreteness of positive charges. The original work on this by Forbes[68] compared the monopole contribution to field variations with the dipole contribution as calculated by the IDP approximation. However, by reference to the full array calculation of the substrate-dipole contribution (choice 3), the monopole contribution is relatively more significant. Including the monopole effects (choice 4) increases the short-range binding energy by approximately 70%, for the SI polarizability value $3.19b^\theta$.

For the higher polarizability value of $7b^\theta$ used in choices 5 and 6, the inclusion of the monopole contribution increases the predicted short-range binding energy by approximately 45%.

7.2.2 The effects of lattice structure

Table 7.2 compares the results for choice 6 above, that are based on a simple square lattice structure of side 0.4476 nm, with those for the two other structure choices specified earlier, assuming the polarizability value $b_E = 7b^\theta$. The binding energy estimate is here based on the full formula for $\Delta B(conv)$, namely eq.4.62 rather than the approximate formula, eq.7.2. The columns in table 7.2 are:

Choice 1: corresponds to choice 6 in table 7.1 (but using full formula), i.e. mdl 1.

Choice 2: represents a square lattice structure with a lattice cell area equal to that of the hexagonal W(111) structure, i.e. mdl 2.

Choice 3: represents the hexagonal W(111) lattice structure.

Choice 4: represents the same hexagonal lattice structure but with the SI proper polarizability for the emitter surface atom $2b^\theta$ (i.e. the lower limit discussed earlier).

The first choice shows that the use of the full formula for β'_A rather than the approximated formula tends to reduce the conventional binding-energy estimate. This is discussed further below.

Comparing choices 1 and 2 shows that, for a given (square) lattice structure, β'_A and $\Delta B(conv)$ are smaller when the interatom spacing is smaller. The monopole contribution to field variations is reduced, and mutual depolarization effects are enhanced.

Comparing choices 1 and 3 shows that, for a given interatom spacing, β'_A and $\Delta B(conv)$ are smaller for the hexagonal than the square structure, essentially because the area per array point is smaller for the former.

Finally, comparison of choices 1 to 3 shows that the modelling of a real hexagonal structure by a square lattice is more successful if the areas per array point (rather than the interatom spacings) are set equal.

TABLE 7.2

Values of the parameters appearing in eq.7.2, and of the conventional short-range field-adsorption binding-energy ΔB(conv.), evaluated for specified lattice structures, without approximations

Lattice type	Square	Square	Hexagonal	Hexagonal
a (nm)	0.4476	0.4165	0.4476	0.4476
b (meV V^2 nm^2)	7.00	7.00	7.00	2.00
β_A	1.233	1.183	1.181	1.111
M_A^{-1}	0.9800	0.9749	0.9753	0.9753
M_A^{-1} β_A	1.208	1.153	1.151	1.083
D^{-1}	1.0044	1.0032	1.0032	1.0015
β_A'	1.213	1.157	1.155	1.085
ΔB(conv.)[a] (eV)	0.106	0.076	0.075	0.040

[a] ΔB(conv.) is evaluated for an external field of 56 V/nm

More generally, one might expect to be able to model a complicated array structure by a square lattice with the same area per lattice point, as has been pointed out by MacDonald and Barlow[85].

7.2.3 The influence of induction effects

Physically, the reduction in the conventional binding-energy estimate when using the full formula is due to induction effects resulting from the presence of the adsorbate layer. The correction to the field ratio is small, about 2% in the case of each lattice structure when the surface polarizability b_E is taken as $7b^\theta$. The correction to $\Delta B(conv)$, however is much greater. For the hexagonal lattice structure, for example, the full-formula result is roughly 15% lower than the approximate result.

To investigate in more detail the effects of the presence of the adsorbed layer, we write eq.4.62 in the form:

$$\beta'_A = D^{-1} M_A^{-1} \beta_A \qquad \ldots\ldots 7.3$$

where D denotes the denominator in eq.4.62. The factor M_A^{-1} in eq.7.3 results from interaction within the adsorbed layer, and acts to reduce the local field acting on an adsorbed atom; the factor D^{-1} relates to mutual induction between the adsorbed atoms and the emitter substrate atoms, and acts to increase the local field acting on an adsorbed atom. As shown in table 7.2 the factor M_A^{-1} has a somewhat greater influence than the factor D^{-1}.

7.2.4 Influence of polarizability value

By comparing choice 3 and 4, in table 7.2 we see the great effect of the polarizability b_E value on the calculation of $\Delta B(conv)$. Setting $b_E = 2b^\theta$ rather than $7b^\theta$ reduces $\Delta B(conv)$ by about 45%. There is still much uncertainty associated with the choice of proper SI polarizability,

for the surface atoms (see sec 3.5) values mentioned in field-ion literature for the "polarizability" of tungsten atoms range from $0.38b^{\theta}$ (for an atom in the (001) plane (ref.(7)) to Thorhalson et al value of $11.7b^{\theta(80)}$, which is a computed value for an atom in free space. In our view there are no reliable experimental or theoretical measurements of the proper SI polarizability of a partially ionized surface atom, and/or of how much it may differ from the SI polarizablity of the same atom (neutral) in free space. Thus we are using upper and lower estimates, as described earlier.

7.2.5 Summary

This section has largely been concerned with possible mathematical approximations in the calculation of the conventional field-induced binding-energy contribution $\Delta B(conv)$. It has been shown that:

(1) The isolated-dipole-pair approximation is not an adequate substitute for a full array calculation.

(2) Mutual depolarisation, and also the field variations due to the discreteness of positive charges, must be taken into account.

(3) Mutual induction effects due to the adsorbate layer can be neglected in a first approximation, but that there is no problem in including them.

(4) The correct lattice structure for the crystallographic plane under discussion should be used.

(5) There is a residual uncertainty by a factor of about two, due to uncertainty over the correct value of surface atom polarizability.

7.3 The calculation of ΔB^{elec}

As we described in section 3.2, the short-range binding energy term

ΔB consists of many terms. Recalling eq.3.2:

$$\Delta B = \Delta B^{elec} + \Delta B^{rep} + \Delta B^{disp} + \Delta B^{lat} + \Delta B^{indir}$$

The term ΔB^{elec} (representing the full electrical component of the induced short-range binding energy) is not identical with the term $\Delta B(conv)$ that represents the conventional expression for short-range field-adsorption binding energy, as described in section 3.2. In the first place there are hyper-polarizability and field-gradient polarizability terms. According to ref.(73), these increase $\Delta B(conv)$ by about 20% in the field range of interest. Secondly, there is the effect of the induced change in the source of the electric field ($- \Delta U_s$). Bearing in mind that the quantity of interest is what we defined earlier as the "differential" short-range binding energy (i.e. the binding energy associated with the removal of a single atom from the adsorbed layer), and that all our short-range binding-energy contributions are of this type, we now consider ΔU_s in more detail.

The evaluation of ΔB^{elec}, by integration of the force acting on the vacancy-site atom along a path away from its adsorption site, is possible in principle but would involve extensive calculations. We think that the following argument may provide a rough estimate.

The effect of mutual induction within the adsorbed layer is to reduce the field acting on each adsorbed atom. If this mutual induction effect could be "turned off", whilst leaving the mutual induction effect between the substrate atoms and the adsorbate-layer atoms "turned on", then the field F* acting on each substrate atom would be:

$$F^* = D^{-1} \beta_A F^{ext} \qquad \ldots\ldots 7.4$$

where the symbols have the same meaning as previously, i.e. β_A is the field ratio for the "bare emitter" situation. Taking F^{ext} as 56 V/nm, and

using the data appropriate to the hexagonal lattice as given in table 7.2, with $b_E = 7b^\theta$, we obtain a binding-energy estimate:

$$\Delta B^{elec}(F^*) = 90 \text{ meV}$$

This result should be compared with the value $\Delta B(conv)$ given in table 7.2, namely 75 meV.

We now argue that during the removal process all the dipoles in the adsorbate layer (except the vacancy-site atom) would, if they remained fixed in position, have strengths intermediate between $b_A F^{loc}$ and $b_A F^*$. Consequently, the work done against electric-field-induced forces in removing the vacancy-site atom should be intermediate between the binding-energy estimates obtained by taking the field acting on the other dipoles as F_A^{loc} and as F^*, respectively. That is, ΔB^{elec} should be intermediate between 75 and 90 meV.

For the same lattice structure, but with $b_E = 2b^\theta$, the conclusion is that ΔB^{elec} should be between 40 and 53 meV.

We thus think that for the field adsorption of helium on the (111) face of tungsten, the (differential) field-induced binding energy contribution ΔB^{elec} could be greater than $\Delta B(conv)$ by roughly 10 meV, when:

$$F^{ext} = 56 \text{ V/nm}$$

Other corrections to ΔB^{elec} might in principle arise from the existence of a permanent surface-atom dipole moment, as discussed in chapter 3. However, it is felt that the corrections will be swamped by the uncertainties in the surface-atom polarizability, and can be neglected at the present time.

Overall, therefore, we feel that ΔB^{elec} will be greater than $\Delta B(conv)$ by perhaps as much as 30% for the fields of interest to field-ion emission.

7.4 The Calculation of ΔB

Next we consider the calculation of the remaining terms in eq.3.2.

7.4.1 Repulsive Forces

The theory of the binding-energy contribution due to repulsive forces was discussed in section 3.7. Using eq.3.33, we computed the repulsive forces ratio η for W(111)/He structure. The results are:

$$\eta = 0.51 \text{ if } b_E = 2b^\theta, \qquad \eta = 0.48 \text{ if } b_E = 7b^\theta$$

Thus the factor $(1 - \eta)$ in eq.3.34 is approximately equal to one half. The effect of repulsive forces cannot be neglected.

7.4.2 Dispersive Forces

The third term in eq.3.2 is the binding-energy component resulting from the interplay of dispersive and repulsive forces. This interplay also exists in the absence of the external field, and has been extensively discussed in past literature [40, 88]. If there were no change in the position of the adsorption site when the field is applied, then the $\frac{1}{2}\Delta B^{disp}$ in eq.3.34 would represent the zero-external-field binding energy, at least approximately. Since the field-adsorption sites are directly above the substrate atoms, but the normal physisorption sites are in the positions that maximise the number of nearest neighbours, differences will exist in the details of the dispersive and repulsive interactions in these two cases. However, it seems reasonable to treat the third term in eq.3.2 as equal to the binding energy in zero external field.

The value of this binding energy, for helium on a metal, is usually taken as approximately 10 meV (see ref.(40), for example). However, a

recent review[88] cites a value of approximately 4 meV for helium on tungsten, derived from scattering experiments[89]. These binding-energy contributions are small, but are not negligible in comparison with the lower of the estimates made for the first term in eq.3.34.

7.4.3 Lateral Interactions

In principle, contributions also result from lateral interactions between adsorbate atoms. The effect of electrostatic dipole-dipole interactions has been taken into account in the estimation of ΔB^{elec}. But in principle there also exist chemical type interactions.

For two helium atoms in free space, calculations suggest that at a separation of 0.4476 nm there is an attractive interaction energy of around 0.1 meV[90]. As each adsorbed helium atom in a monolayer on a (111) face has six nearest neighbours, this would produce a contribution of about 0.5 meV to the short-range binding-energy. A contribution of this size can be neglected.

7.4.4 Indirect Lateral Interactions

When noble-gas atoms are adsorbed, the presence of the surface modifies the interaction between them, even when the surface is neutral. In effect, there is additional contribution to the binding energy, that gives rise to the term ΔB^{indir} induced in eq.3.2. For the heavier inert gases adsorbed on graphite this contribution is known to be repulsive at large separations, and tends to reduce the magnitude of the lateral interaction energy by around 5 - 10%[72]. This effect will presumably exist in the adsorption of helium on a metal, but as far as we know there is no relevant data. However, if its size is comparable with the percentage figure just quoted, then ΔB^{indir} would be of order - 0.1 meV and thus completely negligible.

7.4.5 Summary

Drawing these estimates together, we get the following numerical estimates for He on W(111), at a field of 56 V/nm, (the lower figure in each case corresponding to $b = 2b^{\theta}$, the higher to $b = 7b^{\theta}$):

(1) $\Delta B(conv)$ is estimated to lie between 40 - 75 meV's

(2) Adding about 30% (or somewhat less) to get ΔB^{elec} gives a figure lying between 55 - 100 meV

(3) Taking 50% of the above, to allow for repulsive forces, and adding between 5 meV and 10 meV to allow for dispersive forces gives an estimate of ΔB lying between 30 meV and 60 meV.

Following the same procedure, but for a field of 45 V/nm, ΔB is estimated to lie between 25 and 50 meV.

It will be clear that, although the estimate of $\Delta B(conv)$ is relatively precise, there is considerable uncertainty about the corrections. Better treatments will eventually be required, but for the time being we may formulate a rough rule that, for fields in the range of interest to field-ion emission we may obtain ΔB from $\Delta B(conv)$ by subtracting about 35%.

7.5 Binding energies in other circumstances

7.5.1 Other planes

Using the rule just formulated, we may calculate the binding energies for helium on the other planes of tungsten mentioned in table 6.1. Values obtained using $b_E \doteq 2b^{\theta}$ and F^{ext} 45 V/nm are shown in table 7.3

TABLE 7.3

Plane	A_c	ΔB(conv)/meV	ΔB/meV
100	1	negative	negative
110	$1/\sqrt{2}$	negative	negative
111	$\sqrt{3}$	∿ 50	∿ 30
210	$\sqrt{5}$	∿ 120	∿ 80
211	$\sqrt{6}/4$	negative	negative
310	$\sqrt{10}/2$	∿ 40	∿ 25
411	$3/2\sqrt{2}$	negative	negative

It is seen that several of the planes have negative binding energies. The result indicates that we cannot have a complete field-adsorbed helium layer on these planes, because high mutual depolarization would prevent the formation of a full adsorbed layer. This is because the planes are relatively close-packed, - as demonstrated mathematically by the small value of A_c and the large value of the structure factor T_1.

7.5.2 Partial layers

To follow up this point, we arranged a program to simulate a limited number of helium atoms adsorbed on a full emitter substrate layer, by ignoring mutual induction and artificially reducing the structure factor and hence the relative permittivity M_A for the adsorbed layer. This showed that it is possible to get a partial adsorbed layer (or even few adsorbed atoms) on top of those planes. Admittedly this treatment is not fully correct and we have various reservations.

We also set another program to simulate the c 2 x 2 effect on the

(100) plane (a recent discovered) phenomenon when only every other substrate atom is imaged). This showed that we still have negative values for the short-range binding energy. Very recently Graham (private communication) reported that selective evaporation of emitter surface atoms was noticed in this case. We simulated this situation in a program by setting the surface lattice parameter for a face centred square lattice to be equal to 2 x a. ΔB in this case is positive, the estimated values were 160 meV at F^{ext} = 45 V/nm, and 245 meV at F^{ext} = 56 V/nm. Field adsorption on the c 2 x 2 structure is thus to be expected, and hence its clear imaging can be explained.

7.5.3 The triple-layer case

Stimulated by the results in the preceding sections, we constructed a program to calculate the conventional binding energy for an assumed second adsorbed layer of atoms on top of the first, on the (111)-plane of Tungsten. The theory for this situation was described in section 4.6. For the He on W(111) system, at an external field of 57 V/nm, $\Delta B(conv)$ = 5.6 meV.

Comparing this to the Rendulic and Krautz[39] value, $\Delta B(conv)$ = 20 meV at F^{ext} = 45 V/nm our low value of $\Delta B(conv)$, does not support the Rendulic and Krautz hypothesis of the existence of a second adsorbed layer, since such a weak binding energy cannot hold the adsorbed atoms in the second layer fixed in their positions. More likely, we would have a second layer of mobile atoms, as the more conventional discussion assumes.

CHAPTER EIGHT

CONCLUSIONS AND FUTURE WORK

8.1 Summary

The conclusions of the main work reported in this thesis may be summarised as follows:

First, we have shown that there are many aspects in the theories of field ion imaging, field adsorption, and charged metal surfaces, that are inconsistent or contain basic conceptual errors. We have redefined the main variables, putting forward self-consistent definitions for the concepts of local field, polarizability, and binding energy, and have put forward a new model for charged metal surfaces and for field adsorption.

This model represents the charged surface by an infinite planar array of superimposed point positive charges and dipoles (with a similar array of negative charges at infinity), and the field-adsorbed layer by a similar layer of dipoles. The model can be analysed self-consistently, and incorporates the important physical fact that local structure exists in the charge distribution at the charged surface.

Using calculations based on this model, we have explored the field and potential variations above a charged surface. We have demonstrated that the field above a bare emitter surface is higher above the atomic sites than in between them, but that in the critical surface this variation is not enough to explain image contrast (for He on W(111)) at 80K. When a field-adsorbed layer is present a much higher field difference exists, that is sufficient to explain image contrast. We have also shown that the equipotentials above the emitter plane can be imagined to have an egg-box shape, and that the higher the value of the proper polarizability of the surface atoms the further from the emitter surface will be an equipotential of given V-value. A consequence of this is that

higher surface-atom polarizability can lead to reduced image contrast.

In our studies of field-adsorption binding energy, we have shown the insufficiency of previous treatments when applied to the case of a gas atom adsorbed in the interior of a crystal facet, assuming that the facet can be modelled by an infinite array. In particular, we have shown that ignoring the depolarization effects due to mutual interactions between emitter surface atoms leads to marked over-estimation of the binding energy. In the case of a really close-packed plane, for example W(100), the binding energy is negative, showing that it is impossible to have a full adsorbed layer. We have also shown that, even for W(111), we cannot have a complete second field-adsorbed layer on top of the first one, as has in effect been suggested by Krautz and Rendulic, because the short range binding energy is too low ($\Delta B \sim 5$ meV).

For the paradigm case of He on W(111), when all corrections are taken into account, we have estimated that at the best image field for Helium (45 V/nm) the short-range binding energy probably lies between 25 and 50 meV.

8.2 The adsorption/imaging problem

At this point we reach a very contradictory result. On the one hand we have concluded that it is necessary for a field-adsorbed layer to be present in order to explain image contrast; on the other hand the estimated short-range binding energy (i.e. 25 - 50 meV, at F^{ext} = 45 V/nm) is not sufficient to explain field adsorption itself, as may be demonstrated by the following argument.

If we assume that the mean time interval between ionization events in a given ionization zone is roughly equal to the time interval assumed to cause a continuous bright spot on the phosphor screen of the FIM, that is about 10^{-4} s, then we conclude that 10^{-4} s is the minimum time that

a field-adsorbed atom must be present. We may assume that the time required for an adsorbed atom to escape from a site, where Q is the necessary activation energy, is given by the Arrhenius-type equation:

$$\tau_r = A^{-1} \exp(Q/kT)$$

where kT is the Boltzmann factor, with T the emitter temperature taken to be 80K. A is a pre-exponential whose value is taken[73] as 10^{12} s^{-1}, and $\tau_r = 10^{-4}$ s. Assuming that Q can be identified with the short-range binding energy ΔB, then the value of ΔB necessary for an atom to be field adsorbed for about 10^{-4} s at 80K is about 130 meV.

The estimated binding energy (25 - 50 meV) is substantially less than this. So either the field-adsorbed layer is only partially occupied, or some significant factor has been omitted from our theoretical model or calculations. (For example, the effects of finite plane size may need to be included in a more realistic model).

Clearly, the problem of getting a completely self-consistent theory of field-ion imaging and adsorption has not been fully resolved. Some suggestions for future work are included in the next section.

8.3 Future Work

The opportunity for research in this field (i.e. the theory of the charged metal surface and field adsorption) is still wide open, since all the theoretical work done in this field (including the work reported here) is only a simple step toward the solution of a very complex problem

Even within the framework of the monopole-dipole surface model (the model which constitutes the backbone of this thesis), there is much unfinished work. We have confined this thesis to the case of tungsten as an emitter and helium as imaging and/or adsorbed inert gas, and we have discussed only the cases of the W(111) and W(111)/He systems in detail.

But there is still a wide range of emitter metals to be investigated and compared, and there are also the other gases that are used as imaging gases (in particular neon, argon and hydrogen).

We also need to know more about the possibility of partial occupancy of the adsorbed layer, and about the process of creating vacancies in the adsorbed layer. In particular, we need more accuracy in calculating the short-range differential binding energy ΔB.

Allied to this are problems associated with the use of a mixture of inert gases for imaging (e.g. a He/Ne mixture): the calculation of binding energies in a mixed layer, and the effect of an "impurity" neon atom on contrast.

Generally we need to know more about polarizability and charge localization at metal surfaces. In particular, we need more precise and reliable information about the positions of the electrical surface and the bonding sites, and better ways of estimating what value to choose for surface-atom polarizability within the framework of our charged-surface model.

More fundamentally, we also know that the monopole-dipole model is only a step towards representing a real charged surface. A model that completely represents reality is beyond the reach of mankind, since nothing can completely represent reality except reality itself. A model can only reflect a part of the reality, or certain of its aspects. We judge how truthful this reflection is by how close the results of the application of the model are to the experimental facts in a variety of real situations; and by the self-consistency of the model itself. But we always start with an idealistic model that only vaguely represents a specific reality under specific circumstances. The process of approaching the specific reality then starts by changing some parts of the model, trimming or modifying other parts, or/and may continue by abandoning the

original model in favour of another, better representation of reality.

This is true of our model (the monopole-dipole model). We can now think of many ways of improving it - or we might set up other models - in order to have a better representation of a real charged metal surface. One pathway forwards is to work within the framework of classical physics and modify our model in carefully studied steps. For example, we could:

(1) Introduce negative charges between each pair of nearest-neighbour positive charges (i.e. lattice points) at the surface, and to study field, potential, and binding energy variation;

(2) Investigate in detail the consequence of multipole moments;

(3) A more radical (and much more difficult) endeavour would be to set up a model representing planes of finite size, or a model based on a concave, parabolic, or realistically shaped (in three dimensions) emitter surface. Such models involve the problem of the charge distribution at a shaped surface, or one of a limited area, and this needs to be solved also.

Another pathway would require us to think of charged surface models to replace the classical monopole-dipole model. For example, one can think of a metal surface model consisting of an array of positively charged spheres (representing metal surface atoms) submerged in a sea of negatively charged liquid (representing the conduction electrons). The effect of the impressed field is then to drive this sea of electrons downwards into the interior of the metal. If the external field is strong enough a depletion of sea of negative charges from the top of the spheres gives us a picture of the surface involving positively charged apexes surrounded by negative charges. This imaginary charged metal surface model combines the jellium-type model and the fact that a metal surface contains localised charges, and seemingly has the advantage that we do

not need to worry about metal surface atoms' polarizability, because we do not need to use such a variable.

In principle, the best way to tackle microphysical problems (such as many of those arising with charged metal surfaces) is by general quantum - mechanical means. But this is a task difficult to accomplish. Instead, attempts have been made to introduce some quantum-mechanics to models based on classical physics, as in the jellium-type model. This mixture of classical and quantum physics has many difficulties. Inconsistencies arise between the theory and practice, as described in earlier chapters.

The eventual challenge in this subject area is the production of a fully self-consistent quantum-mechanical theory of realistically-shaped charged surfaces and field adsorption, that takes fully into account the localised detail in the surface charge distribution that is roughly represented in Forbes' monopole-dipole model as used in this thesis. It may be many years before this can be achieved.

APPENDIX A

More general method to calculate the external contributions $S_1(ext)$ and $S_2(ext)$.

(A) The Calculation of $S_1(ext)$

We can express $S_1(ext)$ as:

$$S_1(ext) = \int_{\theta=0}^{2\pi} \int_{n=n_L}^{\infty} \frac{n\, dn\, d\theta}{(n'^2 + z^2)^{3/2}} \quad \ldots\ldots A1$$

where $$n = (x^2 + y^2)^{\frac{1}{2}} \quad \ldots\ldots A2$$

$$n' = [(n \cos\theta - P_x)^2 + (n \sin\theta - P_y)^2]^{\frac{1}{2}} \quad \ldots\ldots A3$$

P_x and P_y are the field point coordinates as explained in chapter 5.

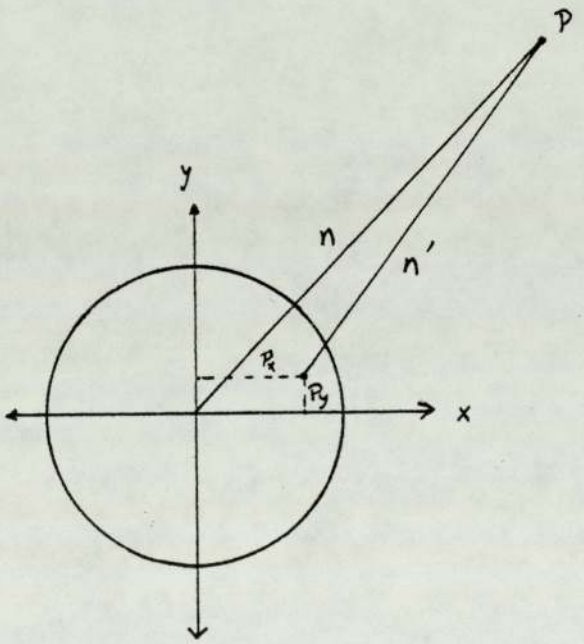

substituting eqs.A2 and A3 into A1, we can write the denominator of eq.A1 in the following form:

$$n^{-3}\left[1 - \frac{2}{n}(P_x \cos\theta + P_y \sin\theta) + \frac{P_x^2 + P_y^2 + Z^2}{n^2}\right]^{3/2} \quad \ldots\ldots A4$$

Knowing that P_x and P_y are usually less than lattice parameter unit length (i.e. P_x or $P_y \ll n$), then by applying binomial expansion theory to eq.A4

and neglecting all higher power terms (i.e. second, third, ... etc), we get:

$$n^{-3}\left[1 + \frac{3}{n}\left(P_x \cos\theta + P_y \sin\theta\right) - \frac{3}{2}\,\frac{P_x^2 + P_y^2 + Z^2}{2n^3}\right] \qquad \ldots\ldots \text{A5}$$

Substituting eq.A5 into eq.A1 and solving the integral, we get:

$$S_1(\text{ext}) \simeq \frac{2\pi}{A_c}\left[\frac{1}{n_L} - \frac{r^2}{2.n_L^3}\right] \qquad \ldots\ldots \text{A6}$$

where

$$r^2 = P_x^2 + P_y^2 + Z^2 \qquad \ldots\ldots \text{A7}$$

(B) The Calculation of $S_2(\text{ext})$

We can express $S_2(\text{ext})$ as:

$$S_2(\text{ext}) = \int_{\theta=0}^{2\pi} \int_{n=n_L}^{\infty} \frac{n\, dn\, d\theta}{\left[(n\cos\theta - P_x)^2 + (n\sin\theta - P_y)^2 + Z^2\right]^{5/2}} \qquad \ldots\ldots \text{B1}$$

Using the same method described above, we finally get:

$$S_2(\text{ext}) \simeq \frac{2\pi}{A_c}\left[\frac{1}{3.n_L^3} \quad \frac{r^2}{2.n_L^5}\right] \qquad \ldots\ldots \text{B2}$$

APPENDIX B

COMPUTER PROGRAM

This program is written in ALGOL 60. Note that this program is written for a specific single value of the coordinate z

#LISTING OF :SPS7807.MKG1(15/) PRODUCED ON 21AUG81 AT 11.25.16

#G8.64AB AT ASTON IN :SPS7807.MOP' ON 21AUG81 AT 11.29.08 USING U15

DOCUMENT MKG1

```
'BEGIN'
'REAL' CNT,SO,S1,S2,S3,PI,CALR,CALR2,CNTR,CR2,S1E,S2E,RL2,SOE,
Z,Z2,BAD2,ETA,PA,PE,PL,FPE,BMA,BME,ME,MA,GAE,GEA,DNOM,BAD,BED,
DB2,T1,TM,TD,AC,ZA,ZH,C,DX,DY,PX,PY,BINCONV,BINCORR,FEXT,RDA,
RDE,RZ,R1,RM3,W,W2,WZ,WM1,WZ2,WLZ,VSL,VDL,VD,VDH,VM,VMR,EPS,
BSL,BDL,BM,BD,BDH,BSH,N,N2,R2,RM1;
'BOOLEAN'CENTRED;

PART 1    DATA:
A INPUT DATA:
SPECIES:
ADSORBED ATOM:
RDA:=0.0          ;'COMMENT'IN NM;
PA:=0.000143      ;
METAL SURFACE ATOM:
RDE:=0.0          ;'COMMENT' IN NM;
PE:=0.002         ;
EXTERNAL FIELD:
FEXT:=45          ;'COMMENT'IN V/NM;
LATTICE PARAMETER:
C:=0.3164             ;'COMMENT'IN NM;
SURFACE ARRAY PARAMETER IN UNITS OF C:
DX:=SQRT(2)       ;
DY:=SQRT(6)       ;
CHOSEN POINT COORDINATES:
PX:=0.0       *DX;'COMMENT'IN UNITS OF DX;
PY:=0.0       *DY;'COMMENT'IN UNITS OF DY;
RZ:=1          ;'COMMENT'IN NM;
RZ IN UNITS OF C IS:
Z:=RZ/C;
SURFACE ARRAY STRUCTURE TYPE:
CENTRED:='TRUE'                ;'COMMENT'PUT FALSE OR TRUE;

B FIXED DATA:

PI:=3.14159265359;
FPE:=0.694456;
PL:=FPE*C*C*C;
CNTR:=70.0001*DX;
CR2:=CNTR*CNTR;
REFERENCE POINT:
WZ:=3*DX;
WZ2:=WZ*WZ;
 FIXING LATTICE CHARACTER:
AC:=DX*DY;
'IF'CENTRED'THEN'AC:=AC/[illegible];
SEPARATION OF [illegible] LAYERS IN UNITS OF C:
ZA:=0.259/C;
```

```
'PART II PROCEDURE :
 
'BEGIN'
'PROCEDURE'SUM(L1,L2,L3,L4,INC1,INC2);
'REAL'L1,L2,L3,L4,INC1,INC2;
'BEGIN'
'REAL'I,J;
'FOR'I:=L1'STEP'INC1'UNTIL'L2'DO'
'BEGIN'
'FOR'J:=L3'STEP'INC2'UNTIL'L4'DO'
'BEGIN'
N2:=I*I+J*J;
'IF'N2'GT'CR2'THEN''GOTO'IT;
CNT:=CNT+1;
R2:=N2+Z2;
R1:=SQRT(R2);
RM1:=1/R1;
RM3:=1/R2/R1;
S1:=S1+RM3;
S2:=S2+RM3/R2;
W2:=N2+WZ2;
WM1:=1/SQRT(W2);
S0:=S0+WM1-RM1;
'END';
IT:'END';
'END';

'PROCEDURE'EVAL(Z);
'VALUE'Z;
'REAL'Z;
'BEGIN'
CNT:=0;
S0:=0;
S1:=0;
S2:=0;
Z2:=Z*Z;

SUM(DX-PX,CNTR,-PY,CNTR,DX,DY);
SUM(-PX,-CNTR,DY-PY,CNTR,-DX,DY);
SUM(-DX-PX,-CNTR,-PY,-CNTR,-DX,-DY);
SUM(-PX,CNTR,-DY-PY,-CNTR,DX,-DY);

'IF'CENTRED'THEN'
'BEGIN'
SUM(DX/2-PX,CNTR,DY/2-PY,CNTR,DX,DY);
SUM(-DX/2-PX,-CNTR,DY/2-PY,CNTR,-DX,DY);
SUM(-DX/2-PX,-CNTR,-DY/2-PY,-CNTR,-DX,-DY);
SUM(DX/2-PX,CNTR,-DY/2-PY,-CNTR,DX,-DY)
'END';

N2:=PX*PX+PY*PY;
R2:=N2+Z2;
'IF'R2'GT'1&-18'THEN''BEGIN'
R1:=SQRT(R2);
RM1:=1/R1;
RM3:=1/R2/R1;
S1:=S1+RM3;
S2:=S2+RM3/R2;
W2:=N2+WZ2;
WM1:=1/SQRT(W2);
S0:=S0+WM1-RM1;
'END';
CNT:=CNT+1;
CALR2:=AC*CNT/PI;
CALR:=SQRT(CALR2);

```

```
115 RL2:=CALR2*Z2;
116 WL2:=CALR2*W*2;
117 SOE:=2*PI*(SQRT(RL2)-SQRT(WL2))/AC;
118 S1E:=2*PI/SQRT(RL2)/AC;
119 S2E:=S1E/3/RL2;
120 SO:=SO+SOE;
121 S1:=S1+S1E;
122 S2:=S2+S2E;
123 S3:=3*Z2*S2-S1;
124 'END' OF PROCEDURE EVAL;
125
126 'PROCEDURE'BAD2CALC(SEP);
127 'VALUE'SEP;
128 'REAL'SEP;
129 'BEGIN'
130 'REAL'A,B;
131 A:=PX;B:=PY;
132 PX:=0;PY:=0;
133 EVAL(SEP);
134 BME:=0.5;
135 ME:=1+PE*T1/PL;
136 MA:=1+PA*T1/PL;
137 GAE:=S3*PA/PL;
138 GEA:=S3*PE/PL;
139 DNOM:=1-GAE*GEA/MA/ME;
140 BMA:=0.5*SEP*AC*S1/4/PI;
141 BAD:=(BMA+GEA*BME/ME)/MA/DNOM;
142 BED:=(BME+GAE*BMA/MA)/ME/DNOM;
143 BAD2:=BAD*BAD;
144 PX:=A;PY:=B;
145 'END'OF PROCEDURE BAD2CALC;
146
147 'PROCEDURE'BINCALC(ZD);
148 'VALUE'ZD;
149 'REAL'ZD;
150 'BEGIN'
151 'REAL'BAD2N,DERIV;
152 BAD2CALC(ZD-0.0005);
153 BAD2N:=BAD2;
154 BAD2CALC(ZD+0.0005);
155 DERIV:=(BAD2-BAD2N)/0.001;
156 BAD2CALC(ZD);
157 DB2:=BAD2-1;
158 ETA:=-1*(ZD/12)*DERIV/DB2;
159 BINCONV:=DB2*PA*FEXT*FEXT;
160 BINCORR:=(1-ETA)*BINCONV;
161 'END'OF PROCEDURE BINCALC;
162
163 'PROCEDURE'TCALC;
164 'BEGIN'
165 'REAL'A,B;
166 A:=PX;B:=PY;
167 EVALUATE T1:
168 PX:=0;PY:=0;
169 EVAL(0);
170 T1:=S1;
171
172 EVALUATE TM TD:
173 EVAL(ZA);
174 TM:=S1;
175 TD:=S1;
176 PX:=A;PY:=B;
177 'END' OF PROCEDURE TCALC;
178
179 'PROCEDURE'VMMCALC;
180 'BEGIN'
```

```
EVALUATE MONOPOLS REFERENCE POTENTIAL;
EVAL(-BOO);
VMR:=-(.5*(-BOO+AZ)+(AC/4/PI)*SO);
*END* OF PROCEDURE VMRCALC;

*PROCEDURE*SCALC;
*BEGIN*
MS:=1-PE*T1/PL;
BES:=0.5/MS;
EVAL(Z);
BM:=0.5*Z*AC*S1/4/PI;
BD:=PE*BES*S3/PL;
BSL:=BM+BD;
VM:=0.5*(Z+AZ)*AC*SO/4/PI+VMR;
VD:=-(PE*BES/PL)*(2*PI/AC+Z*S1);
VSL:=VM+VD;
*END* OF PROCEDURE SCALC;

*PROCEDURE*DCALC;
*BEGIN*
BAD2CALC(ZA);
ZH:=Z-ZA;
EVAL(ZH);
BDH:=PA*BAD*S3/PL;
VDH:=-(PA*BAD/PL)*(2*PI/AC*ZH*S1);
EVAL(Z);
BM:=0.5*Z*S1*AC/4/PI;
BD:=PE*BED*S3/PL;
BDL:=BM+BD+BDH;
VM:=0.5*(Z+AZ)*AC*SO/4/PI+VMR;
VD:=-(PE*BED/PL)*(2*PI/AC*Z*S1);
VDL:=VM+VD+VDH;
*END* OF PROCEDURE DCALC;

PART 3:

MAIN PROGRAM STARTS HERE:

TCALC;
VMRCALC;
SCALC;
DCALC;
BINCALC(ZA);


PART 4  PRINT OUT:

NEWLINE(1);
PRINT(T1,3,6);
PRINT(T*,3,6);
PRINT(TD,3,6);
PRINT(VMR,3,6);
PRINT(BSL,3,6);
PRINT(BDL,3,6);
PRINT(VSL,3,6);
PRINT(VDL,3,6);
PRINT(BINCORR,3,6);
*END*
*END*
*END*;
****

```

REFERENCES

1. Harrison, W.A., Pseudopotentials in the theory of metals, (Benjamin, New York, 1966)
2. Rice, T.M., Landau Fermi - Liquid parameters in Na and K, Phys. Rev. 175, (1968), 858.
3. Ewald, P.P. and Juretschke, H., Structure and properties of solid surfaces, P82 (University of Chicago Press, Chicago, 1953).
4. Lang, N.D. and Kohn W., Theory of metal surface: charge density and surface energy, Phys. Rev., B1, 4555 (1970).
5. Bardeen, J., Theory of work function: The surface double layer, Phys. Rev. 49, (1936) 653.
6. Lennard-Jones, J.E. and Dent, B.M., The change in lattice spacing at a crystal boundary, Proc. Roy. Soc., A121, (1928), 247.
7. Müller, E.W. and Tsong, T.T., Field Ion Microscopy, Principles and applications, (Elsevier, New York, 1969).
8. Becker, J.A., Part I: Thermoionic emission, Rev. Mod. Phys., 7, No.2, (1935), 95.
9. Swanson, L.W. and Bell, A.E., Recent advances in field electron microscopy of metals, Adv. in electronics and electron Phys., 32, (1973), 193.
10. Müller, E.W., The imaging process in field ion microscopy from the FEM to the Atom-Probe, Chemistry and Physics of solid surfaces (CRC Press, Cleveland, Ohio, 1977).
11. Müller, E.W., (German) elektronmikroskopische beobachtugen von feldkathoden, Z. phys. 106, (1937), 541.
12. Müller, E.W., The field ion microscope (German), Z. phys., 131, (1951), 136.

13. Inghram, M.G. and Gomer, R., Mass spectrometric analysis of ions from the field microscope, J. Chem. Phys., 22, (1954), 1279.

14. Tsong, T.T. and Müller, E.W., Field adsorption of inert gas atoms on field ion emitter surface, Phys. Rev. Lett. 25, (1970), 911.

15. Tsong, T.T. and Müller, E.W., Field adsorption of inert-gas atoms, J. Chem. phys. 55, (1971), 2884.

16. Forbes, R.G., Field ion microscopy at very low temperatures, Ph.D. Thesis, University of Cambridge (1970).

17. Müller, E.W., Field desorption, Phys. Rev. 102, (1955), 618.

18. Panitz, J.A., Surface characterisation by single atom mass spectroscopy, Crit. Rev. Sol. Stat. Sci., 5, (1975), 153.

19. Waugh, A.R., Boyes, E.D., and Southon, M.J., Field-desorption microscopy and the atom probe, Nature, 253, (1975), 342.

20. Forbes, R.G., A theory of field-ion imaging: I.A quasi-classical site-current formula, J. of Microscopy, 96, (1972), 57.

21. Müller, E.W., Field ionization and field-ion microscopy, Adv. in Electron and Electron Phys., 13, (1960), 83.

22. Knor, Z. and Müller, E.W., A refined model of the metal surface and its interaction with gases in the field ion microscope, Surface Sci., 10, (1968), 21.

23. Knor, Z., Comments on "Field-Ion Image Formation", Nature Physical Sci., 239, (1972), 15.

24. Tsong, T.T., Surface states and field ion image formation, Surface Sci., 10, (1968), 102.

25. Forbes, R.G., Field-ion image formation, Nature Physical Sci., 230, No. 16, (1971), 165.

26. Forbes, R.G., A theory of field-ion imaging: II. on the origin of site-current variations, J. of Microscopy, 98, pt 1, (1972), 63.

27. Moore, A.J.W., The structure of atomically smooth spherical surfaces, J. Phys. Chem. Solids, 23, (1962), 907.

28. Iwasaki, H. and Nakamura, S., Ionization probability calculations in field ion microscopy, surface Sci., 43, (1974), 301

29. Iwasaki, H. and Nakamura, S., Model Calculation of field ionization through adsorbed atoms in a field-ion microscope, surface Sci. 49, (1975), 664.

30. Nolan, D.A. and Herman, R.M., Increased image brightness caused by field adsorption in field-ion microscopy. II. Effects of field distortions in atomic orbitals., Phys. Rev. B. 10 (1974), 50.

31. Duffell, J. and Forbes, R.G., Field-ion image contrast: the gas distribution hypothesis re-examined, J. Phys. D: Appl. Phys., 11, (1978), L 123.

32. Müller, E.W. and Bahadur, K., Field ionization of gases at a metal surface and the resolution of the field ion microscope, Phys. Rev. 102, (1956), 624.

33. Müller, E.W., Study of atomic structure of metal surfaces in the field ion microscope, J. Appl. Phys. 28, (1957), 1.

34. Chen, Y.C. and Seidman, D.N., On the atomic resolution of a field ion microscope, Surface Sci., 26, (1971), 61

35. Iwasaki, H. and Nakamura, S., Ion-current generation in the field ion microscope. Pt.1. Dynamic approach, Surface Sci., 52, (1975), 588.

36. Iwasaki, H. and Nakamura, S., Ion-current generation in the field ion microscope. Pt.2. Quasi-static approach, Surface Sci., 52, (1975), 597.

37. Forbes, R.G., More about mechanisms of field-ion imaging: sources of local contrast, (21st international field emission symposium, Marseille, 1974)

38. Sakurai, T. and Müller, E.W. Field ionization within the forbidden zone, Surface Sci., 49, (1975), 497

39. Rendulic, K.D. and Krautz, E., Is the field ion microscope a desorption microscope?, Acta Physica Austriaca, 42, (1975), 357.

40. Crowell, A.D., on: The solid-gas interface, (ed: Flood, E.A.) (Dekker, New York, 1967)

41. Nishikawa, O. and Müller, E.W., Operation of the field ion microscope with neon, J. Appl. Phys. 35, (1964), 2806.

42. Müller, E.W., Hydrogen promotion of field ionization and rearrangement of surface charge, Surface Sci., 7, (1967), 462.

43. Müller, E.W., Field ion microscopy and electronic structure of metal surfaces, Quarterly Rev. 23, (1969), 177.

44. Forbes, R.G., Field-ion imaging theory: on the visibility of adsorbates, Surface Sci, 27, (1971), 659

45. Weizer, V.G., Investigation of intermittent enhancement of ion emission from a tungsten surface using FIM, J. Appl. Phys. 42, (1971) 5886

46. Rendulic, K., Measurements of field adsorption of Ne and He and the field ionization of a He-Ne mixture, Surface Sci, 28, (1971), 258.

47. Schmidt, W.A., Reisner, Th. and Krautz, E., Field ion microscopic phenomena of neon atoms with platinum and platinum-gold alloy surface, Surface Sci., 26, (1971), 297.

48. Janssen, A.P. and Jones, J.P., The effect of neon on helium ion imaging in the field ion microscope, Surface Sci, 33, (1972), 553.

49. Lewis, R.T. and Gomer, R., Adsorption studies in the field ion microscope with argon imaging, Surface Sci., 26, (1971), 197.

50. Röllgen, F.W. and Becke y, H.D., Field induced chemisorption and promoted field ionization, Surface Sci., 26, (1971), 100.

51. Forbes, R.G., Problems in the theory of field-ion imaging, Vacuum, 22, (1972), 517.

52. Tsong, T.T., Field ion image formation, Surface Sci., 70, (1978), 211.

53. Forbes, R.G., Conceptual errors in the theory of field adsorption, Surface Sci., 87, (1979), L278.

54. Wafi, M.K., Field adsorption and field ion imaging (a computer study of field and potential variations above charge arrays), M.Sc. thesis, University of Aston (1977)

55. Blyholder, G. and Coulson, C.A., Molecular-orbital models of chemisorption, Trans. Far. Sci. 63, (1967), 1782.

56. Frenkel, J., Physik, 51, (1928), 232.

57. March, N.H., Thomas-Fermi approximations in quantum mechanics , Advan. phys., 6, (1957), 1

58. Smoluchouski, R., Anisotropy of the electronic work function of metals, Phys. Rev., 60, (1941), 661.

59. Kohn, W., and Sham, L.J., Self-consistent equations including exchange and correlation effects, phys. Rev., 140, (1965), 1133 A.

60. Lang, N.D., and Kohn, W., Theory of metal surfaces: charge density and surface energy, Phys. Rev., B1, (1970), 4555.

61. Lang, N.D., and Kohn, W., Theory of metal surfaces: work function, phys. Rev. B3, (1971), 1215.

62. Rice, O.K., Application of the Fermi statistics to the distribution of electrons under fields in metals and the theory of electro-capillarity, Phys. Rev. 31, (1928), 1051.

63. Mott, N.F., and Watts-Tobin, R.J., The interface between a metal and an electrolyte, Electrochim Acta, 4, (1961), 79.

64. Gomer, R. and Swanson, L.W., Theory of field desorption, J. Chem. Phys. 38, (1963), 1613

65. Tsong, T.T., and Müller, E.W., Effects of static field penetration and atomic polarization on the capacity of a capacitor, field evaporation, and field ionization processes, Phys. Rev., 181, (1969), 530.

66. Lang. N.D. and Kohn, W., Theory of metal surface: induced surface charge and image potential, phys. Rev., 7, (1973), 3541B.

67. Theophilou, A.K. and Modinos, A., Metallic-field effect and its consequences in field emission, field ionization and the capacitance of a capacitor, phys. Rev., 6, (1972), 801B.

68. Forbes, R.G., Field adsorption - the monopole-dipole interaction, Surface Sci., 78, (1978), L504.

69. Müller, E.W. and Krishnaswamy, S.V., Energy spectrum of field ionization at a single atomic site, Surface Sci., 36, (1973), 29.

70. Sakurai, T. and Müller, E.W., Field ionization within the forbidden zone, Surface Sci., 49, (1975), 497.

71. Culbertson, R.J., Sakurai, T. and Robertson, G.H., Field ionization of surface absorbates, Phys. Rev., B19, (1979), 4427.

72. Freeman, D.L., The interaction of rare gas atoms with graphite surface., J. Chem. Phys., 62, (1975), 4300.

73. Forbes, R.G., The influence of hyperpolarizability and field-gradient polarizability on field adsorption binding energies for He on W(111), Surface Sci., 108, (1981), 311.

74. Feynman, R.P. and Leighton, R.B., in: Lectures on Physics, VII (Addison-Wesley, London, 1964).

75. Forbes, R.G., Atomic Polarizability values in the SI system, Surface Sci., 64, (1977), 367.

76. Tsong, T.T. and Kellogg, G., Direct observation of the directional walk of single adatoms and the adatom polarizability, Phys. Rev., B12, (1975), 1343.

77. Forbes, R.G. and Wafi, M.K., An array model for the field adsorption of helium on tungsten (111), Surface, Sci., 93, (1980), 192.

78. Tsong, T.T., Measurement of the polarizabilities and field evaporation rates of individual tungsten atoms, J. Chem. Phys., 54, (1971), 4205.

79. Forbes, R.G., Field evaporation theory; the atomic jug formalism, Surface Sci., 70, (1978), 239.

80. Thorhallsson, J., Fisk, C. and Fraga, S., Use of atomic functions with minimal basic sets., J. Chem. Phys., 49, (1968), 1987.

81. Miller, T.M. and Bederson, B., in: Advances in atomic and molecular physics, 13, (Academic Press, London, 1977).

82. Forbes, R.G., Derivation of surface-atom polarizability from field-ion energy deficits, Appl. phys. Lett. 36, (1980), 739.

83. Reitz, J.R. and Milford F.J., in: Foundation of electromagnetic theory (Addison-Wesley, London, 1971).

84. Topping, J., On the mutual potential energy of a plane network of doublets, Proc. Roy. Soc., (London), A114, (1927), 67.

85. MacDonald, J.R. and Barlow, C.A., Work function change of monolayer adsorption, J. Chem. Phys., 39, (1963), 412.

86. Chibane, K., Field-adsorption of a single helium atom on a charged surface, (M.Sc. thesis, Aston University, 1980)

87. Nicholas, J.F., in: An altas of models of crystal surface, (Gordon and Breach, Science Publishers, Inc., London, 1965).

88. Landmand,U. and Kleiman G.G., in : Surface and defect properties of solids, V6, (Chem.Soc.,London, 1977)

89. Weinberg,W.H., Ph.D. Thesis, Univ. of California, Berkeley (1971)

90. Bertoncini, P., and Wahl, A.C. Calculation of the helium-helium $^1\Sigma^+$ Potential at intermediate and large separations, Phys.Rev.Letters 25, (1970), 991.